

MULTISCALE ANALYSIS OF HEMOSTASIS AND THROMBOSIS

By

Hari Hara Sudhan Lakshmanan

A DISSERTATION

Presented to the Department of Biomedical Engineering

Of the Oregon Health & Science University

School of Medicine

In partial fulfillment of the requirements for the degree of

Doctor of Philosophy

In Biomedical Engineering

December 2021

© Hari Hara Sudhan Lakshmanan

All Rights Reserved

School of Medicine

Oregon Health & Science University

CERTIFICATE OF APPROVAL

This is to certify that the PhD Dissertation of
Hari Hara Sudhan Lakshmanan
“Multiscale analysis of hemostasis and thrombosis”
has been approved

Mentor: Owen J. T. McCarty, Ph.D.

Member/Chair: Daniel M. Zuckerman, Ph.D.

Member: Carmem S. Pfeifer, D.D.S, Ph.D.

Member: Carolyn S. Ibsen, Ph.D.

Member: Xubo Song, Ph.D.

TABLE OF CONTENTS

TABLE OF CONTENTS	i
List of Figures	vii
List of Tables	x
List of Abbreviations	xi
Acknowledgements	xiv
Abstract	1
Chapter 1.Introduction	4
1.1 Overview – Hemostasis and Thrombosis.....	4
1.2 Biochemistry of coagulation	6
1.2.1 Coagulation pathways.....	6
1.3 Platelets	9
1.4 Platelet receptors and signaling.....	10
1.4.1 GPIb and initial platelet adhesion.....	10
1.4.2 GPVI-induced platelet activation	11
1.4.3 Role of PARs in platelet activation	12
1.4.4 Integrins and platelet aggregation.....	13

1.4.5	P2Y receptors and feedback activation.....	14
1.5	ECM proteins – Platform for hemostasis and thrombosis	16
1.5.1	von Willebrand factor (vWF)	17
1.5.2	Collagen.....	17
1.5.3	Laminin.....	18
1.5.4	Nidogen	18
1.5.5	Other ECM proteins with plausible roles in hemostasis and thrombosis.....	19
1.6	Platelet granule secretion	19
1.7	Platelets in coagulation	22
1.8	Physics of hemostasis and thrombosis	24
1.8.1	Blood rheology	24
1.8.2	Convection and diffusion.....	27
1.8.3	Dimensionless numbers	28
1.9	Platelets, coagulation and flow	29
1.10	Thesis Overview	33
Chapter 2. Materials and Methods		36
2.1	Ethical Considerations	36
2.2	Common reagents	36
2.3	Human blood collection.....	36

2.4	Platelet isolation.....	37
2.5	<i>In vitro</i> platelet spreading studies	37
2.6	Microscopy	38
2.6.1	General protocol	38
2.6.2	Image analysis	38
2.7	Statistical analysis	38
Chapter 3.Revised model of the tissue factor pathway of thrombin generation: role of the feedback activation of FXI		39
3.1	Abstract.....	39
3.2	Introduction.....	40
3.3	Background	41
3.4	Materials and Methods.....	43
3.4.1	Reagents	43
3.4.2	Thrombin generation - Experiments.....	44
3.4.3	Thrombin generation – Simulations	45
3.4.4	Estimation of kinetic constants.....	46
3.4.5	Statistical analysis	47
3.5	Results.....	48
3.5.1	FXI increases TF-initiated thrombin generation in a TF concentration- dependent manner	48
3.5.2	Effect of FXI on FXa-initiated thrombin generation.....	51

3.5.3	A systems biology model of TF-pathway of thrombin generation.....	52
3.5.4	Extending the mod.HM model to include FXI	59
3.5.5	Validating the ext.HM model	62
3.6	Discussion	66
Chapter 4.The basement membrane protein nidogen-1 supports platelet adhesion and activation.....		70
4.1	Abstract	70
4.2	Introduction.....	71
4.3	Background	71
4.4	Materials and Methods.....	73
4.4.1	Reagents	73
4.4.2	Isolation of human platelets.....	74
4.4.3	Static platelet adhesion and spreading assay	74
4.4.4	Statistical Analysis	74
4.5	Results.....	75
4.5.1	Nidogen supports platelet adhesion and activation	75
4.6	Discussion	80
Chapter 5.Design of a microfluidic bleeding chip to evaluate antithrombotic agents		82
5.1	Abstract.....	82
5.2	Introduction.....	83

5.3	Background	83
5.4	Materials and Methods.....	85
5.4.1	Design and fabrication of microfluidic pillar device	85
5.4.2	Experimental setup	88
5.5	Results and discussion	90
5.5.1	Modeling blood flow in the microfluidic pillar device.....	90
5.5.2	Hemostatic plug formation in the microfluidic pillar device.....	92
Chapter 6. Modeling the effect of blood vessel bifurcation ratio on occlusive thrombus formation		96
6.1	Abstract	96
6.2	Introduction.....	97
6.3	Background	97
6.4	Materials and methods	100
6.4.1	Modeling the circulatory system as a hydraulic circuit	100
6.4.2	Mathematical modeling of flow and shear rate in microvascular bifurcations	103
6.5	Results.....	105
6.5.1	Complete occlusion and partial occlusion in terms of bifurcation ratios.....	110
6.6	Discussion	112
Chapter 7. Conclusions and Future Directions		117

7.1	Conclusions.....	117
7.2	Future directions	119
7.2.1	Analyze the role of TFPI in modifying the contribution of FXI to TF-mediated fibrin generation under flow	120
7.2.2	Sensitivity analysis of the kinetic parameters of the ext. HM model .	122
7.2.3	Role of polyphosphates in thrombin generation.....	124
	References	128
	Biographical Sketch.....	146
	Appendix A	150

List of Figures

Figure 1.1 Hemostasis and thrombosis.....	5
Figure 1.2 Coagulation network.....	8
Figure 1.3 Platelet signaling.....	15
Figure 1.4 Extracellular matrix proteins.....	16
Figure 1.5. Platelets in coagulation.	24
Figure 1.6 Velocity and shear stress in laminar flow.	26
Figure 1.7 Thrombus formation in atherosclerosis.....	30
Figure 1.8. Multiscale events of hemostasis and thrombosis.	33
Figure 3.1. Sensitivity of TF-initiated thrombin generation to FXI.....	50
Figure 3.2. Sensitivity of FXa-initiated thrombin generation to FXI.....	52
Figure 3.3. Comparison of in vitro and in silico TF-initiated thrombin generation in FXI-depleted plasma	58
Figure 3.4. Comparison of in vitro and in silico TF-initiated thrombin generation in plasma with FXI.....	61

Figure 3.5. Validation of the extended Hockin-Mann model.....	64
Figure 4.1. Adhesion and spreading of human platelets on nidogen-1.	76
Figure 4.2. Effect of platelet inhibitors on platelet adhesion and spreading on nidogen-1.....	79
Figure 5.1 Design and development of a polydimethylsiloxane based microfluidic bleed chip.....	87
Figure 5.2 Experimental setup for the use of bleed chip with the blood sample.....	90
Figure 5.3 Estimation of shear rate and velocity in the bleed chip using numerical modeling.....	92
Figure 5.4 Dynamics of blood flow and hemostatic plug formation in the bleed chip.	94
Figure 6.1 Modeling a microvasculature bifurcation with a thrombus as a series of resistances.....	102
Figure 6.2 Estimation of the shear rate on thrombus surface in a microvascular bifurcation.....	106
Figure 6.3 Effect of boundary conditions and thrombus length ratio (ϕ) on the dynamics of shear rate in a bifurcation.....	108

Figure 6.4 Sensitivity of critical shear ratio on bifurcation ratios – Phase plot.	111
Figure 6.5 Effect of microvascular plaque on occlusive thrombus formation.	114
Figure 7.1 Schematic of flow chamber setup to assess fibrin generation under flow.	121
Figure 7.2 Example sobol indices plot for a six-parameter system.....	124
Figure 7.3 Polyphosphates enhance TF-mediated thrombin generation.	126

List of Tables

Table 3.1 Average initial plasma concentrations of enzymes and inhibitors 56

Table 3.2 Reactions and kinetic constants of the extended Hockin-Mann model..... 65

List of Abbreviations

ADP	adenosine diphosphate
aPTT	activated partial thromboplastin time
APC	activated protein C
ATIII	anti-thrombin
ATP	adenosine triphosphate
BSA	bovine serum albumin
Btk	Bruton's tyrosine kinase
cAMP	cyclic adenosine monophosphate
C1inh	C1inhibitor
CLEC-2	C-type lectin receptor-2
CRP	collagen-related peptide
CTI	corn trypsin inhibitor
DAG	diacylglycerol
DIC	differential interference contrast
DNA	deoxyribonucleic acid
ECM	extracellular matrix
ETP	endogenous thrombin generation potential
FcR γ	Fc receptor γ
FII	coagulation factor II (prothrombin)
FIIa	activated coagulation factor II (thrombin)
FVII	coagulation factor VII (zymogen)
FVIIa	activated coagulation factor VII
FVIII	coagulation factor VIII

FVIIIa	activated coagulation factor VIII
FIX	coagulation factor IX (zymogen)
FIXa	activated coagulation factor IX
FX	coagulation factor X (zymogen)
FXa	activated coagulation factor X
FXI	coagulation factor XI (zymogen)
FXIa	activated coagulation factor XI
FXII	coagulation factor XII (zymogen)
FXIIa	activated coagulation factor XII
GP	glycoprotein
GPCR	G-protein coupled receptor
GPIb	glycoprotein Ib
GPIX	glycoprotein IX
GPV	glycoprotein V
GPVI	glycoprotein VI
GSA	global sensitivity analysis
HBSS	Hank's balanced salt solution
HBS	HEPES buffered saline
IKK	I κ B kinase
ITAM	immunoreceptor tyrosine-based activation motif
LAT	linker for activation of T cells
LMWH	low molecular weight heparin
mIIa	meizothrombin
NETs	neutrophil extracellular traps
NaCit	sodium citrate

ODE	ordinary differential equation
PAR	protease-activated receptor
PBS	phosphate buffer saline
PDMS	polydimethylsiloxane
PFA	paraformaldehyde
PGI ₂	Prostaglandin I ₂ or prostacyclin
PI3K	phosphoinositide 3-kinase
PIP ₃	phosphatidylinositol-3,4,5-triphosphate
PKA	protein kinase A
PKC	protein kinase C
PLC	phospholipase C
PolyP	polyphosphate
PPP	platelet-poor plasma
PRP	platelet-rich plasma
PS	phosphatidylserine
PT	prothrombin time
RBC	red blood cell
SEM	standard error of means
Syk	spleen tyrosine kinase
SFK	Src family kinases
TAFI	thrombin-activatable fibrinolysis inhibitor
TF	tissue factor
TFPI	tissue factor pathway inhibitor
TXA ₂	thromboxane A ₂
vWF	von Willebrand factor

Acknowledgements

மாதா, பிதா, குரு, தெய்வம் (Mother, Father, **Teacher (Guru)**, God) is a popular adage often quoted in India to reflect the significance of a teacher in one's life. My mentor, Dr. Owen J.T. McCarty, was an embodiment of this saying and possibly even more. From the moment I joined Owen's lab, he has incessantly encouraged me to explore the unknown. More often than not, he regulated my scientific enthusiasm by repeating 'slowly, slowly' to make me a thoughtful scientist. His support during the worst phase of the pandemic during the lockdown in India, was vital in keeping me on track despite being miles away from Oregon. I will cherish those 'zoompuffs', and 'gym times', two important factors for the productivity of the McCarty lab. I look forward to witnessing greater accomplishments and careers made from the McCarty lab in the future.

My dissertation advisory committee (DAC) has been an important part of my support during my time at OHSU. I am grateful to them for keeping me on track with every step of the process and motivating me to do more and go the extra mile. During every DAC meeting that I have had, I was nourished with fresh ideas and positive feelings towards planning my research and career. Dr. Daniel Zuckerman, my committee chair, Dr. Carmem Pfeifer and Dr. Carolyn Ibsen, as the members of my DAC, are inspiring scientists and excellent mentors. I thank Dr. Xubo Song for serving as an external member in my examination committee.

Thanks to Dr. Monica Hinds, an inspiration to all the academics, for keeping the grad students on track with everything academic in the Biomedical Engineering

department. Thanks to Erica, Alex, Holly and Caitlin for making it look easy in the administration. Thanks to Dr. Nakayama for her support towards the last leg of the grad school.

I am glad to have collaborated with an array of incredible scientists and physicians at and outside OHSU. Their feedback, insights and contribution were invaluable in steering projects towards successful publications. Thanks to Dr. Joseph Shatzel, Dr. Sven Olson, Dr. Monica Hinds, Dr. Joseph Aslan, Dr. Michael Wallisch, Dr. Christina Lorentz, Dr. Norah Verbout, Dr. Annachiara Mitrugno, Benjamin Elstrott, Novella Bates, Meghan Fallon, Dr. Patrick Journey, Dr. Siva Vanapalli, Adity Pore, Dr. Jeevan Maddala et al. Thanks to Mo, from PDX pharma for the constant support, encouragement, guidance and feedback.

Words cannot express my gratitude for everyone I have worked with in the McCarty lab. I am glad for the opportunity to work with some incredible scientists and excellent friends. The mentorship of the McCarty lab ‘wonder woman’ Dr. Cristina Puy is the pillar we all rely on. Thank you, Cristina, for all the inspiration, advice and encouragement. A big thanks to Tony, Tia, Nhu, Kelley, Alex, JP, Stephanie, Daniel, Graham, Aki, Annachiara, for making the lab environment so much fun and lively to learn and work. I am looking forward to seeing the greater heights everyone will achieve in the coming future.

This would be impossible without the support of my parents, sisters and friends, Jayaram, Irfan, Keshav, Jothi, Christabel and Josh. My deepest thanks to my wife Preethi for traveling along this wonderful path with me. To the future!

Abstract

Multiscale analysis of hemostasis and thrombosis

Hari Hara Sudhan Lakshmanan

Department of Biomedical Engineering
School of Medicine
Oregon Health & Science University

December 2021

Dissertation Advisor: Owen J. T. McCarty, Ph.D.

Hemostasis is the process of sealing a vascular leak through concomitant activation of the blood coagulation cascade and blood platelet adhesion to and activation by the subendothelial extracellular matrix (ECM) proteins. On the other hand, thrombosis is the obstruction of blood flow in an otherwise intact blood vessel due to uncontrolled growth of a thrombus. Currently available drugs and therapies that abrogate thrombosis invariably affect hemostasis, thus increasing the risk of bleeding. Hence, there exists a need to develop therapeutics that are effective in mitigating thrombosis without interrupting hemostatic safety.

A hemostatic plug or a thrombus is an aggregate of red blood cells and activated platelets bound by fibrin that is formed under the influence of the shear forces associated with blood flow. The present research analyzes molecular, cellular and physical events across various length scales involved in hemostasis and thrombosis

through the development and integration of *in vitro* and *in silico* models of coagulation biochemistry and the identification of novel ligands of platelet activation.

At the molecular level, both hemostasis and thrombosis are the result of a network of biochemical reactions involving enzymes, inhibitors and cofactors controlled in part by the feedback loops that converge on the serine protease thrombin. Mechanistically, the serine protease coagulation factor XI (FXI) appears to be a common node for the contact and tissue factor (TF) pathway of thrombin generation, as FXI can be activated by thrombin as well as activated coagulation factor XII (FXIIa) – the initiator of the contact pathway of coagulation. Importantly, FXI deficiency causes a mild bleeding disorder, whereas there are no bleeding symptoms associated with FXII deficiency. In the first part of this dissertation, we take an integrative biology approach to evaluate the relative contribution of the serine protease FXI towards the TF-mediated thrombin generation. We developed and experimentally validated an *in silico* model of thrombin generation that provides insights into the role of endogenous inhibitors in determining the effect of FXI in thrombin generation.

Platelets respond rapidly to a vascular injury in part due to their capacity to be activated by the extracellular matrix (ECM) proteins to spread, adhere and aggregate. Herein, we describe a novel role for nidogen-1, the ECM protein that bridges collagen and laminin in the subendothelial matrix, in activating platelets and supporting adhesion. Utilizing a combination of pharmacological inhibitors, gel-electrophoresis and adhesion assays, we identified that nidogen-1 may activate platelets through the transmembrane receptor glycoprotein VI (GPVI) and the integrin $\beta 1$.

Preclinical evaluation of the hemostatic safety of drugs and therapies is limited in part due to the lack of *in vitro* models that faithfully represent the diversity of the physics associated with hemostasis and thrombosis. To model the formation of a hemostatic plug under physiologically relevant flow conditions *in vitro*, we designed a polymer-based microfluidic pillar device with two orthogonal channels, an injury channel, and a blood channel. The microfluidic device was utilized to demonstrate the role of shear gradients and mass transport in hemostasis. Finally, to assess how geometry may predispose microvasculature to occlusive thrombus formation, an analytical mathematical model was developed to estimate the shear stress dynamics on the thrombus surface during growth. The model was utilized to identify that the microvessels that bifurcate according to the Murray's law of bifurcations may be protected from occlusive thrombus formation.

Overall, the studies presented in this dissertation provide novel insights into the biochemical, cellular and biomechanical events governing hemostasis and thrombosis. The results from the studies could be useful in the development of devices and therapeutic strategies that improve the hemostatic safety of anticoagulant and antiplatelet agents.

Chapter 1. Introduction

1.1 Overview – Hemostasis and Thrombosis

Blood coagulation is the formation of a semi-solid blood clot from liquid blood. The phase change of blood in clotting is due to the formation of an aggregate of circulating cells, specifically platelets and red blood cells (RBCs) and a fibrous protein called fibrin. There are two major outcomes of blood coagulation *in vivo*: hemostasis and thrombosis. Hemostasis is a physiologic phenomenon where an injury to a blood vessel exposes tissue factor (TF) from the extravascular region to flowing blood that triggers fibrin formation and platelet aggregation to seal the blood vessel for continuous flow of blood (1). On the other hand, thrombosis is a pathologic event where a thrombus induced by vascular inflammation or flow disturbances blocks the flow of blood (**Figure 1.1**). Thrombosis is the underlying cause of death in cardiovascular diseases, the world's major cause of death (2-4). The current treatments and therapies for thrombosis target biomolecular and cellular aspects of coagulation that invariably affect hemostasis to increase the risk of bleeding (5). Success in abrogating thrombosis without jeopardizing hemostasis requires an understanding of the subcellular, cellular and the extracellular processes that drive blood coagulation during hemostasis and thrombosis; concepts that make up the substance of this dissertation.

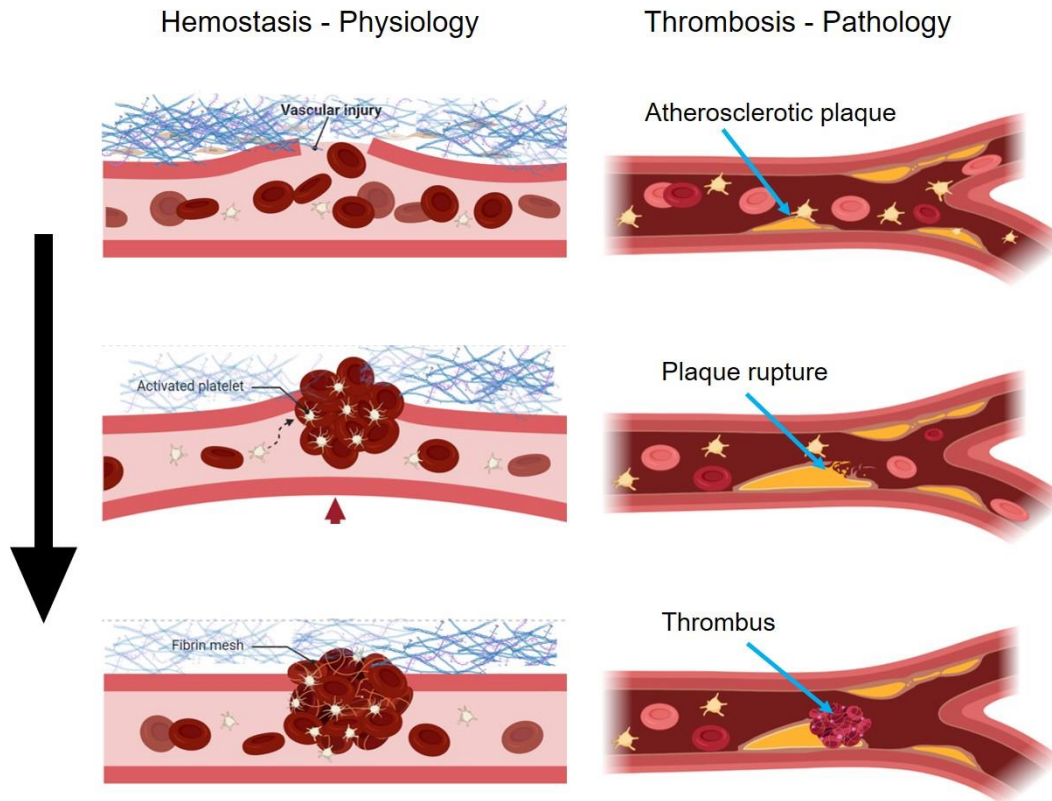


Figure 1.1 Hemostasis and thrombosis. Hemostasis is the physiological process of sealing a vessel injury with an aggregate of platelets bound by a mesh of fibrin generated from coagulation. Thrombosis is the pathological phenomenon of vessel occlusion due to a thrombus, aggregate of platelets and fibrin, most often triggered by the rupture of atherosclerotic plaque in an inflamed blood vessel. Figure created with Biorender.com
 ©Hari Hara Sudhan Lakshmanan

Hemostasis and thrombosis involve a set of biochemical reactions that generate thrombin and cellular signaling events that activate platelets to cause aggregation, all under the influence of physical forces associated with blood flow (6). In the first part of this chapter, we will explore the biochemical reactions and proteins involved in coagulation, in particular the generation of thrombin and fibrin. In the second and third parts of the chapter the biology of platelets and the physics relevant to hemostasis and thrombosis will be discussed.

1.2 Biochemistry of coagulation

The coagulation system is an orchestrated set of biochemical reactions involving enzymes, inhibitors and cofactors connected with the goal of regulating the generation of thrombin – the serine protease responsible for fibrin formation and for regulatory feedback within the cascade. The proteins involved in the coagulation cascade are identified using roman numerals such as I and II placed after ‘F’ (to denote factor) and their activated forms are described with a lowercase ‘a’ next to the roman numerals e.g. FVIIa – denotes the activated coagulation factor VII and reads as ‘factor seven a’.

1.2.1 *Coagulation pathways*

Two distinct pathways of coagulation have been described based on how coagulation is initiated. The ‘TF pathway’ also known as the ‘extrinsic pathway’ is initiated when the activated coagulation factor VII (FVIIa) forms a complex with the TF that is exposed from the subendothelium to circulating blood due to injury (1). The ‘contact pathway’ also referred to as the ‘intrinsic pathway’ is initiated when coagulation factor XII (FXII) is autoactivated to FXIIa due to contact with artificial surfaces or negatively charged molecules, such as DNA, RNA or bacteria-released polyphosphates (7). FXIIa activates coagulation factor XI (FXI) that in turn activates coagulation factor IX (FIX) to participate in the generation of thrombin.

Around 1% of FVII circulates as FVIIa in plasma and it immediately forms a complex with TF upon exposure during injury or inflammation (8). TF is a glycoprotein that serves as a cofactor for FVIIa to activate circulating coagulation

factors X (FX), FIX and FVII (1). Activated coagulation factor X (FXa) sparks thrombin production by directly cleaving prothrombin to thrombin (9). Thrombin is central to the coagulation network, due to its capacity to self-regulate its production through the feedback activation of serine proteases FVII and FXI, the activation of cofactors coagulation factor VIII (FVIII) and factor V (FV) and the activation of an inhibitory serine protease protein C (10). FVIIa, FIXa, FXa, FXIa and FXIIa are the serine proteases of the coagulation cascade that can activate other enzymes through cleavage, while TF, FVa and FVIIIa are cofactors that promote the activity of serine proteases towards their substrates. FVa is the cofactor for the cleavage of prothrombin to thrombin by FXa, while FVIIIa is the cofactor for FIXa-induced activation of FX (11).

The success of hemostasis localized to the injury site should be attributed to an appropriate balance between the procoagulant reactions of the coagulation network and the endogenous inhibitors of the system. Tissue factor pathway inhibitor (TFPI) is a Kunitz-type inhibitor that circulates in plasma at a concentration of around 2.5 nM and is also present in platelets, endothelial cells and monocytes (12). TFPI binds to TF-FVIIa complex, FXa and the TF-FVIIa-FXa complex to impede the serine proteases from participating in thrombin generation (1). Antithrombin (ATIII) is a serine protease inhibitor that derives its name by its capacity to inhibit thrombin by binding to the active site of thrombin; however, it can also inhibit FVIIa, FXa, FIXa, FXIIa and FXIa. As such ATIII plays a major role as an inhibitor of activity and generation of thrombin (13). Unsurprisingly, one of the most commonly used anticoagulants – heparin, enhances the inhibitory action of antithrombin to curtail coagulation (14). Among the endogenous inhibitors, protein C requires activation to

activated protein C (APC) by thrombin bound to endothelial thrombomodulin. APC can inhibit FVa and FVIIIa, a mechanism that is enhanced by the cofactors protein S and FV (15). Together, these serine proteases, cofactors and inhibitors make up the coagulation network as depicted in (Figure 1.2).

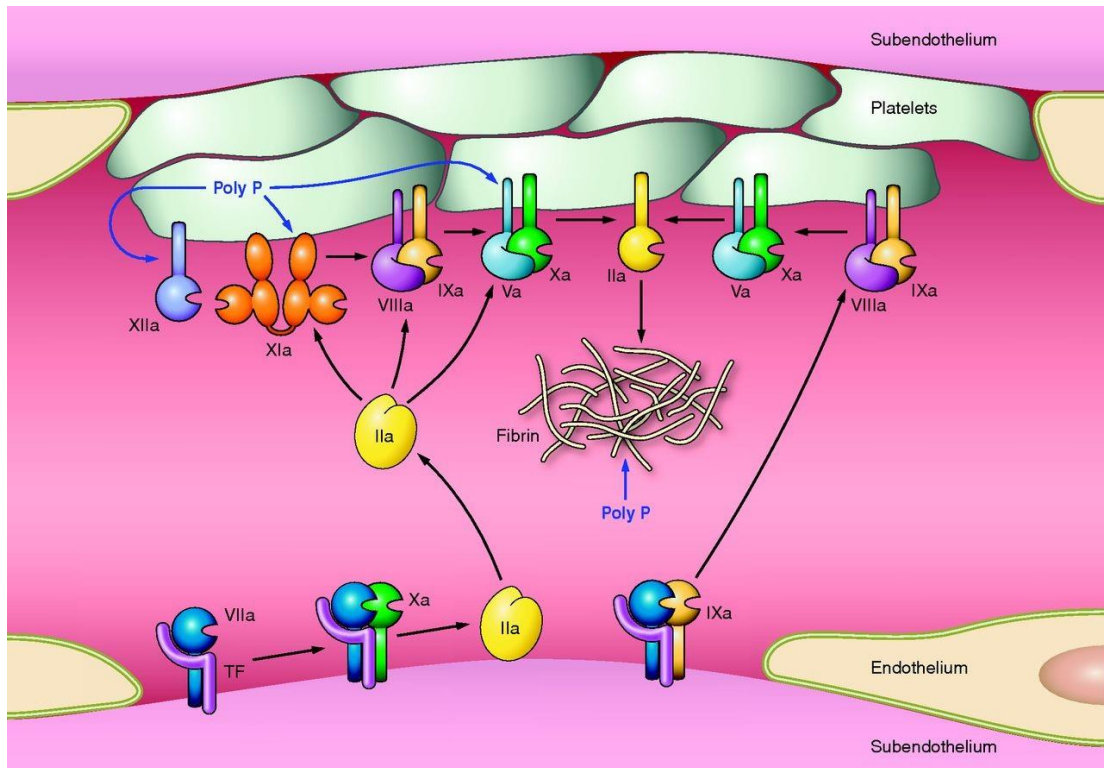


Figure 1.2 Coagulation network. The exposure of TF allows for the formation for TF-FVIIa complex that activates FX to FXa which activates prothrombin (FII) to thrombin (FIIa). Thrombin converts fibrinogen to fibrin that cements the platelet aggregate together. In addition, thrombin serves as a master regulator of the coagulation network by feedback activation of FXI, FVIII and FV to further its own production. Moreover, polyphosphates secreted by the activated platelets can serve as a cofactor to enhance several reactions involved in the network of reactions that lead to the generation of fibrin. Figure adapted from Versteeg et al. *Physiological Reviews* 2013, 93(1):327-358. Reprinted with permission from the publisher.

Disorders in the coagulation system may arise either due to deficiency or surplus in the levels of the coagulation factors or due to mutations that alter the enzymatic

activity of coagulation factors. For example, a lack or deficiency in FVIII or FIX, clinically referred to as hemophilia A or B respectively, can cause either spontaneous or post-traumatic bleeding. On the other hand, mutations in FV gene causes FV-Leiden that reduces the binding of the endogenous thrombin inhibitor APC to FV. As APC binding to FV is an essential step in regulating the activity of APC to inhibit thrombin generation and regulate coagulation, FV-Leiden is associated with hypercoagulability. While almost all cases of hemophilia are inherited, few patients may still acquire hemophilia due to autoantibodies developed against FVIII or FIX. Hemophilia C is a rare and relatively milder bleeding disorder due to the lack of or deficiency of FXI. Deficiencies in inhibitors such as protein C, ATIII and protein S or high plasma levels of procoagulant enzymes such as FXI, prothrombin, FX and FIX can cause thrombophilia (hypercoagulability) that could result in thrombosis. Deep vein thrombosis (DVT), arterial thrombosis, and cerebral thrombosis (stroke) are possible fatal outcomes associated with thrombophilia.

1.3 Platelets

Platelets, also known as ‘thrombocytes’, are anuclear cells that are formed as fragments of megakaryocytes, which are large cells derived from the bone marrow. Around 1 trillion platelets circulate in blood, which translates to roughly 150,000 – 450,000 platelets per microliter of blood, with an average lifespan of 7-10 days (16). As the cellular building blocks of a blood clot, platelets play a vital role in securing vascular integrity. Decrease in platelet count, usually < 150,000 per microliter, is clinically termed as ‘thrombocytopenia’ and is associated with internal bleeding (17).

In the following sections we will explore the fundamentals of platelet biology that are relevant to hemostasis and thrombosis.

1.4 Platelet receptors and signaling

Platelets survey the circulatory system in a discoid shape that denotes their resting state. Due to their relatively smaller size (2 μm) compared to red blood cells (10 μm), platelets are forced closer to the vessel walls during circulation – a phenomenon defined as margination that allows platelets to respond rapidly to a vascular injury (18). The recruitment of circulating platelets to a site of injury or inflammation involves: 1) initial adhesion, 2) activation and shape change governed by intracellular signaling events and 3) sustenance of activation through feedback activation by platelet granule secretion. The following sections will discuss the numerous platelet receptors that orchestrate the recruitment of platelets to respond to an injury or a site of endothelial damage.

1.4.1 GPIb and initial platelet adhesion

The initial adhesion of platelets to an injury site involves the binding of a receptor that is exclusive to platelets and megakaryocytes called glycoprotein (GP) Ib α to von Willebrand factor (vWF) bound to subendothelial collagen (19). vWF is produced by endothelial cells and megakaryocytes and is released into circulation in a globular form. At the site of injury, vWF binds to collagen to facilitate platelet recruitment to the injury. GPIb α is a transmembrane platelet receptor that is a major functional subunit of the GPIb-IX-V glycoprotein complex with more than 25,000-35,000

copies per platelet. GPIb β , GPIX and GPV are the three other subunits that form the GPIb-IX-V complex. The current body of evidence suggests that the activation of GPIb α by vWF initiates a sequence of signaling events that include the phosphorylation of Src family kinases (SFK), the effectors phospholipase C γ 2 (PLC γ 2), and phosphoinositide 3-kinase (PI3K), to increase intracellular Ca²⁺ levels and inside-out activation of integrin α IIb β 3 (20,21). The advent of proteomics could lead to more clarity in the signaling events that regulate the inside-out activation of platelets by GPIb. The binding of GPIb α to vWF is vital to hemostasis as defects in either the quantity or quality of GPIb α in humans has been associated with a congenital bleeding disorder called Bernard-Soulier syndrome (BSS) (22). Although primarily a vWF receptor, it is suggested that GPIb α can also interact with coagulation factors such as thrombin, FXI and FXII, and extracellular matrix (ECM) proteins such as thrombospondin and cell adhesion proteins such as P-selectin and integrins (23-25).

1.4.2 *GPVI-induced platelet activation*

Platelet binding to vWF has a fast off-rate that causes platelets to roll on the ECM surface. Although weak by itself to induce complete activation, the on-off binding of platelets to vWF establishes contact of platelets with one of the most abundant proteins of the ECM – collagen. Collagen binds to glycoprotein VI (GPVI) to activate platelets through immunoreceptor tyrosine-based activation motif (ITAM) signaling (26). GPVI is an immunoglobulin super family protein that serves as a transmembrane receptor for platelet activation. Although initially identified as a receptor for collagen, recent studies added a plethora of ECM proteins such as

laminin, fibrin, fibrinogen, fibronectin, vitronectin and nidogen to the list of ligands that can bind to and activate platelets through GPVI (27-29). Upon ligand binding, GPVI dimers cluster together to initiate the ITAM-mediated signaling cascade. The extent of clustering is proportional to the strength of the activation signal. Ligand binding to GPVI induces phosphorylation of the FcR γ -chain that leads to the phosphorylation of the tyrosine kinase Syk. This leads to the assembly of several kinases, adaptor and effector proteins, such as linker for activation of T-cells (LAT), PLC γ 2, and Bruton's tyrosine kinase (BTK), to form a signaling complex (signalosome). The phosphorylation of the effector protein PLC γ 2 induces the formation of inositol 1,4,5-triphosphate (IP $_3$) and 1,2-diacylglycerol (DAG) leading to the release of calcium (Ca $^{2+}$) from stores and the phosphorylation of protein kinase C (PKC). Eventually these molecular events result in the inside-out activation of platelets to release their granule content and activate the integrins α IIb β 3 to support platelet aggregation. However, the exact molecular events of the inside-out signaling cascade is still ill-defined.

1.4.3 *Role of PARs in platelet activation*

One of the many ways by which platelets and the coagulation network are connected is through the activation of platelets by thrombin generated in the coagulation network. Protease activated receptors (PARs) are transmembrane G-protein coupled receptors (GPCRs) named after their capacity to be cleaved by proteases to induce cell activation. Thrombin generated during coagulation is one of the major proteases that can cleave PAR1, PAR3 and PAR4 to induce intracellular signaling events that activate platelets (21). The cleavage of PAR1 and PAR4 by thrombin has been

studied the most as platelets express very low levels of PAR3 (30). Upon cleavage by thrombin, PAR1 and PAR4 recruit the G-proteins G_q and G_{12}/G_{13} to stimulate the formation of inositol triphosphate (IP3) and DAG, which increases the intracellular calcium levels, inducing shape change and granule content release in platelets. FXa and fibrinolytic plasmin can also cleave PARs to induce platelet activation, and in some cases platelet aggregation (31,32). Antagonists against PAR1 and PAR4 are actively being developed for clinical use as anti-platelet agents and vorapaxar, a PAR1 antagonist, is clinically used in the United States of America (USA) for reducing thrombotic events in patients with a history of cardiovascular diseases since 2014 (33).

1.4.4 *Integrins and platelet aggregation*

Aggregation of platelets is mediated through one of their highly expressed unique membrane receptors, integrin $\alpha IIb\beta 3$ (GPIIb-IIIa complex / CD41/CD61). In a resting state, $\alpha IIb\beta 3$ is expressed in a low affinity state characterized by a bent conformation with minimal capacity to bind ligands. However, the activation of platelets changes its conformation to increase the affinity of $\alpha IIb\beta 3$ towards its ligands such as fibrinogen, fibronectin, vitronectin, thrombospondin-1, and vWF (21). Ligand binding to $\alpha IIb\beta 3$ induces outside-in activation of platelets through Ras family of small Guanosine triphosphatases (GTPases) (34). Outside-in activation causes platelets to maintain or further the release of granule content and spreading. Inhibitors against the function of $\alpha IIb\beta 3$ such as abciximab, eptifibatide and tirofiban are frequently used in the clinic either to prevent or treat thrombosis (35-37). These

inhibitors inevitably increase the risk of bleeding as blocking integrins invariably affects platelet aggregation in both hemostasis and thrombosis.

$\alpha 2\beta 1$ (CD49b/CD29) is the second most important integrin found on platelet membranes that is established as a receptor for collagen (38). Similar to $\alpha \text{IIb}\beta 3$, $\alpha 2\beta 1$ needs to be activated to a high affinity state through inside-out signaling mechanisms before it can bind to its ligands. Information from humans with defects in $\alpha 2\beta 1$ is not sufficient to make conclusions on the relevance of this receptor towards hemostasis and thrombosis. The other platelet integrins that share similar signaling mechanisms to $\alpha \text{IIb}\beta 3$ are: $\alpha \text{v}\beta 3$ (CD51/CD61) the receptor for vitronectin and collagen, $\alpha 5\beta 1$ (CD49e/CD29) the fibronectin receptor, and $\alpha 6\beta 1$ (CD49f/CD29) the laminin receptor (39).

1.4.5 *P2Y receptors and feedback activation*

P2Y receptors are transmembrane proteins of molecular mass 40-50 kDa that belong to the class of GPCRs (40). Human platelets express P2Y₁ and P2Y₁₂ that are coupled to G proteins G_q and G_i, respectively. Activated platelets secrete their granules containing molecules, such as ADP, that can feedback to promote platelet activation and aggregation by binding to the P2Y receptors (21). The binding of ADP to P2Y₁ activates the PLC β to induce the formation of IP3, which increases intracellular calcium levels. The rise in Ca²⁺ levels activates the integrin $\alpha \text{IIb}\beta 3$ through inside-out signaling causing platelet aggregation. P2Y₁₂ activation by ADP results in the activation of PI3K which activates integrins into the high affinity state, inducing shape change through the phosphorylation of protein kinase B (PKB), also known as

Akt (41). Although feedback activation of P2Y₁ and P2Y₁₂ by ADP is weak by itself to induce robust activation and granule secretion, it is critical to the growth of a thrombus or a hemostatic plug. While patients and mice lacking functional P2Y₁₂ receptors exhibit prolonged bleeding times, P2Y₁₂ antagonists clopidogrel, ticlopidine, ticagrelor, prasugrel and cangrelor are frequently used in clinics in the USA as antiplatelet agents to prevent or treat thrombotic disorders (42). **Figure 1.3** is a depiction of major platelet receptors and signaling proteins associated with them in the activation of platelets and secretion of platelet granules.

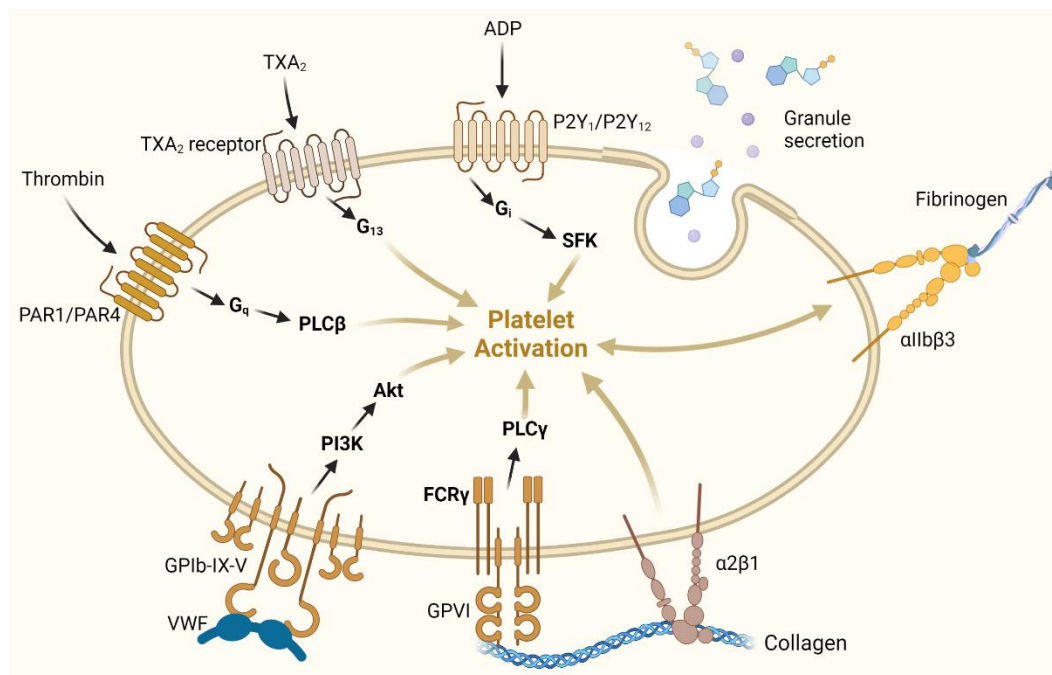


Figure 1.3 Platelet signaling. Activation of platelet receptors by ECM proteins and soluble agonists instigates a series of downstream signaling events including the phosphorylation of proteins that result in the activation of platelets, secretion of granules and cytoskeletal rearrangements. Figure created with Biorender.com © Hari Hara Sudhan Lakshmanan

1.5 ECM proteins – Platform for hemostasis and thrombosis

Blood vessels are lined with endothelial cells that are supported by the sub-endothelium containing the sheets of ECM protein that create the basement membrane (**Figure 1.4**). An injury or an increase in permeability of the endothelial layer exposes the ECM proteins to blood, specifically to coagulation proteins and platelets. ECM is made up of fibrillar proteins and glycosaminoglycans that provide support to the blood vessel structure and serve as ligands to activate major proteins and receptors involved in hemostasis and thrombosis (43).

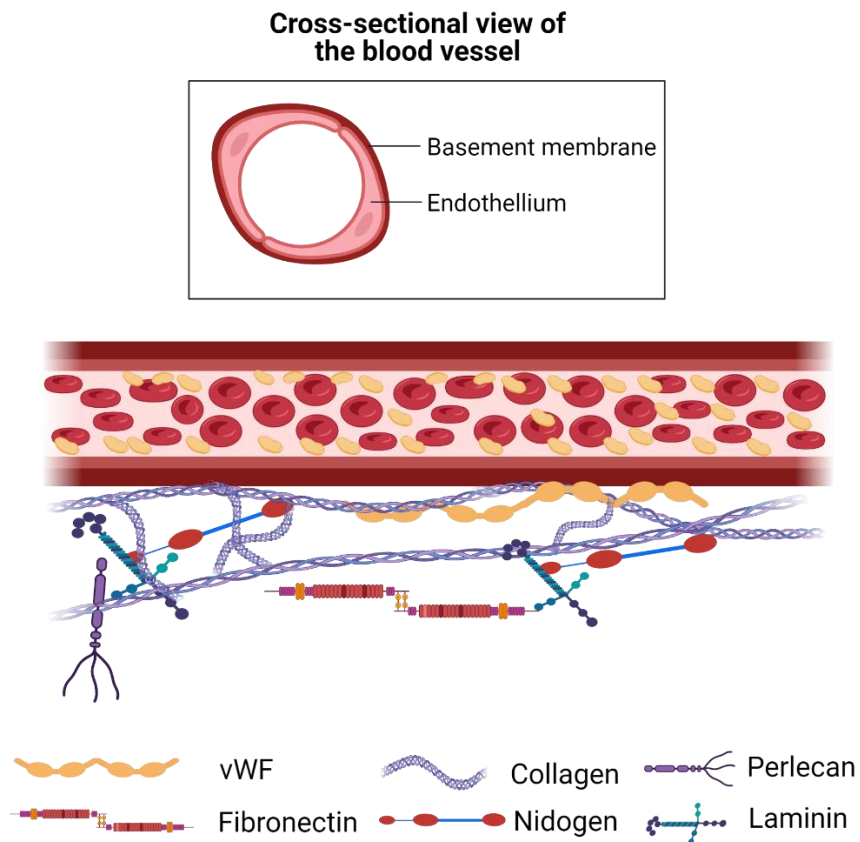


Figure 1.4 Extracellular matrix proteins. The subendothelium is lined with a thin sheet of glycoproteins such as the collagens, laminins, nidogens, fibronectin, vWF and perlecans. The ECM provides stability and support to the endothelial cells that make up the vasculature. Figure created with Biorender.com ©Hari Hara Sudhan Lakshmanan

1.5.1 *von Willebrand factor (vWF)*

vWF is a multimeric glycoprotein present in the ECM and circulates in plasma in complex with FVIII. In addition, vWF is stored in platelet α granules and released from damaged endothelial cells. The molecular mass of vWF ranges from 500 to 20,000 kDa based on the number of subunits that comprise the protein (44). The multimeric units of vWF are cleaved by a plasma metalloprotease known as “a disintegrin and metalloprotease with thrombospondin type motifs 13 (ADAMTS13)”. Deficiency in ADAMTS13 has been associated with microvessel occlusion due to thrombus formation clinically termed as thrombotic thrombocytopenic purpura (45). Upon injury, the shear forces in circulation unfold vWF to expose the GPIIb/IIIa-binding A1 domain to platelets. The catch-and-release fashion of the bonds between platelets and vWF causes platelets to roll and tether before finally coming to rest following complete activation provided by other ECM proteins such as collagen. vWF binds to fibrillar collagen through the A1 and A3 domains to form a bridge between platelets and collagen during aggregation (46). The initial attachment of platelets to vWF is critical to the formation of hemostatic plugs under arterial shear ($> 1000 \text{ s}^{-1}$) and is modestly involved under venous shear ($< 500 \text{ s}^{-1}$) conditions (18).

1.5.2 *Collagen*

Collagen is a triple helical structural protein of the ECM made up of polypeptide chains coiled together. Type I collagen is the predominant form of collagen among the 28 known subtypes of collagen (47). While type IV collagen is exposed in superficial injuries, type I and III are found in the deeper layers of the ECM and are

exposed mostly under serious injuries. As the most abundant fibrous protein present in the ECM, collagen participates in both coagulation and platelet activation.

Collagen can activate FXII to FXIIa to trigger the contact pathway of coagulation and activate platelets through the receptors GPVI and $\alpha 2\beta 1$ (26).

1.5.3 *Laminin*

Laminin is an approximately 800 kDa heterotrimeric glycoprotein, composed of α , β , and γ chains coiled together, that provides structural support to the basement membrane along with the nidogens and collagens. Laminins 8 and 10 are found in the sub-endothelium while platelets store laminins 8, 10, and 11 in their granules (43).

Laminin was the first non-collagenous protein discovered with the capacity to stimulate GPVI (29). Studies in mice and humans suggests that integrin $\alpha 6\beta 1$ mediates the adhesion of platelets to laminin.

1.5.4 *Nidogen*

Nidogen, also known as entactin, is a 150 kDa sulfated glycoprotein with three globular domains that non-covalently links collagens, perlecan and laminins together providing a structural framework to the ECM. In addition, nidogen is stored in platelet granules and is released upon activation (48). So far, two types of nidogen, nidogen-1 and nidogen-2, have been identified in humans and other mammals.

Attempts at understanding the physiological relevance of nidogens in mice revealed that knocking out either nidogen-1 or nidogen-2 was non-lethal and did not alter birth and development (49). However, abrogation of both nidogen-1 and nidogen-2 resulted in death of mice at birth with defects identified in the development of the

heart, lung and limbs. While the physiological significance of nidogen-1 and nidogen-2 remains unclear, *in vitro* studies presented in this dissertation suggest a plausible role for nidogen-1 in hemostasis and thrombosis due to its capacity to activate platelets and support platelet adhesion.

1.5.5 *Other ECM proteins with plausible roles in hemostasis and thrombosis*

Fibronectin, thrombospondin and vitronectin are some of the other proteins of the ECM that have been identified so far as ligands for platelet receptors. Fibronectin is a ligand for two integrins, α IIb β 3 and α 5 β 1, and can support the spreading of platelets (50). In addition, fibronectin secreted by hepatocytes circulates in plasma and may play a vital role in providing stability to thrombus in microvasculature according to studies conducted in mice (51). Thrombospondin is another constituent of the ECM that also circulates in plasma and is stored in the α -granules of the platelets. Thrombospondin binds to activated platelet surface and potentiates the aggregation of platelets induced by thrombin or ADP or fibrinogen (52-54).

1.6 Platelet granule secretion

Platelets contain several organic and inorganic molecules stored in three different types of granules: α -granules, dense granules and lysosomes. Some of these granules include coagulation factors, ECM proteins, nucleotides, divalent cations, polyphosphates and membrane-associated receptors that are vital to promote and sustain platelet activation (55). While granule formation starts in megakaryocytes,

circulating platelets continue to endocytose proteins and microparticles to be stored in granules. The type, amount and the rate of granule content release has been observed to vary based on the strength and length of stimulation, however, the precise details on the regulation of granule release is still unclear.

Each platelet contains about 50-80 α -granules that occupy an average of 14 μm^2 area of the platelet. Some of the important proteins and molecules inside of α -granules that are involved in coagulation and platelet activation include FV, FIX, FXIII, ATIII, protein S, TFPI, plasminogen, fibrinogen, vWF, nidogen, laminin, vitronectin, fibronectin, GPIb α , GPVI, α IIB β 3 and P-selectin (56). While some of these proteins can be found on the surface of resting platelets, P-selectin (CD62P) is translocated to the platelet membrane surface only upon robust platelet activation. P-selectin enables the adhesion of platelets to leukocytes and endothelial cells, in addition to being suggested as an additional receptor for platelet-platelet aggregation (57).

Platelet dense granules, also called as δ -granules, are primarily composed of nucleotides, inorganic molecules such as polyphosphates, divalent cations such as Ca^{2+} and bioactive amines that include serotonin (58). Among these, ADP and polyphosphates are important players in platelet activation and coagulation, respectively. ADP released by platelets induces activation of platelets through P_2Y receptors – a feedback mechanism that is vital to sustain and promote activation and aggregation of platelets in a hemostatic plug or a thrombus (59). Polyphosphates released by platelets are usually shorter than 100 units of phosphates and are termed as short-chain PolyP. These polyphosphates have been shown to accelerate the activation of FV by thrombin, FXa, and FXIa, enhance the cleavage of TFPI by FXIa,

enhance the activation of FXI by thrombin and weakly activate FXII to instigate the contact pathway of coagulation (60). Recent discoveries on the potentially vital role of platelet- PolyP have led to the development of nontoxic PolyP inhibitors as novel antithrombotics that promise to be safer than the current standard of care (61).

Lysosomes are the least understood category of the platelet granules that comprise acid proteases and glycohydrolases such as collagenase and heparinase (55).

Lysosomes are generally observed to be in much smaller concentrations than the other two types of granules and the current understanding of platelet lysosomes is insufficient to associate this category of granules with hemostasis and thrombosis.

Recent discoveries of the involvement of the transcription factor nuclear factor-kappa B (NF- κ B) in granule release have stimulated research towards understanding the intricate mechanisms behind platelet activation. The presence of NF- κ B, a protein that lies at the heart of inflammatory responses in immune cells, in platelets was discovered by Liu et al. in 2002 and led to the paradigm shift in understanding platelet functions beyond hemostasis and thrombosis (62). As observed in other cells, NF- κ B is generally kept in an inactivated state by its complex formation with the inhibitory protein I-kappa B (I κ B). ECM proteins such as thrombin, collagen and nidogen can initiate the intracellular signals that causes phosphorylation of I κ B by I κ B kinase (IKK) in platelets. Phosphorylated I κ B degrades and exposes active NF- κ B to participate in granule secretion. In addition, inhibition of NF- κ B activation has been shown to affect platelet spreading and thrombus stability suggesting non-classical roles for the nuclear transcription factor in platelets (63). It is vital to study the mechanisms through which NF- κ B is involved in platelet activation and

degranulation as it could have major implications in the treatment of autoimmune disorders.

Advances in microscopy techniques such as super resolution microscopy and electron microscopy have spurred our interests in understanding the location and content of platelet granules. However, there remains much to be discovered in terms of the physiological and pathological importance of the granule content and its release kinetics. Understanding the biology of granule endocytosis and release could potentially aid in the development of safer antithrombotics, novel diagnostics, and even the creation of synthetic platelets (64).

1.7 Platelets in coagulation

The surface of activated platelets can greatly accelerate the reactions of the coagulation network. On the other hand, products of the coagulation network such as thrombin can induce robust platelet activation and aggregation. In addition, activated platelets can secrete coagulation factors and coagulation inhibitors from their granules to influence coagulation. Thus, both the coagulation network and platelets work hand-in-hand in the construction of a blood clot.

In resting platelets, the anionic phospholipid called phosphatidylserine (PS) is in the inner monolayer of the membrane while phosphatidylcholine and sphingomyelin are present in the outer monolayer of the platelet membrane (65). Upon platelet activation, PS is exposed on the platelet membrane surface allowing for several coagulation proteases to assemble on the negatively charged PS surface.

Fluorescently tagged annexin V is routinely used to assess PS exposure on platelets

by flow cytometry as a way of establishing the procoagulant capacity of platelets (66). Annexin V binding to platelet PS surface is a way of regulating coagulation as antibody-mediated destruction of annexin V can lead to a procoagulant phenotype that is commonly associated with anti-phospholipid syndrome, an autoimmune disorder. The exposure of PS is vital to coagulation *in vivo*, as evidenced by the bleeding diathesis associated with platelets deficient of PS exposure in Scott syndrome (67). The activation of FX by the FIXa-FVIIIa complex and the activation of prothrombin by the FXa-FVa complex are the major reactions of the coagulation network that have been identified to be accelerated by PS exposed on the platelet surface (68). Besides, platelet receptors may even offer protection from inhibition to coagulation proteases through receptor binding (69). On the other hand, platelet releasates, such as protease nexin – 2 (PN-2), can inhibit serine protease FXIa by acting as an anticoagulant (70). **Figure 1.5** is a simplified representation of the interplay between platelets and coagulation. Thrombin activates platelets and in turn platelets catalyze the reactions involved in the generation of thrombin.

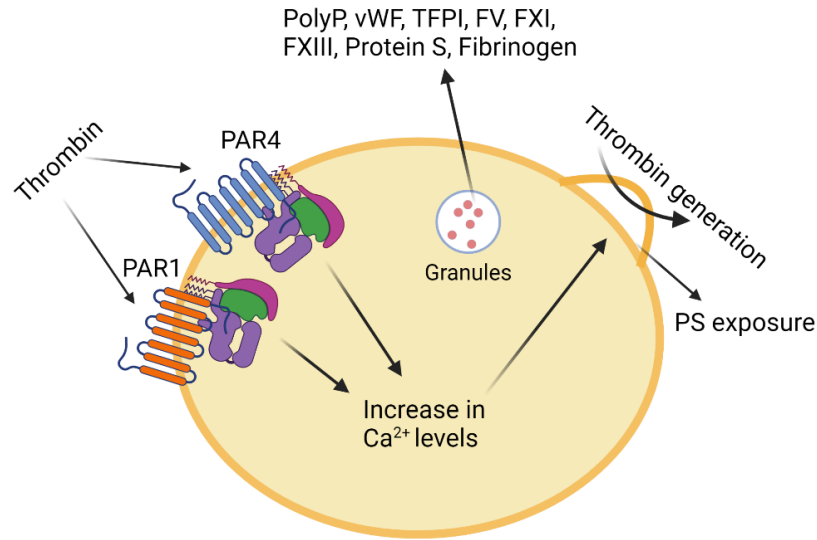


Figure 1.5. Platelets in coagulation. Thrombin induced platelet activation through PAR1 and PAR4 leads to phosphatidylserine (PS) exposure that enhances coagulation. Furthermore, PolyP secreted by platelets can also promote coagulation. Figure created with Biorender.com ©Hari Hara Sudhan Lakshmanan

1.8 Physics of hemostasis and thrombosis

Platelets and fibrin are the essential building blocks of both a hemostatic plug and a thrombus. While the activation of platelets and the activity of enzymes at the sites of injury is subject to biology, the quantity of cells and enzymes available for the formation and growth of a platelet-fibrin aggregate are subject to the physics of flow around the injury. Flow can determine the kinetics of clot formation by controlling the transport rates of proteins and platelets to the sites of injury or inflammation.

1.8.1 *Blood rheology*

Flow of viscous fluids such as blood is conventionally described as a collection of layers of fluids sliding past one another. The flow is called ‘laminar’ when the

adjacent layers glide smoothly past each other along the axis of the vessel, and ‘turbulent’ when there is chaotic movement and mixing between the layers. The layers adjacent to the wall of the vessel experience the maximum resistance to flow in the form of frictional shear stress offered by the stationary vessel walls. This leads to ‘zero velocity’ at the wall that is often termed as the ‘no-slip’ boundary condition meaning the layer closest to the wall is stuck to the wall and does not have a velocity of its own. (71). The resistance offered by the wall creates a gradient in blood velocity across the radial direction of the vessel with $v = 0$ at the walls and $v = v_{max}$ at the center of the vessel where the shear stress is zero (**Figure 1.6**). The velocity gradient across the cross-section of the vessel, dv/dr , is termed as the shear rate denoted by ‘ γ ’ with the unit of s^{-1} . The ratio of shear stress to shear rate defines the capacity of a fluid to transfer momentum across layers measured by a fluid property called ‘viscosity’ denoted by ‘ μ ’ with the units of Pa s (pascal second). Lower the viscosity, larger the velocity gradient as it is more difficult to transport momentum across fluid layers. Newton’s law of viscosity states that the shear stress applied on the fluid is directly proportional to the gradient of velocity with the viscosity as the constant of proportionality. The following equation is the mathematical description of the law,

$$\tau = \mu \frac{dv}{dr}; r - \text{radius of vessel}$$

$$\tau = \text{Shear stress, } \frac{dv}{dr} = \text{Velocity gradient, } \mu = \text{Viscosity}$$

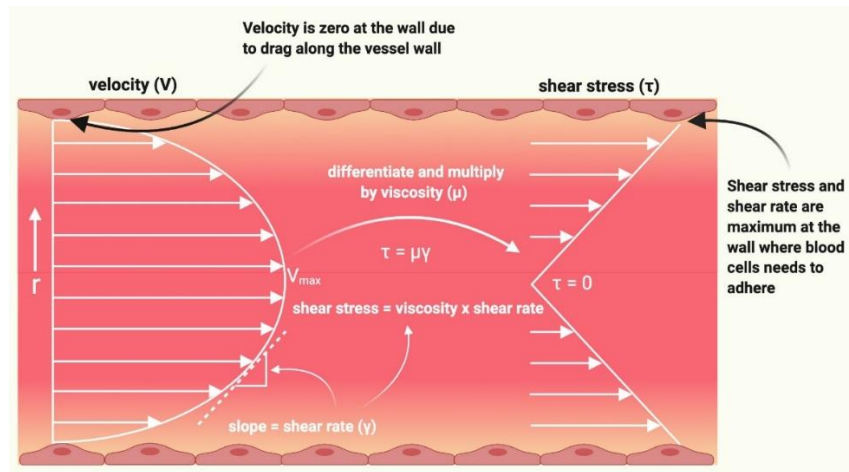


Figure 1.6 Velocity and shear stress in laminar flow. Figure adapted from Lin et al. (2021) originally published in *Res Pract Thromb Haemost* (Lin 2021). Reprinted under the CC BY-NC-ND 4.0 license.

Fluids that obey the Newton's law of viscosity with a constant viscosity that is independent of the shear stress applied on the fluid and are called 'Newtonian'. If the viscosity of the fluid changes with the amount or period of applied shear stress it is called 'non-Newtonian'. Blood is a non-Newtonian fluid, although under shear rates $> 100 \text{ s}^{-1}$ it behaves like a Newtonian fluid with a constant viscosity of approximately 3 mPa.s (milli Pascal seconds). For comparison, blood is at least thrice as viscous as water ($\mu = 1 \text{ mPa.s}$) and 50 times thinner than engine oil ($\mu = 200 \text{ mPa.s}$) (72). In addition, the viscosity of blood is directly proportional to the percentage of red blood cells often termed as 'hematocrit'. The average hematocrit is estimated to be from 40% to 50% in males and 36% to 48% in females (73).

1.8.1.1 Hagen-Poiseuille's equation

The flow rate of the blood through the circulatory system can be estimated using the Hagen Poiseuille's equation which relates flow rate as a function of the pressure drop

across the length of the blood vessel, the cross-sectional area of the vessel and the viscosity of blood as described by the following equation:

$$Q = \frac{\Delta P A^2}{8\pi\mu L}$$

Q – flow rate, ΔP – pressure drop, A – cross sectional area, μ – viscosity and

L – length of the vessel

This equation applies for incompressible (fluids with a constant density) Newtonian fluids – a valid assumption that results in very small error for blood under high shear rate (18). The average blood velocity is the ratio of the flow rate to the cross-sectional area, $\frac{Q}{A} = \frac{Q}{\pi r^2}$, where r – is the radius of the vessel.

1.8.2 *Convection and diffusion*

Blood contains water, proteins, red blood cells, platelets and other cells. Although the bulk of blood is moving at a rate dictated by the pressure gradient across the vessel, individual protein molecules and cells move at velocities that also depend on their concentration gradient. The phenomenon of bulk motion driven by pressure is called convection and the molecular motion driven by concentration is referred to as the diffusion. Similar to viscosity, diffusivity is the experimentally measured property of a protein molecule that defines the rate at which a molecule or cell can diffuse through the medium (74). Based on flow conditions either convection or diffusion can dominate as the primary mechanism of transport

where the slower of the two dictates the overall rate of transport and is often termed as the ‘rate limiting step’.

1.8.3 *Dimensionless numbers*

Blood vessels range in sizes from 5 μm to 1.5 cm with blood flow velocities ranging from 0.03 to 40 cm s^{-1} (75). Dimensional analysis of hemodynamics through dimensionless numbers that relate various forces that drive transport can aid in the understanding of the rate limiting steps in the development of a hemostatic plug or thrombus. In addition, it also helps in the design of *in vitro*, *in vivo* and *in silico* models to study clotting under (patho)physiologically relevant conditions and later in the translation of the knowledge to the clinic.

1.8.3.1 *Reynolds number – laminar and turbulent flow*

For a given flow rate, laminar or turbulent flow is determined by the ratio of inertial and viscous forces present in the flow. Reynold’s number (Re) is the ratio of the inertial to viscous forces that are available during the flow of a liquid inside the blood vessel (76). Re is a function of vessel diameter, velocity, density and viscosity represented by the following equation,

$$Re = \frac{Dv\rho}{\mu}$$

D – diameter, v – velocity, ρ – density and μ – viscosity

Based on empirical observations, for Re lower < 2000 the flow is generally laminar and for $Re > 4000$ the flow is turbulent where inertial forces dominate leading to mixing between layers and chaotic flow. Between 2000-4000, the flow can be either laminar or turbulent, based on other factors involved in the flow. Re normally ranges from 0.01-5000 in the human circulatory system (77).

1.8.3.2 Péclet number – convective and diffusive transport

Péclet number (Pe) is the ratio of velocity of convective transport to that of diffusive transport of a molecule per unit area. Physiologically, convection dominates as the primary mechanism of protein transport and $Pe \gg 1$. However, during the formation of a hemostatic plug the transport of coagulation factors and soluble platelet agonists can be expected to be dominated by diffusion based on the architecture of the aggregate, thus leading to $Pe < 1$ (78). Pe for a biomolecule ‘ i ’ is mathematically described as follows,

$$Pe_i = \frac{\text{convective velocity per unit area}}{\text{diffusive velocity per unit area}} = \frac{v d}{D_i}$$

D_i – Diffusivity of molecule ‘ i ’, v – bulk flow velocity, d – vessel diameter

1.9 Platelets, coagulation and flow

The formation of a platelet-fibrin aggregate is the culmination of numerous biochemical reactions of the coagulation network that are catalyzed by platelet surfaces and constrained by flow. Hemodynamics can determine the kinetics of reactions involved in coagulation by limiting the transport rate of coagulant enzymes,

cofactors and inhibitors to the site of thrombosis or hemostasis. Additionally, flow can also directly influence platelets through shear-dependent activation and aggregation independent of soluble agonists such as thrombin, ADP or thromboxane.

Atherosclerosis is the buildup of plaque in the sub endothelium that leads to vascular stenosis, defined as the narrowing of the blood vessel (79). Stenosis creates a throat in the vessel that has a growing constriction and an expansion upstream and downstream of the stenotic region respectively as shown in **Figure 1.7**.

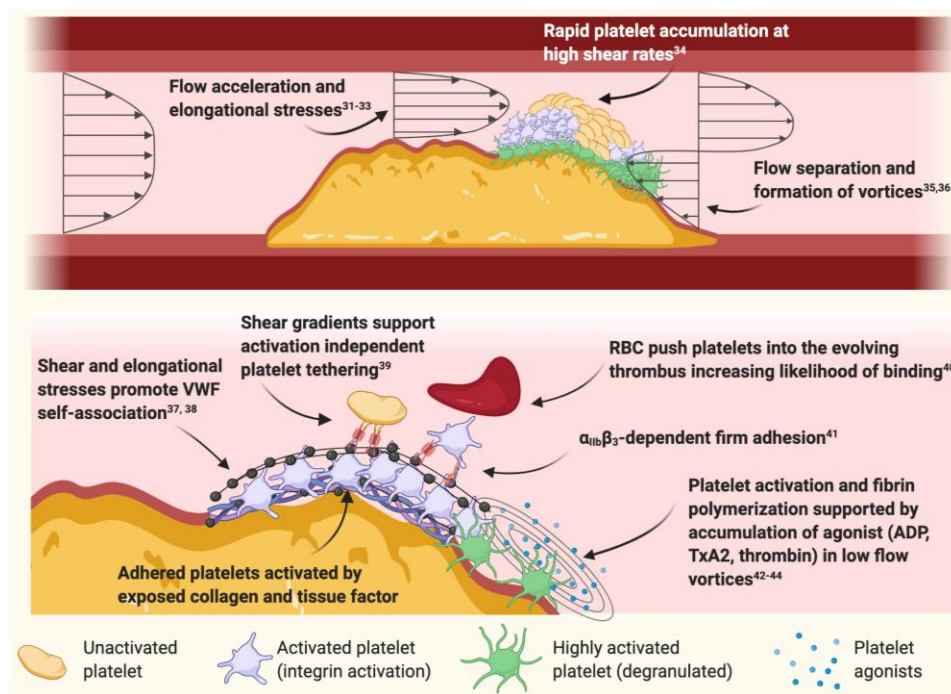


Figure 1.7 Thrombus formation in atherosclerosis. Atherosclerotic plaque growth narrows the vessel and causes acceleration in flow around the constricted region. Distal to the stenosis, flow decelerates rapidly leading to the formation of vortices and recirculation zones. In addition, rapid changes in shear around the stenotic region creates high shear gradients that causes vWF unfolding and platelet aggregation. Figure adapted from Lin et al. (2021) originally published in *Res Pract Thromb Haemost* (Lin 2021). Reprinted under the CC BY-NC-ND 4.0 license.

The reduction in cross-sectional area leads to a rapid increase in velocity and shear rate around the upstream region of the stenosis. The maximum shear rate on the surface of an atherosclerotic plaque can reach up to $40,000 \text{ s}^{-1}$, which is 40 times the physiological shear rate in arteries (72). The shear gradient established around the stenotic region may trigger platelet aggregation in a GPIIb/IIIa-dependent manner, which was discovered by Nesbitt et al. using microfluidic devices *in vitro* (80).

Interestingly, the shear-dependent platelet aggregation may be reversible and not even require platelet activation, degranulation or shape change. Moreover, high shear stress can unfold soluble vWF to serve as an additional mechanism of platelet activation in pathology. The rapid expansion that follows the stenotic throat creates turbulence resulting in recirculation zones and eddies distal to the stenotic throat. Simulation and experiments have shown that the platelets and the plasma proteins trapped under these recirculation zones can potentially lead to microaggregates in circulation that may block microvascular flow (81).

The effect of hemodynamics on thrombus formation is evident from the comparison of thrombi formed *in vivo* in arteries and veins. Arterial thrombi formed under high flow velocities tend to be richer in platelets, while venous thrombi are primarily composed of red cells and fibrin (18). This can be explained due to the difference in flow velocities and shear rates between arteries and veins. High shear rate environments enhance the margination of platelets towards the vascular wall, thereby increasing the near-wall concentration of platelets, and thus could be a reason for platelet-rich thrombi in arteries (82). In addition, pathological shear rates in arteries can be much higher than in veins and can induce platelet aggregation by itself, contributing to the high percentage of platelets observed in arterial thrombi. In

contrast, low velocities in veins lead to lower concentration of platelets near the wall and possibly less flow-induced activation (6).

The coagulation network contains numerous enzymatic steps of various timescales that culminates in the generation of thrombin. Likewise, platelets comprise several receptors that can induce activation based on the strength and period of stimulation by an agonist. While these may seem redundant at first glance, perhaps the complexity and redundancy are shaped by the distinct fluid dynamic environments of the arteries and veins. Profound implications of flow on hemostasis and thrombosis suggests that understanding the interplay between the biophysics and biochemistry of thrombus formation holds potential to unlock disease and patient specific treatment strategies. **Figure 1.8** illustrates the molecular and cellular events with an emphasis on the role of platelets and flow in the formation of a hemostatic plug.

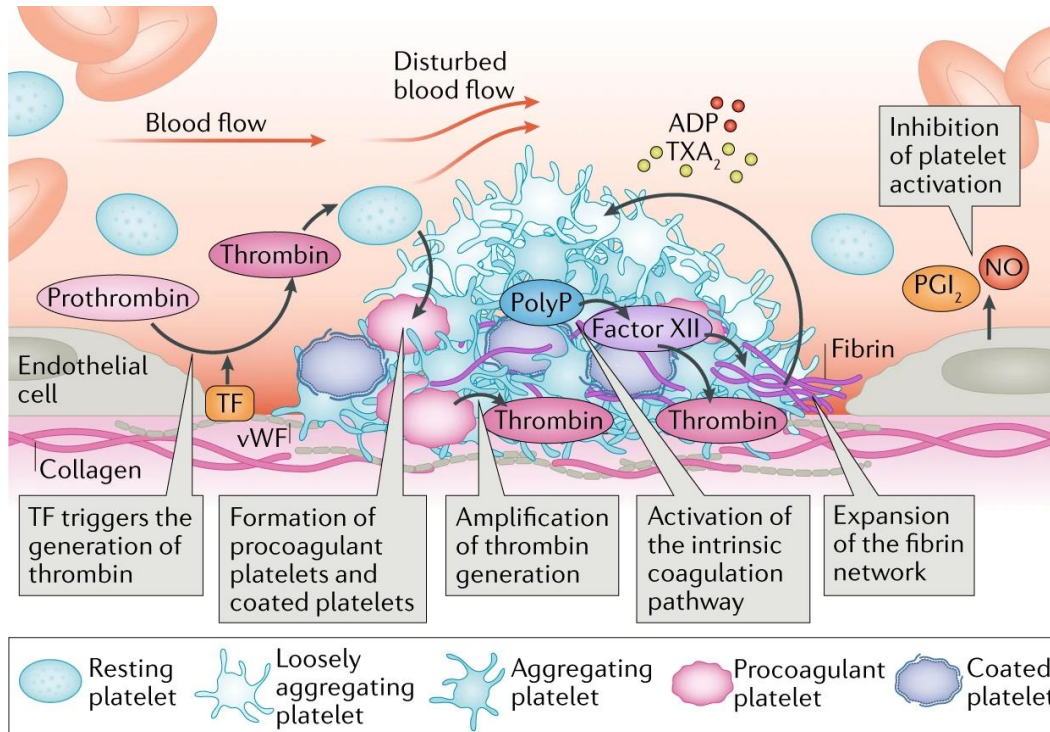


Figure 1.8. Multiscale events of hemostasis and thrombosis. Biochemical reactions triggered during coagulation result in the generation of thrombin that activates resting platelets to become procoagulant (PS exposing) and cleaves fibrinogen to fibrin for the formation of a platelet-fibrin clot. Procoagulant platelets coated with fibrin can catalyze the surface reactions involved in thrombin generation. The ECM proteins also activate the platelets to a loosely aggregating or a procoagulant state based on the strength of stimulation. Activated platelets secrete ADP and TXA₂ to activate the circulating platelets and secrete polyphosphates (PolyP) to enhance coagulation. Healthy endothelial cells secrete prostacyclin (PGI₂) and nitric oxide (NO) to inhibit platelet activation. Figure adapted from van der Meijden et al. *Nat Rev Cardiol* 2019; 16:166-179. Reprinted with permission from the publisher.

1.10 Thesis Overview

The molecular and cellular events that influence hemostasis and thrombosis range from the reactions of the coagulation network to the activation of platelets governed by the shear forces of blood flow. This thesis presents the results of research aimed at understanding the biochemical reactions of the coagulation network, the activation of

platelets by ECM proteins and the role of vascular geometry and flow in regulating hemostasis and thrombosis.

The generation of thrombin is an essential step in hemostasis and thrombosis due to the multifarious roles thrombin plays in regulating the activation of coagulation factors as well as platelets. In Chapter 3, the contribution of FXI towards TF-mediated thrombin generation is analyzed by using an integrative approach that involves an ordinary differential equation (ODE)-based model of thrombin generation and *in vitro* thrombin generation experiments. The ODE model, developed as a part of this study, enables the temporal analysis of the reactions in the coagulation network and their impacts on the generation of thrombin.

Platelets are anchored to the site of injury through the interactions of their receptors with the ECM proteins. The two major components of the ECM collagen and laminin are linked together by the globular proteins nidogen-1 and nidogen-2. While it is established that both collagen and laminin can activate platelets through GPVI and support platelet adhesion, in Chapter 4 we present experimental evidence to demonstrate that nidogen-1 could support platelet adhesion and activate platelets through GPVI and $\beta 1$ integrin.

Flow is an important mediator of platelet and protein transport that connects the microscopic and macroscopic scale of events that occur during hemostasis and thrombosis through diffusion and convection. In addition, shear rates can cause platelet activation and aggregation independent of biochemical agonists. Chapter 5 describes the development of a polymer-based microfluidic device that models the

extravascular clot formation with an injury channel and a blood channel to represent hemostatic plug formation. The preliminary data from the device suggests that it holds potential to be used in interrogating the role of flow in hemostasis and in the preclinical evaluation of bleeding risk associated with novel drugs.

Due to their small diameters, microvessels such as arterioles and capillaries offer the most resistance to blood flow that is increased further when a growing thrombus reduces the vessel diameter. To understand the role of evolving geometry during thrombus formation, in Chapter 6, a first principles-based mathematical model was developed to estimate the dynamic change in shear rate on the thrombus surface as it grows to alter the geometry of the microvasculature. Analysis of the microvascular geometry using these models indicates that the ratios of diameters by which the microvessels bifurcate into smaller vessels may determine the occlusive scenario of a thrombus. In addition, the model also holds potential to be used in the design and analysis of microfluidic oxygen transfer devices.

Chapter 2. Materials and Methods

2.1 Ethical Considerations

Human whole blood for the studies were obtained from healthy volunteers with consent in accordance with an Oregon Health & Science University (OHSU) Institutional Review Board (IRB)-approved protocol.

2.2 Common reagents

Collagen was from Chrono-Log (Havertown, PA). Collagen-related peptide (CRP) was from R. Farndale (Cambridge University, UK). Hanks' Balanced Salt Solution (HBSS) was from Corning cellgro (Manassas, VA, USA). Prostacyclin (PGI₂) was from Cayman Chemical (Ann Arbor, MI, USA). All other reagents were from Sigma, unless specified otherwise.

2.3 Human blood collection

Human blood was collected via venipuncture from healthy volunteers above the age of 18 who had been free of aspirin or ibuprofen for at least two weeks prior to the donation. Syringes with trisodium citrate (NaCit; 0.38% w/v; Sigma-Aldrich, St Louis, MO) were used to collect blood directly from the veins in the ratio of 9:1 (blood:citrate). All blood was used for experiments within 2 hours of collection.

2.4 Platelet isolation

Washed platelets were prepared from human blood drawn into a syringe containing 3.8% sodium citrate in the volume ratio of 9:1 (blood:citrate). Acid-citrate-dextrose buffer (ACD) was added at 1:10 (volume of ACD:volume of blood). Platelet-rich plasma (PRP) was prepared by centrifuging the mixture of ACD and blood at $200\times g$ at room temperature for 20 minutes. PGI₂ at 0.1 $\mu\text{g/ml}$ was added to PRP before centrifugation at $1000\times g$ for 10 minutes to obtain a platelet pellet. Platelets from the pellet were resuspended into modified HEPES/Tyrode buffer (129 mM NaCl, 0.34 mM Na₂HPO₄, 2.9 mM KCl, 12 mM NaHCO₃, 20 mM HEPES, 1 mM MgCl₂, pH 7.3, supplemented with 5 mM glucose). Resuspended platelets were centrifuged again at $1000\times g$ for 10 minutes before resuspension again into modified HEPES/Tyrode buffer to obtain the necessary platelet count.

2.5 *In vitro* platelet spreading studies

Circular glass coverslips of 12 mm diameter #1.5 thickness (0.16 to 0.19 mm) were placed in wells, coated with desired proteins for 1 hour at room temperature, washed 3 times with phosphate buffered saline (PBS), blocked with 5 mg/ml denatured bovine serum albumin (BSA) for 1 hour at room temperature, and washed with PBS. Washed platelets in solution with vehicle or specified inhibitors were added to the coverslip surface and incubated at 37⁰C for 45 minutes. Coverslips were then washed 3 times with PBS to remove unadhered platelets before fixing with 4% paraformaldehyde (PFA) for 15 minutes at room temperature and stained with phalloidin to detect actin filaments and other fluorescent antibodies against proteins

of interest. Coverslips were then mounted onto glass slides and stored at 4⁰C for imaging and analysis by differential interference contrast (DIC) and immunofluorescence microscopy.

2.6 Microscopy

2.6.1 General protocol

Köhler-illuminated Nomarski DIC optics with a Zeiss 63× magnification oil immersion lens (numerical aperture 1.4) was used to image the coverslips. Zeiss Axiocam MRc5 camera operated using Slidebook 5.5 software (Intelligent Imaging Innovations, Denver, CO) was used to capture images.

2.6.2 Image analysis

Platelets were outlined manually to compute the surface area and number of adherent platelets per field of view using ImageJ. The total area of the field of view was 14,587 μm².

2.7 Statistical analysis

Experimental data are represented as mean ± standard error of the means (SEM), unless noted otherwise. Experiments were repeated at least 3 times for each condition. For image analysis, 3 random fields of view are captured, analyzed and averaged for each condition per experiment to be counted as n=1. Appropriate statistical tests as mentioned in each chapter were performed to compare groups and treatments. $P < 0.05$ was considered statistically significant.

**Chapter 3. Revised model of the tissue factor pathway of thrombin
generation: role of the feedback activation of FXI**

Hari hara sudhan Lakshmanan, Aldrich Estonilo, Stephanie E. Reitsma, Alexander R.
Melrose, Jayaram Subramanian, Tony J. Zheng, Jeevan Maddala, David Gailani,
Owen J.T. McCarty, Patrick L. Journey and Cristina Puy

3.1 Abstract

Biochemical reaction networks are self-regulated in part due to feedback activation mechanisms. The tissue factor (TF) pathway of blood coagulation is a complex reaction network controlled by multiple feedback loops that coalesce around the serine protease thrombin. Our goal was to evaluate the relative contribution of the feedback activation of coagulation factor XI (FXI) in TF-mediated thrombin generation using a comprehensive systems-based analysis. To accomplish this, we developed a systems biology model that improves the existing Hockin-Mann (HM) model through an integrative approach of mathematical modeling and *in vitro* experiments. Thrombin generation measured using *in vitro* assays revealed that the feedback activation of FXI contributes to the propagation of thrombin generation based on the initial concentrations of TF or activated coagulation factor X (FXa). We utilized experimental data to improve the robustness of the HM model to capture thrombin generation kinetics without a role for FXI before including the feedback activation of FXI by thrombin to construct the extended (ext.) HM model. Using the ext.HM model, we predicted that the contribution of positive feedback of FXI activation by thrombin can be abolished by selectively eliminating the inhibitory

function of tissue factor pathway inhibitor (TFPI), a serine protease inhibitor of FXa and TF-activated factor VII (FVIIa) complex. This prediction from the ext.HM model was experimentally validated using thrombin generation assays with function blocking antibodies against TFPI and plasmas depleted of FXI. Together, our results demonstrate the applications of combining experimental and modeling techniques in predicting complex biochemical reaction systems.

This work is currently under review in
Journal of Thrombosis and Haemostasis

3.2 Introduction

Studies in this chapter were designed to elucidate the role of feedback activation of FXI by thrombin in TF-mediated thrombin generation. Here, we use TF-initiated thrombin generation measured *in vitro* to modify and extend the HM model of thrombin generation. Utilizing the ext. HM model and *in vitro* experimental data we show that the contribution of FXI towards thrombin generation initiated by low concentrations of TF is inversely correlated to the inhibitory role of TFPI. This study explains the significance of feedback and inhibitory mechanisms involved in coagulation.

3.3 Background

Blood coagulation is a network of complex reactions dependent upon the conversion of inactive species (zymogens) of coagulation factors to active serine proteases. Often portrayed as a waterfall, the plasma coagulation was originally described as a series of enzymatic events initiated by two sources, tissue factor (TF) and coagulation factor XII (FXII), converging in the activation of coagulation factor X (FX). TF-initiated coagulation, referred to here as the TF-pathway, starts when blood is exposed to extravascular TF which forms a complex with coagulation factor VII (FVII) to catalyze the conversion of FVII to its activated version FVIIa (1,83). The TF-FVIIa complex then activates coagulation factors X (FX) and IX (FIX) leading to the generation of thrombin. Thrombin is the central serine protease that serves as a master regulator of coagulation by activating both procoagulant and anticoagulant species. For instance, thrombin amplifies its generation by direct activation of the cofactors factor V (FV) and factor VIII (FVIII) (84,85). Moreover, thrombin acts upstream to activate a member of the contact activation pathway, coagulation factor XI (FXI), which in turn activates FIX to create a feedback loop of thrombin generation (86).

While experimental studies utilizing purified components or selective inhibitors have been useful for delineating the contribution of each individual component of the coagulation system, an integrative systems biology approach is required to enable data-driven knowledge discovery and predict yet unknown pathways for thrombin generation. With this as a goal, Hockin et al. built one of the first mathematical models of the TF pathway of thrombin generation by assembling 42 individual

coagulation factor activation or inhibition reactions into ordinary differential equations (ODEs) (87). The Hockin-Mann (HM) model enabled an understanding of the temporal variation of individual species involved in the TF pathway and their sensitivity to variable initial conditions (88-91). Naturally, the HM model was quickly adapted into several models of coagulation that included contributions of flow, diffusion, fibrin formation and platelets to thrombin generation (92-95). While the HM model has proven extremely useful in studying the TF pathway, it was built specifically to exclude coagulation factor XI, in part due to an incomplete mechanistic understanding of the role of FXI in thrombin generation. Moreover, at that time, the physiological relevance of FXI to TF-mediated thrombin generation was in question in part due to *in vitro* studies that utilized supraphysiological concentrations of TF as initiators (96). Therefore, by definition, the utility of the HM model is limited to conditions in which FXI does not play a role in thrombin generation.

In this work, we aim to extend the applications of the HM model for studying the TF pathway of thrombin generation by including the feedback activation of FXI by thrombin. Towards this goal, we used an integrative approach of thrombin generation experiments and numerical analysis to extend the capacity of the HM model to predict the effect of FXI on TF-mediated thrombin generation. We added the mechanisms of feedback activation of FXI by thrombin, activation of FIX by FXIa and inhibition of FXIa by plasma proteins. We utilized *in vitro* thrombin generation assays to support the development of our model. Finally, we tested the robustness of our model by predicting and experimentally validating the role of FXI in the TF pathway with respect to tissue factor pathway inhibitor (TFPI), an endogenous

inhibitor circulating in plasma. Our model and experiments suggest the hypothesis that the effect of FXI in TF-mediated thrombin generation can be modified by neutralizing the function of TFPI in plasma. Our work is a demonstration of how mathematical models can be a useful method for testing and deriving novel mechanistic ideas that can be experimentally verified.

3.4 Materials and Methods

3.4.1 Reagents

FXI-depleted plasma was from Affinity Biologicals Inc. (Ancaster, ON, Canada). Innovin from Siemens Healthcare Diagnostics (Deerfield, IL, USA) was used as the source of TF. Neutralizing monoclonal mouse anti-human TFPI antibodies, specific for the Kunitz 1 or Kunitz 2 domains, was from MyBiosource (San Diego, CA, USA). CTI was obtained from Enzyme Research Laboratories, Inc (South Bend, IN, USA). Plasma-derived FXa and FXI were from Haematologic technologies Inc. (VT, USA). The anti-factor XI antibody 1A6, that blocks the activation of FIX by FXIa was generated as previously described (97). The fluorogenic substrate and calibrator for thrombin generation assay was from Techno Thrombin TGA kit (Technoclone, GmbH, Vienna, Austria). TGA kit consists of the fluorogenic substrate, 1 mM Z-G-G-Ar-AMC in 15 mM CaCl₂, and the calibrator of 1 nM thrombin. Black 96-well plates were from Corning (Corning, NY, USA). All reagents were stored and prepared according to recommendations from the manufacturers. HEPES buffered saline (HBS) containing 25 mM HEPES and 150 mM NaCl (pH 7.4) was used as the buffer for all dilutions unless stated otherwise.

3.4.2 *Thrombin generation - Experiments*

Thrombin generation in plasma was measured by following the cleavage of fluorogenic substrate Z-G-G-Ar-AMC at 37°C on a Tecan's Infinite M200 microplate reader. Experiments were performed in 96-well black plates coated with PEG 20000 (2%). In all experiments, FXI-depleted plasma was supplemented with 30 nM FXI or vehicle and with 40 µg/ml corn trypsin inhibitor (CTI). In select experiments, plasma was additionally supplemented with 30 µg/ml 1A6 or vehicle or anti-TFPI antibodies (6 µg/ml) for 30 minutes before use. All treatments were done at room temperature. HBS with 15 mM CaCl₂ was used as the buffer in the preparation of various concentrations of TF (0.125-1 pM) or FXa (0.1-0.5 nM) as the fluorogenic substrate is contained in 15 mM CaCl₂.

Thrombin generation was initiated by mixing 40 µL of supplemented plasma with 60 µL of reagent substrate mixture, containing 50 µL of fluorogenic substrate and 10 µL of TF or FXa. The fluorescence was recorded at 60 second intervals with an excitation wavelength of 360 nm and emission wavelength of 460 nm for 60 minutes. Thrombin generation was calculated by using Technothrombin[®] TGA evaluation software. The resulting thrombin generation curves from the software were analyzed to estimate the endogenous thrombin generation potential (ETP) – area under the curve, lag time – time to reach 2 nM thrombin, peak thrombin – maximum thrombin concentration and peak time – time to reach peak thrombin.

3.4.3 *Thrombin generation – Simulations*

The mathematical models of tissue factor pathway of thrombin generation were set up as systems of ordinary differential equations (ODEs) as described in (87,92) and solved using odeint from Scipy in Python with a tolerance of 1.5×10^{-8} . Odeint uses Livermore Solver for Ordinary Differential Equations (LSODA) algorithm with dynamic step sizing to solve ODEs. A classic example of the algorithm's usage for a similar purpose is the original implementation of the Hockin-Mann model (87). Initially, simulations were performed using just SciPy which led to an average run time of 5 minutes making it computationally very expensive to run further studies using the model. Therefore, to improve the speed of our simulations, we utilized Numba, an open-source just-in-time compiler that translates python functions to machine code. This led to a decrease in average run time from 204 to 30 seconds. For this work, all computations were implemented in Spyder 4.2.5 IDE running on an Intel i7 core system with 16 GB RAM.

Both the models assume the plasma is well-mixed without any spatial variations in enzyme levels and transport limitations such as diffusion. The models assume that all reactions occur in the fluid phase and do not explicitly model the surface reactions. Our models do not include FXII mediated thrombin generation and it does not affect comparison to our experimental data as all our experiments include CTI to block FXIIa-mediated thrombin generation. The HM model also does not include fibrin related reactions and these conditions were unchanged when we improved the model. A detailed description of reactions along with their respective kinetic constants used in the model are provided in **Table 3.2**. In all cases, 60 minutes of thrombin

generation from the addition of initiator was simulated, with an average computational time of 30 seconds.

The Hockin-Mann model is referred to as the “HM” model and is taken from the work of Hockin and Mann (87) without any modifications. The initial concentrations of enzymes used in all simulations are normal plasma concentrations as provided in **Table 3.1**, and all these concentrations were diluted 2/5th to match the experimental conditions used in the study. To simulate conditions of FXI-depleted plasma or TFPI neutralized plasma, the initial concentrations of FXI or TFPI were set to ‘0’.

The following output parameters were determined from the simulations as described below:

1. ETP (nM.min) – area under the thrombin generation curve.
2. Lag time (min) – time taken to generate 2 nM thrombin; if less than 2 nM thrombin was generated within the simulated 60 minutes (maximum timespan of simulation), lag time is counted as 60 minutes.
3. Peak thrombin (nM) – maximum thrombin concentration observed within the simulated 60 minutes of thrombin generation.
4. Peak time (min) – time taken to reach peak thrombin.

3.4.4 *Estimation of kinetic constants*

Kinetic constants of the mod.HM model were estimated by simultaneously fitting all 4 outputs of thrombin generation, ETP, lag time, peak thrombin and peak time to the experimental data by using the Sequential Least Squares Programming (SLSQP)

algorithm available in the SciPy package. Values of kinetic constants from the HM model were used as initial guesses to estimate the kinetic constants for modified (mod.) HM model. For estimating the kinetics of FXI-related reactions to use in the extended (ext.) HM model, the values of kinetic constants obtained from the literature were used as starting points (92). The estimated kinetics of FXI activation by thrombin were at least two fold less than the literature values, this can be explained by the fact that literature kinetics was determined in the presence of dextran sulfate, a cofactor for this reaction. The estimated kinetics of FIX activation by FXIa was 10 fold higher than the values reported in the literature (98). The kinetics of FXIa inhibition by C1 inhibitor and anti-thrombin (ATIII) were estimated to be 3 fold and 1.5 fold higher than the values reported in the literature (99). **Table 3.1** and **Table 3.2** include details on the initial plasma concentrations and the values of the estimated kinetic constants used in the model.

3.4.5 *Statistical analysis*

Experimental data were analyzed using GraphPad Prism 9 software (San Diego, CA). Data are shown as means \pm standard error of means (SEM) of 3 independent experiments. Illustrated curves from experiments are representative of three independent trials performed in duplicates. Single pair comparisons were analyzed by 2-tailed student's *t* test. Dunnett's multiple comparisons tests with two-way analysis of variance (ANOVA) were performed to compare vehicle with treatments for more than two groups.

3.5 Results

3.5.1 *FXI increases TF-initiated thrombin generation in a TF concentration-dependent manner*

First, we experimentally analyzed the contribution of FXI to thrombin generation initiated via TF *in vitro* to understand conditions for which the Hockin-Mann (HM) model required extension to include the contribution of FXI. To achieve this, we measured thrombin generation in FXI-depleted human plasma supplemented with either a physiological concentration of human FXI (30 nM) or vehicle. We used a fluorogenic substrate assay to measure thrombin generation (100). In this assay, the thrombin concentration was measured every minute by recording the fluorescent signal resulting from the cleavage of the fluorogenic substrate, Z-G-G-Ar-AMC. The thrombin concentration at each time point was computed and used to prepare a thrombin generation curve. The resulting curves were used to derive the following 4 output parameters to assess different aspects of thrombin generation: Endogenous Thrombin Potential (ETP) – area under the curve (nM.min), peak thrombin – maximum thrombin concentration measured during the observation period (nM), lag time – time to generate 2 nM of thrombin (min), and peak time – time to reach peak thrombin (min). Increases in ETP and/or peak thrombin or decreases in lag time and/or peak time is indicative of enhanced thrombin generation. To restrict our study to the TF-initiated FXI feedback pathway for thrombin generation, we pretreated all plasmas with the FXIIa inhibitor CTI (40 µg/ml) (101). This eliminates any potential contribution from FXI activation by FXIIa.

When thrombin generation was initiated in FXI-depleted plasma with 0.125 pM TF, the inclusion of FXI dramatically increased the rate and extent, but not the peak time of thrombin generation (**Figure 3.1A**). This was exemplified by a 145% increase in ETP (1166 ± 90 to 2859 ± 121 nM.min; mean \pm S.E; **Figure 3.1E**) and a 140% increase in peak thrombin (49.67 ± 1.17 to 119.87 ± 3.13 nM **Figure 3.1F**) coupled with a 50% decrease in lag time observed in the presence of FXI (**Figure 3.1G-H**). Similar trends were observed for 0.25 pM TF-initiated thrombin generation (**Figure 3.1B, E-H**). As the initiating concentration of TF increased up to 1 pM, the relative contribution of FXI to the overall rate and extent of thrombin generation fell below 10% (**Figure 3.1A-H**). As expected, no thrombin generation was observed in the absence of TF (data not shown). Activated coagulation factor XI (FXIa) activates coagulation factor IX (FIX) to promote thrombin generation. To determine if the observed increase in thrombin generation in the presence of FXI was due to the activation of FIX by FXIa, we pretreated plasmas with an anti-factor XI mAb 1A6, to selectively eliminate the activation of FIX by FXIa (97,102,103). Note that, 1A6 does not inhibit the activation of FXI by thrombin (104). Indeed, pretreatment with 1A6 reversed the FXI-dependent increase in thrombin generation in plasma induced to clot with 0.125 or 0.25 pM TF but did not produce a significant change with 0.5 or 1 pM TF (**Figure 3.1A-H**).

These experimental results established a range of TF concentrations for which FXI makes substantial contribution to the rate and extent of thrombin generation. Based on these results, the inclusion of the feedback loop of FXI activation to the Hockin-Mann (HM) model of thrombin generation at low concentrations of TF is warranted.

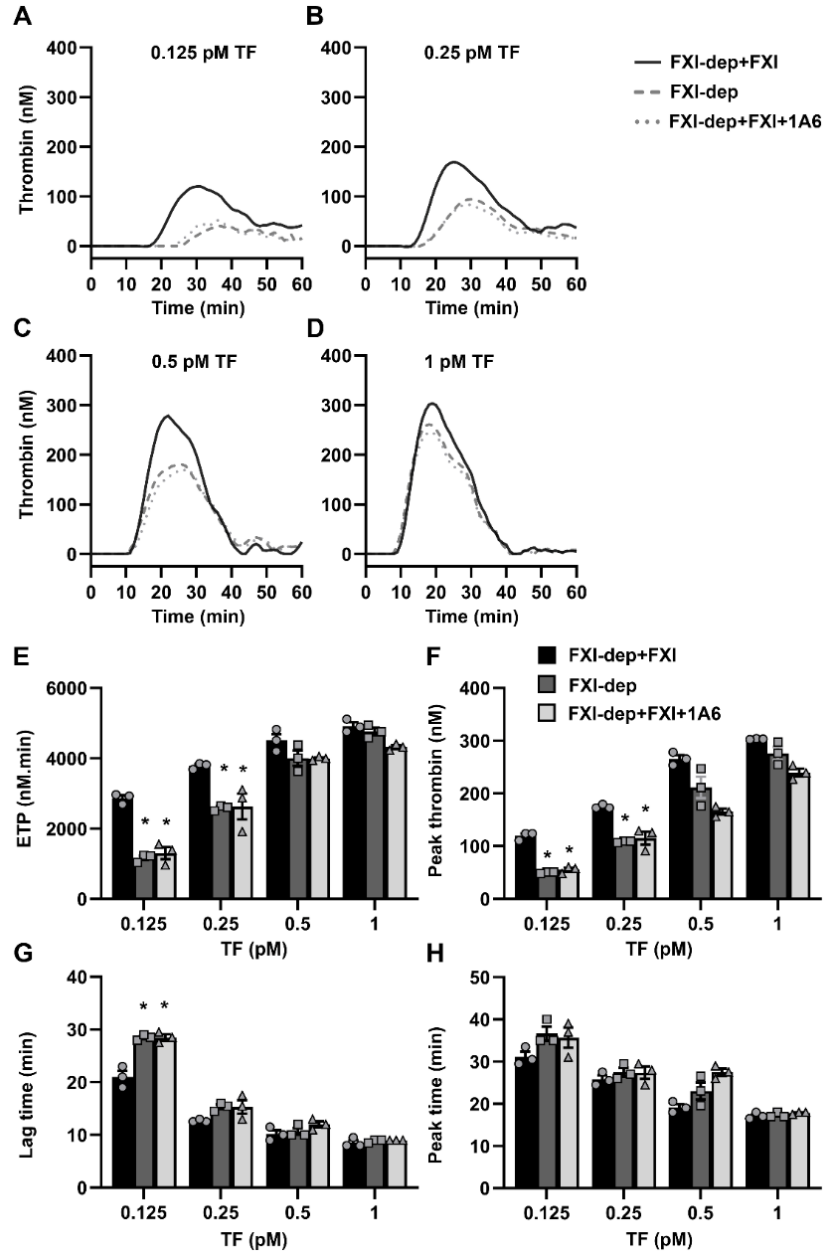


Figure 3.1. Sensitivity of TF-initiated thrombin generation to FXI. (A-D) Thrombin generation in FXI-depleted plasma (FXI-dep) supplemented with 30 nM FXI or vehicle was initiated by the addition of TF (0.125 – 1 pM) and Ca²⁺. Experiments were run in the presence or absence of the anti-FXI mAb, 1A6 (30 µg/ml). (E) Endogenous thrombin generation potential (ETP), (F) Peak thrombin concentrations, (G) Lag time and (H) Peak time were estimated from the thrombin generation curves for each condition. Data are means ± SEM (n = 3). * P < 0.05 with respect to FXI-dep+FXI.

3.5.2 *Effect of FXI on FXa-initiated thrombin generation*

As the TF-FVIIa complex drives thrombin generation by activating coagulation factor X (FX), we sought to identify the range of FXa concentrations at which FXI contributes to the rate and extent of FXa-mediated thrombin generation. When thrombin generation was initiated with 0.1 nM FXa, similar to our observations with low TF, the addition of FXI to FXI-depleted plasma dramatically increased the rate and extent of thrombin generation (**Figure 3.2A**). Under these conditions, both the FXa-generated ETP (258.6 ± 149.2 to 3721.5 ± 399.5 nM.min; **Figure 3.2C**) and the peak thrombin (13 ± 6 to 154.8 ± 19.5 nM; **Figure 3.2D**) increased more than 1000% in the presence of FXI compared to the presence of vehicle. We also observed a decrease in lag time (**Figure 3.2E**) and peak time (**Figure 3.2F**) in the presence of FXI. As with TF-initiated thrombin generation, the selective blockade of FIX activation by FXIa with 1A6 eliminated the contribution of FXI to FXa-initiated thrombin generation at low FXa levels (**Figure 3.2A and C**). As the initiating concentration of FXa increased up to 0.5 nM, the relative contribution of FXI to the overall rate and extent of thrombin generation fell below 10% (**Figure 3.2B-F**).

Together, these results demonstrate that the contribution of FXI to thrombin generation is dependent on the initial concentration of FXa or TF used to trigger coagulation.

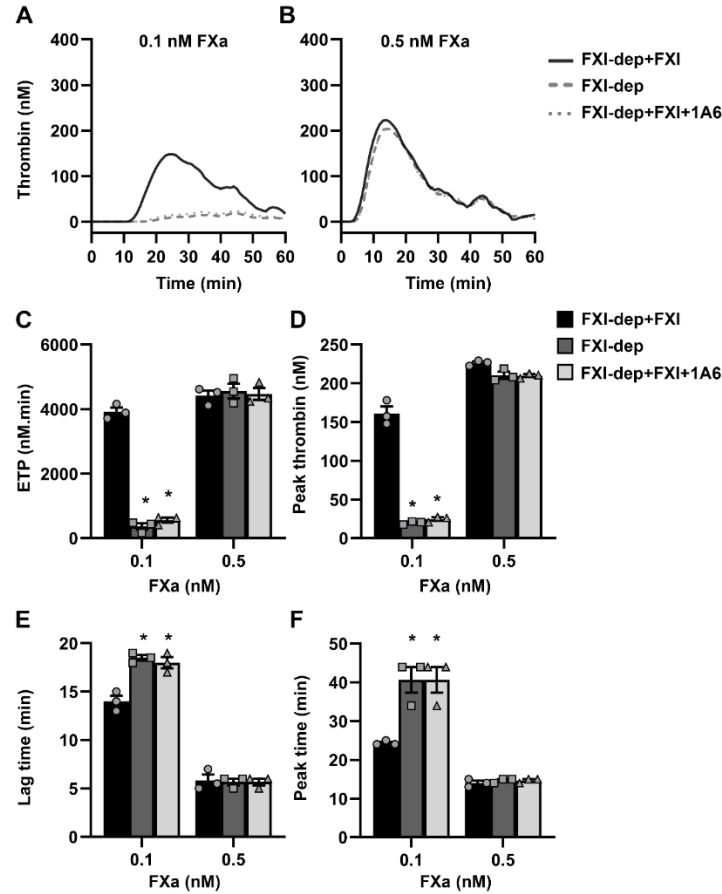


Figure 3.2. Sensitivity of FXa-initiated thrombin generation to FXI. (A-B) FXa (0.1 or 0.5 nM) was used to initiate thrombin generation in FXI-depleted plasma (FXI-dep) supplemented with 30 nM FXI or vehicle in the presence or absence of the anti-FXI mAb, 1A6 (30 μ g/ml). (C) Endogenous thrombin generation potential (ETP), (D) Peak thrombin concentration, (E) Lag time and (F) Peak time were estimated from the thrombin generation curves recorded for each condition. Data are means \pm SEM (n = 3). * P < 0.05 with respect to FXI-dep+FXI.

3.5.3 A systems biology model of TF-pathway of thrombin generation

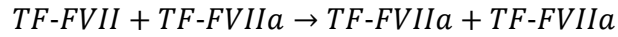
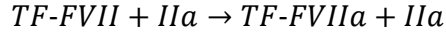
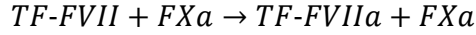
The HM model was one of the first mathematical models to describe the TF pathway of thrombin generation. The model does not include FXI as the mechanistic role of FXI in thrombin generation was unclear at the time the HM model was developed (86,105). The HM model was built for simulating *in vitro* thrombin generation and was originally validated with measurements of thrombin concentrations formed in a

mixture of purified plasma zymogens at their physiologic concentrations rather than in plasma itself (85,106). It is noteworthy that this ‘synthetic’ plasma did not include FXI and was studied at TF-initiating concentrations of more than 1 pM. Thus, we suspect that the original HM model would be unable to predict the thrombin generation dynamics observed in our studies with low concentrations of TF where thrombin generation is most dependent on FXI.

To test this hypothesis, we compared our experimental results for thrombin generation initiated by 0.125 and 0.25 pM TF in FXI-depleted plasma. The initial concentrations of the plasma species were computationally set to the physiological levels of zymogens and enzymes normally found in plasma (**Table 3.1**). The computed thrombin curves from the simulations were used to derive ETP, peak thrombin, lag time and peak time. As shown in **Figure 3.3A-F**, the HM model was unable to predict the thrombin generation curve or the four kinetic outputs to match the experimentally derived data for either 0.125 or 0.25 pM TF. This was particularly evident for the condition using 0.125 pM TF, where the HM model predicted an $ETP < 1 \text{ nM}\cdot\text{min}$ compared with an experimental average of 1150 $\text{nM}\cdot\text{min}$ ETP (**Figure 3.3C**). The inability of the HM model to capture the kinetics of thrombin generation in a system depleted of FXI provided the rationale for making the following modifications:

1. Include reactions describing the activation of FVII in the TF-FVII complex to FVIIa by FXa, thrombin and the TF-FVIIa complex, itself. We assumed that the kinetics of TF-FVII activation is similar to the activation of FVII by FXa, thrombin and TF-FVIIa complex allowing us to use the same kinetic

parameters for both sets of reactions. This is required in light of recent studies suggesting that FVII can be activated by several proteases while in a complex with TF (93,107). The following chemical expressions were used to represent the reactions added to the HM model.



2. The kinetic constants of the reactions were updated by fitting them to the experimental data derived from 0.125 and 0.25 pM TF-initiated thrombin generation in FXI-depleted plasma. The error between the experimental data and the predicted values from the model simulations was minimized according to an objective function as described below. The objective function consists of experimentally estimated average values of ETP, peak thrombin, lag time and peak time and the corresponding predictions from the HM model simulations. We used these outputs from thrombin generation curves as a way of representing the average experimental data for parameter estimation. The estimated parameters were used to simulate thrombin generation curves and compared with the thrombin generation curves from the experiments (44).

$$\text{Objective} = \text{Objective 1} + \text{Objective 2}$$

$$\begin{aligned} \text{Objective 1} = & \sum_{0.125 \text{ pM TF}} \left(\frac{ETP_{exp} - ETP_{model}}{ETP_{exp}} \right)^2 + \left(\frac{Peak_{exp} - Peak_{model}}{Peak_{exp}} \right)^2 \\ & + \left(\frac{LT_{exp} - LT_{model}}{LT_{exp}} \right)^2 + \left(\frac{PT_{exp} - PT_{model}}{PT_{exp}} \right)^2 \end{aligned}$$

$$\text{Objective 2} = \sum_{0.25 \leq p_{M_{TF}}} \left(\frac{ETP_{exp} - ETP_{model}}{ETP_{exp}} \right)^2 + \left(\frac{Peak_{exp} - Peak_{model}}{Peak_{exp}} \right)^2 \\ + \left(\frac{LT_{exp} - LT_{model}}{LT_{exp}} \right)^2 + \left(\frac{PT_{exp} - PT_{model}}{PT_{exp}} \right)^2$$

where, LT – Lag time and PT – Peak time

Hereafter, we refer to the HM model after modifications 1 and 2 as the modified (mod.) HM model. As shown in **Figure 3.3A and B**, thrombin generation curve derived from the mod.HM model was in close agreement with the experimental data using FXI-depleted plasma based on visual inspection. All the four outputs of thrombin generation from the mod.HM model were fitted within 10% of the experimentally derived values. The kinetic parameters of reactions involving TF and FVIIa, reactions 1,3, 4, 17, 39,40 and 41 were estimated to be at least 10-fold different from the original HM model. These reactions are either procoagulant, involved in the generation of proteases that will accelerate thrombin generation, (1,3,4 and 17) or anticoagulant, such as the inhibition of FXa and TF-FVIIa complex by TFPI. Most importantly, the kinetics of TF and FVIIa complex formation was estimated to be 100-fold more than the HM model. This is expected as these reactions control the initiation phase, based on sensitivity studies in the literature, of the thrombin generation which is predicted to be at least 5 times slower than the experimental data by the original HM model as can be seen in **Figure 3.3 (108)**. Reaction 7, FVII activation by FXa is also a part of the initiation phase, parameters of which are increased by more than 100-fold to fit the experimental thrombin generation curve. It is noteworthy that the original HM model used synthetic plasma

that lacked the natural cofactors such as microparticles and lipids that have been shown to accelerate several reactions of the coagulation network including the TF-initiated thrombin generation (109).

Thus, our modifications improved the robustness of the HM model of TF-mediated thrombin generation under conditions in which plasma lacks FXI activity.

Table 3.1 Average initial plasma concentrations of enzymes and inhibitors

Species	Initial concentration (nM)
TF	Varied
FVII	10
TF-FVII	0
FVIIa	0.1
TF-FVIIa	0
FXa	0
IIa (thrombin)	0
FX	160
TF-FVIIa-FX	0
TF-FVIIa-FXa	0
FIX	90
TF-FVIIa-FIX	0
FIXa	0
II (prothrombin)	1400
FVIII	0.7
FVIIIa	0
FIXa-FVIIIa	0
FIXa-FVIIIa-FX	0
FVIIIa1.L	0
FVIIIa2	0
FV	20
FVa	0
FXa-FVa	0
FXa-FVa-II	0
mIIa (meizothrombin)	0
TFPI	2.5
FXa-TFPI	0
FVIIa-TF-FXa-TFPI	0
ATIII	3400
FXa-ATIII	0

Table 3.1 (continued)

Species	Initial concentration (nM)
mIIa-ATIII	0
FIXa-ATIII	0
IIa-ATIII	0
TF-FVIIa-ATIII	0
FXI	30
FXI-IIa	0
FXIa	0
FXIa-FIX	0
C1inh	2500
FXIa-C1inh	0
FXIa-ATIII	0

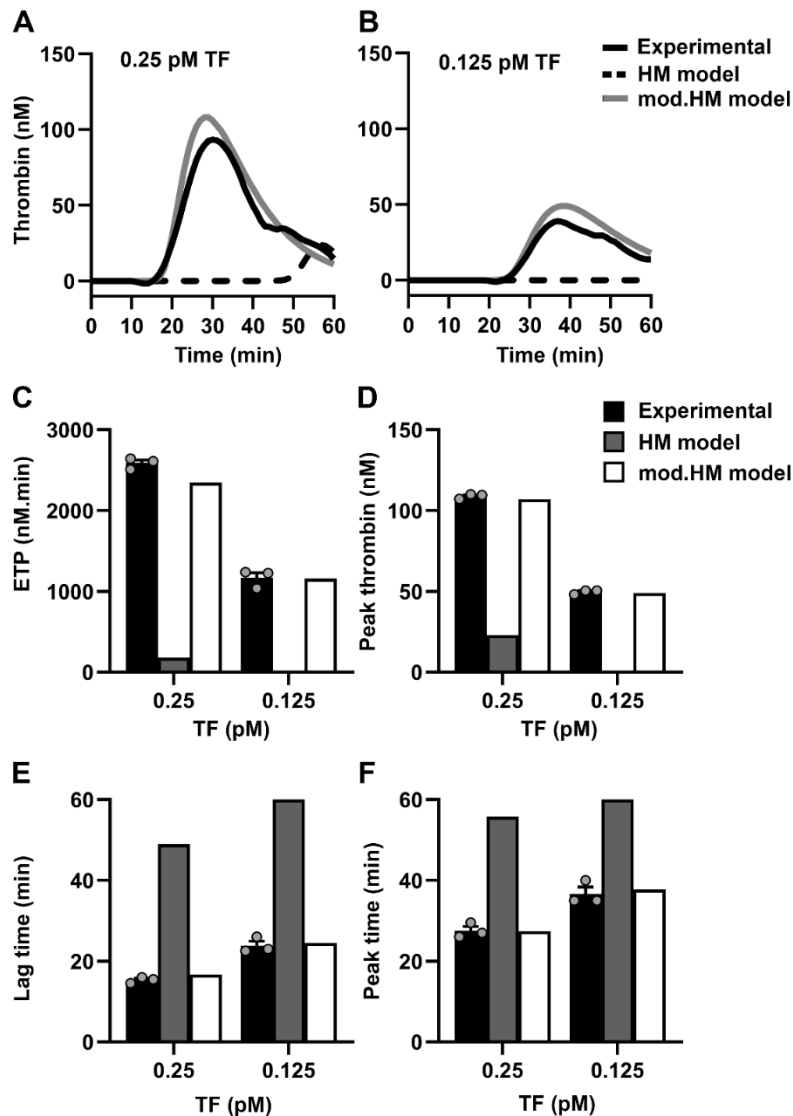
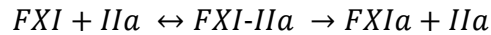


Figure 3.3. Comparison of in vitro and in silico TF-initiated thrombin generation in FXI-depleted plasma Thrombin generation in FXI-depleted plasma was simulated using the Hockin-Mann (HM) model (black dotted line) or the modified Hockin-Mann (mod.HM) model (grey line) with physiological concentrations of enzymes as described in methods, 0 nM FXI and (A) 0.25 or (B) 0.125 pM TF and (A-B) plotted alongside the curves obtained from experiments in FXI-depleted plasma with vehicle (black solid line). (C) Endogenous thrombin generation potential (ETP), (D) Peak thrombin concentration, (E) Lag time and (F) Peak time were estimated from HM (grey bars), m.HM (white bars) and experiments in FXI-depleted plasma (black bars). Lag time and peak time were recorded as 60 minutes if < 2 nM thrombin was generated within 60 min. No bars in (C) and (D) for the HM model indicate that < 2 nM of thrombin generation was recorded within 60 min of simulation. Experimental data are shown as mean \pm SEM (n = 3).

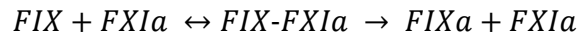
3.5.4 Extending the mod.HM model to include FXI

As the mod.HM model does not include FXI, it cannot capture effects of FXI on thrombin generation. To address this limitation, we included the following mechanisms related to FXI activation and activity in the mod.HM model (herein referred to as the ‘extended HM model’, or ext.HM model):

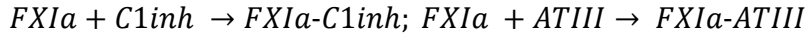
1. FXI activation by thrombin.



2. FIX activation by FXIa.



3. FXIa inhibition by antithrombin (ATIII) and C1-inhibitor (C1inh).



We took parallel approaches to extend the mod.HM model. First, we incorporated the literature values for kinetic constants of the activation of FXI by thrombin. In the second approach, we estimated the kinetic constants based on fitting curves to our experimental data. The caveat for the literature values was that they were measured in the presence of dextran sulfate – an exogenous cofactor of FXI activation by thrombin – and thus may overestimate the kinetics of endogenous FXI activation by thrombin (92). Our experimental data were derived from conditions under which thrombin generation was most sensitive to FXI: 0.125 and 0.25 pM TF-initiated thrombin generation in FXI-depleted plasma supplemented with 30 nM FXI.

Both simulation approaches were performed for initial TF concentrations of 0.125 or 0.25 pM TF and the initial concentration of FXI computationally set to 30 nM.

Simulated thrombin generation curves (**Figure 3.4A-D**) and the outputs derived from the curves were then compared to the experimental data (**Figure 3.4E-H**).

The ext.HM model run with kinetic parameters from the literature predicted peak thrombin values that were >2-fold higher than the experimentally-derived values (**Figure 3.4A, C and F**). Moreover, the literature-based model predictions were insensitive to changes in TF concentration (**Figure 3.4A and C**). For example, the model predicted a <1% decrease in ETP and peak thrombin when the TF concentration fell from 0.25 to 0.125 pM, whereas a >33% decrease was observed experimentally (**Figure 3.4E-F**). Similarly, both the lag time and peak time were insensitive to TF concentration when ext.HM model was run with kinetic parameters from the literature (**Figure 3.4G-H**). However, the predicted thrombin generation curves were sensitive to TF concentration in a manner consistent with experimental observation when the ext.HM model was simulated with estimated kinetic constants (**values listed Table 3.2**). Ext.HM model simulations with estimated kinetic parameters predicted a decrease in ETP and peak thrombin consistent with the experimental observation when the TF concentration was decreased from 0.25 pM to 0.125 pM (**Figure 3.4E and F**). Therefore, we chose to use experimentally-derived estimated kinetics for extending the mod.HM model to extended HM (ext.HM) model. The ext.HM model is used further to predict the role of the FXI feedback mechanism in thrombin generation.

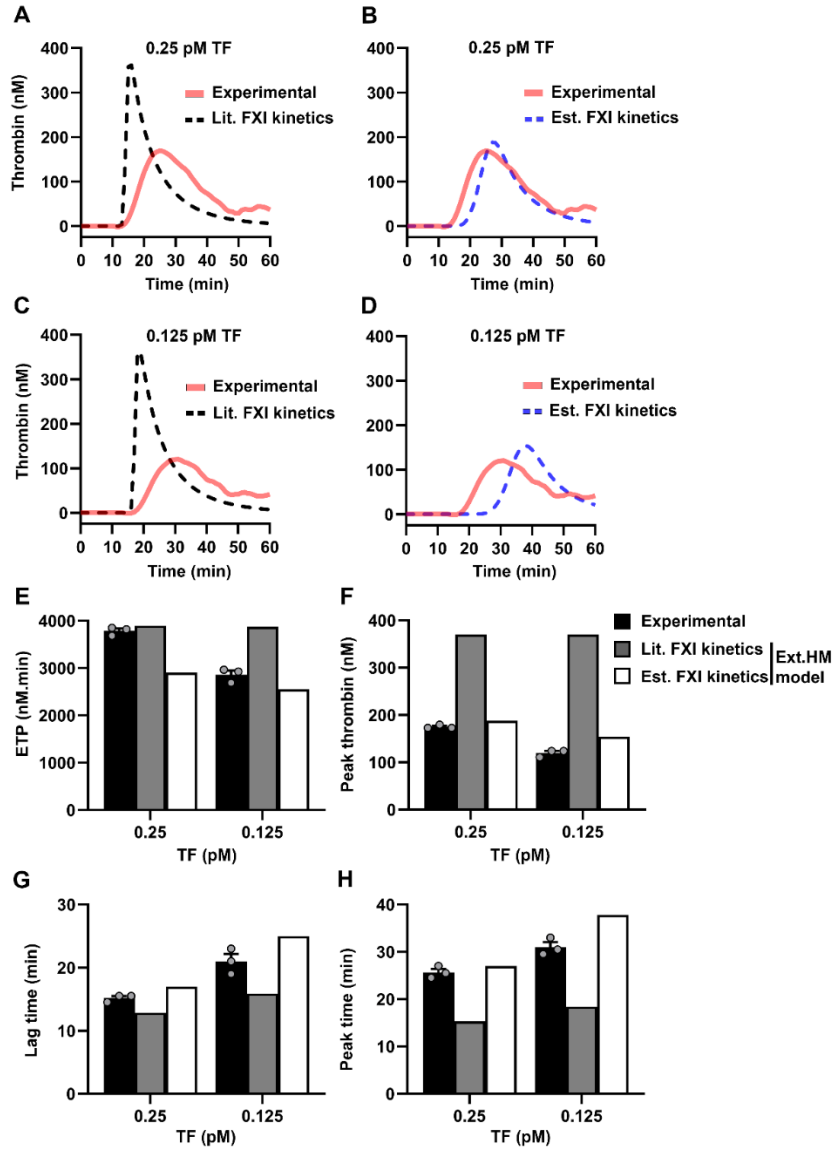


Figure 3.4. Comparison of in vitro and in silico TF-initiated thrombin generation in plasma with FXI. Experimental curves are from the experiments in FXI-depleted plasma supplemented with 30 nM FXI as described in **Figure 3.1**. Sensitivity of TF-initiated thrombin generation to FXI. **(A)** and **(C)** Thrombin generation curves from the simulations of extended (ext.)-HM model with FXI-related kinetics from literature (Lit. FXI kinetics) (black broken line) and experiments (red solid line). **(B)** and **(D)** Thrombin generation from simulation using ext.HM model with FXI-related kinetic parameters estimated by fitting to the experimental data (Est. FXI kinetics) (blue broken line) and experiments (red solid line). **(E)** ETP, **(F)** peak thrombin, **(G)** lag time and **(H)** peak time were estimated from the experiments (black bars) and the simulations of mod.HM model with literature kinetic parameters (dark grey bars) and estimated kinetic parameters (white bars) as described in methods. Experimental data are expressed as means \pm SEM ($n = 3$).

3.5.5 Validating the ext.HM model

We tested the predictive capabilities of the ext.HM model using a novel set of conditions not previously used during kinetic parameter estimation. We chose to predict and experimentally validate the role of FXI in TF-mediated thrombin generation in the presence or absence of an endogenous inhibitor of the TF/FVIIa/FXa complex, tissue factor pathway inhibitor (TFPI). The ability of TFPI to reduce thrombin generation becomes more pronounced as TF concentrations decrease (6,26) and for the purpose of our study, we predicted that this effect would be maximal for conditions of low TF where FXI makes its most substantial contribution to thrombin generation. Simulations were performed for TF concentrations of 0.125 or 0.25 pM with or without physiological levels of FXI (30 nM) or TFPI (2.5 nM).

The simulations indicate that removing TFPI from the *in silico* system eliminates the contribution of FXI to thrombin generation (**Figure 3.5A and E**). In particular, our model predicts that for the initiating condition of 0.125 pM TF, removing TFPI from the system caused a 10-fold reduction in the sensitivity of ETP to FXI (**Figure 3.5E-F**). This suggests that the inhibitory function of TFPI is absolutely necessary in order to observe the effect of FXI on thrombin generation under conditions of low TF.

Next, we took an integrative approach to validate the effect of TFPI on thrombin generation predicted by the ext.HM model under conditions of low TF. We measured thrombin generation initiated with 0.125 or 0.25 pM TF, in FXI-depleted plasma supplemented with vehicle or 30 nM FXI. We neutralized the function of plasma

TFPI with anti-TFPI antibodies. Any potential effects of the FXII-mediated contact activation pathway to thrombin generation were abrogated by inclusion of CTI (40 $\mu\text{g/ml}$) in plasma.

In agreement with the effect predicted by the ext.HM model for TFPI on FXI-mediated thrombin generation, we observed that blocking plasma TFPI abrogated the potentiating effect of FXI on the total extent of thrombin generated, ETP (**Figure 3.5D and H**), as well as the kinetics of the thrombin generation curve (**Figure 3.5B and F**). This integrative approach demonstrates the robustness and utility of the ext.HM model to predict the influence of FXI on thrombin generation.

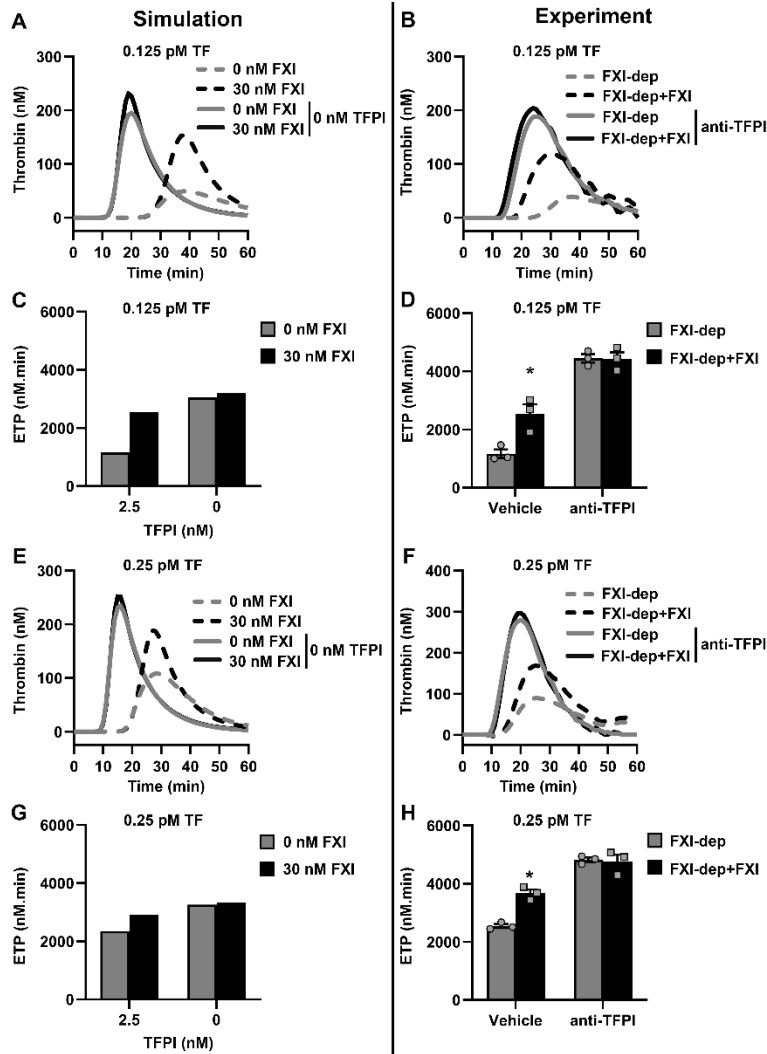


Figure 3.5. Validation of the extended Hockin-Mann model. The effect of TFPI on TF-initiated thrombin generation in the presence or absence of FXI is predicted using the extended (ext.) HM model. Experiments were conducted in FXI-depleted plasma (FXI-dep) supplemented with 30 nM FXI or vehicle in the presence or absence of TFPI blocking antibodies (5 μ g/ml). All plasmas were incubated with CTI to block FXIIa activity. Thrombin generation curves from simulations initiated with (A) 0.125 or (E) 0.25 pM TF and 0 or 30 nM FXI with 0 or 2.5 nM TFPI. Thrombin generation was initiated with (B) 0.125 or (F) 0.25 pM TF in FXI-depleted plasma supplemented with 30 nM FXI or vehicle. In select experiments, plasma was pretreated with blocking antibodies against K-1 and K-2 domains of TFPI. (C) and (D) show the ETP of 0.125 pM TF-initiated thrombin generation as estimated from simulations and experiments for each condition, respectively. (G) and (H) show the ETP of 0.25 pM TF-initiated thrombin generation from simulations and experiments, respectively. Experimental data are shown as means \pm SEM (n = 3). * P < 0.05 with respect to FXI-dep plasma with vehicle.

Table 3.2 Reactions and kinetic constants of the extended Hockin-Mann model

No.	Reactions	Kinetic constant	Units	Fold change from the HM model
1	TF + FVII = TF-FVII	1.7×10^5	$M^{-1}s^{-1}$	18
2	TF-FVII = TF + FVII	3.0×10^{-3}	s^{-1}	1
3	TF + FVIIa = TF-FVIIa	2.2×10^8	$M^{-1}s^{-1}$	9.6
4	TF-FVIIa = TF + FVIIa	3.1×10^{-5}	s^{-1}	100
5	TF-FVIIa + FVII = TF-FVIIa + FVIIa	4.4×10^5	$M^{-1}s^{-1}$	1
6*	TF-FVIIa + TF-FVII = TF-FVIIa + TF-FVIIa	4.4×10^5	$M^{-1}s^{-1}$	-
7	FXa + FVII = FXa + FVIIa	2.5×10^9	$M^{-1}s^{-1}$	196
8*	FXa + TF-FVII = FXa + TF-FVIIa	2.5×10^9	$M^{-1}s^{-1}$	-
9	IIa + FVII = IIa + FVIIa	2.3×10^4	$M^{-1}s^{-1}$	1
10*	IIa + TF-FVII = IIa + TF-FVIIa	2.3×10^4	$M^{-1}s^{-1}$	1
11	TF-FVIIa + FX = TF-FVIIa-FX	7.5×10^6	$M^{-1}s^{-1}$	3.3
12	TF-FVIIa-FX = TF-FVIIa + FX	5.2×10^{-1}	s^{-1}	2
13	TF-FVIIa-FX = TF-FVIIa-FXa	1.1×10^1	s^{-1}	1.92
14	TF-FVIIa + FXa = TF-FVIIa-FXa	2.2×10^7	$M^{-1}s^{-1}$	1
15	TF-FVIIa-FXa = TF-FVIIa + FXa	3.9×10^1	s^{-1}	2
16	TF-FVIIa + IX = TF-FVIIa-IX	2.7×10^7	$M^{-1}s^{-1}$	2.7
17	TF-FVIIa-IX = TF-FVIIa + IX	4.2×10^2	s^{-1}	177
18	TF-FVIIa-IX = TF-FVIIa + FIXa	1×10^1	s^{-1}	5.9
19	II + FXa = IIa + FXa	9.2×10^3	$M^{-1}s^{-1}$	1.2
20	IIa + FVIII = IIa + FVIIIa	2.5×10^7	$M^{-1}s^{-1}$	1.2
21	FVIIIa + FIXa = FIXa-FVIIIa	5×10^7	$M^{-1}s^{-1}$	5
22	FIXa-FVIIIa = FVIIIa + FIXa	2.8×10^{-3}	$M^{-1}s^{-1}$	1.75
23	FIXa-FVIIIa + X = FIXa-FVIIIa-FX	1.3×10^8	$M^{-1}s^{-1}$	1.34
24	FIXa-FVIIIa-X = FIXa-FVIIIa + X	1.0×10^{-3}	s^{-1}	1
25	FIXa-FVIIIa-X = FIXa-FVIIIa + FXa	4.2×10^1	s^{-1}	5.1
26	FVIIIa = FVIIIa1 + FVIIIa2	7.5×10^{-3}	s^{-1}	1.2
27	FVIIIa1 + FVIIIa2 = FVIIIa	2.1×10^4	$M^{-1}s^{-1}$	1
28	FIXa-FVIIIa-FX = FVIIIa1 + FVIIIa2 + FX + FIXa	1.4×10^{-4}	s^{-1}	7.1
29	FIXa-FVIIIa = FVIIIa1 + FVIIIa2 + FIXa	6.1×10^{-4}	s^{-1}	1.6
30	IIa + FV = IIa + FVa	2.3×10^7	$M^{-1}s^{-1}$	1.1
31	FXa + FVa = FXa-FVa	4.9×10^8	$M^{-1}s^{-1}$	1.2
32	FXa-FVa = FXa + FVa	3×10^{-1}	s^{-1}	1.5
33	FXa-FVa + II = FXa-FVa-II	2.5×10^7	$M^{-1}s^{-1}$	3.9
34	FXa-FVa-II = FXa-FVa + II	7.8×10^1	s^{-1}	1.3
35	FXa-FVa-II = FXa-FVa + mIIa	1.3×10^1	s^{-1}	4.8
36	FXa-FVa + mIIa = FXa-FVa + IIa	2.3×10^7	s^{-1}	1.6
37	FXa + TFPI = FXa-TFPI	2.2×10^7	$M^{-1}s^{-1}$	24

Table 3.2 (continued)

No.	Reactions	Kinetic constant	Units	Fold change from the HM model
38	$\text{FXa-TFPI} = \text{FXa} + \text{TFPI}$	3.7×10^{-5}	s^{-1}	9.7
39	$\text{TF-FVIIa-FXa} + \text{TFPI} = \text{TF-FVIIa-FXa-TFPI}$	1×10^7	$M^{-1}s^{-1}$	31
40	$\text{TF-FVIIa-FXa-TFPI} = \text{TF-FVIIa-FXa} + \text{TFPI}$	1×10^{-5}	s^{-1}	10
41	$\text{TF-FVIIa} + \text{FXa-TFPI} = \text{TF-FVIIa-FXa-TFPI}$	4.4×10^8	$M^{-1}s^{-1}$	8.7
42	$\text{FXa} + \text{ATIII} = \text{FXa-ATIII}$	1.2×10^3	$M^{-1}s^{-1}$	1.2
43	$\text{mIIa} + \text{ATIII} = \text{mIIa-ATIII}$	1×10^4	$M^{-1}s^{-1}$	1.4
44	$\text{FIXa} + \text{ATIII} = \text{FIXa-ATIII}$	7×10^2	$M^{-1}s^{-1}$	1.4
45	$\text{IIa} + \text{ATIII} = \text{IIa-ATIII}$	2.1×10^3	$M^{-1}s^{-1}$	3.4
46	$\text{TF-FVIIa} + \text{ATIII} = \text{TF-FVIIa-ATIII}$	3.3×10^2	$M^{-1}s^{-1}$	1.4
47*	$\text{FXI} + \text{IIa} = \text{FXI-IIa}$	5×10^7	$M^{-1}s^{-1}$	-
48*	$\text{FXI-IIa} = \text{XI} + \text{IIa}$	9.9	s^{-1}	-
49*	$\text{FXI-IIa} = \text{FXIa} + \text{IIa}$	1.1×10^{-4}	s^{-1}	-
50*	$\text{FXIa} + \text{FIX} = \text{FXIa-FIX}$	6.1×10^5	$M^{-1}s^{-1}$	-
51*	$\text{FXIa-IX} = \text{FXIa} + \text{IX}$	9.9×10^{-1}	s^{-1}	-
52*	$\text{FXIa-IX} = \text{FXIa} + \text{FIXa}$	1.1×10^{-1}	s^{-1}	-
53*	$\text{FXIa} + \text{ATIII} = \text{FXIa-ATIII}$	3.2×10^2	$M^{-1}s^{-1}$	-
54*	$\text{FXIa} + \text{C1inh} = \text{XIa-C1inh}$	1.8×10^3	$M^{-1}s^{-1}$	-

II – prothrombin, FVIIIa1 and FVIIIa2 – trimeric forms of FVIIIa, mIIa – meizothrombin, ATIII – antithrombin, C1inh – C1 inhibitor. *Reactions not part of the original HM model that are added in this study.

3.6 Discussion

Feedback activation mechanisms are central to the self-regulation of biological processes ranging from cellular signaling to protein synthesis (110-114). For instance, an organized set of positive and negative feedback mechanisms control the complex biochemical reaction networks observed in metabolic pathways, complement pathways of the immune system, and the pathways of blood coagulation. Due to the inherent complexity associated with the presence of several series and parallel reactions in biochemical reaction networks, intuitive analysis alone is insufficient to assess the importance of individual reactions, necessitating a systems-

based approach. In this work, we present a case example of the TF pathway of thrombin generation to demonstrate the utility of synchronizing experimental and computational systems biology models to map the feedback mechanisms of a complex reaction network. We believe our approach is versatile and simple and can be extended to the study of any complex reaction system with feedback loops.

In the initiation phase of coagulation, formation of a complex of TF and FVIIa catalyzes a series of enzymatic reactions that culminate in the generation of thrombin (115). In the propagation phase, thrombin self-regulates its production through feedback of activation of FVII, FVIII, FV and FXI (116). The mean plasma concentration of FXI (30 nM) is higher than the other zymogens FVII (10 nM), and cofactors FVIII (0.3 nM) and FV (20 nM), yet the catalytic efficiency (k_{cat}/K_m) of FXI activation by thrombin is at least 100-fold lower than those for activation of the other coagulation factors (10,84,86). Moreover, the primary substrate for FXIa is FIX, which can also be directly activated by the TF-FVIIa complex. Thus, robust thrombin generation driven by relatively high concentrations of TF or FXa would be predicted to be insensitive to FXI. This has led some to question the physiological relevance of FXI activation by thrombin (96,117). However, we and others hypothesize that FXI activation by thrombin affects the propagation of thrombin generation when the initial thrombin generation rate through the main reaction pathways is initiated by relatively low initial concentrations of TF or FXa (97,102). By incorporating the FXI feedback activation mechanism, we have improved an established network model that encompassed not only the major reaction pathways but also the role of regulatory mechanisms in the generation of thrombin.

Our network model predicts that manipulating the initial rates of thrombin generation by selectively neutralizing a specific inhibitor also changes the sensitivity of thrombin generation to FXI. TFPI is an endogenous inhibitor of FXa and the TF-FVIIa complex. In simulations of thrombin generation initiated with a low TF concentration, the model predicted that eliminating TFPI will increase the initial rate of thrombin generation and abolish the effect of FXI on TF-mediated thrombin generation. Our experimental validation of this computationally-derived hypothesis provides credence to the theory that amplifying the propagation phase of thrombin generation through feedback activation of FXI is important in low tissue factor environments.

Applied to physiology, this pathway could underlie a spatial role for FXI in propagating thrombin generation during the growth and stabilization phase of hemostatic plug development beyond the initial burst of thrombin generated by surface-expressed TF at the site of a vascular breach (65,103,118-120). Furthermore, this mechanism could propagate the growth of pathologic occlusive thrombi, suggesting it may be a useful target for antithrombotic therapy. For instance, several biological substances that are likely to be present in a growing thrombus, including polyphosphates released from platelets (121), the platelet surface itself (122), and neutrophil extracellular traps (NETs) (123,124) have been shown to affect the activation rate of FXI or the kinetics of FXI activity.

Similar to the HM model we approximate surface and bulk reactions together as bulk reactions but this did not affect the capacity of ext.HM model to predict qualitative changes in thrombin generation profiles in response to changes in stimulus as

observed *in vitro*. Potential roles for the surface-based FXI activation or inhibition are not included in our model. Future work focused on modifying the kinetics of FXI feedback activation by cofactors and biologically relevant surfaces can establish the effect of this feedback mechanism on thrombin generation and thrombus formation differentially in a disease setting.

In addition to activating FIX, FXIa can contribute to thrombin generation by activating FX, FV, and FVIII and by inhibiting TFPI (125-127). Further refinements to the model will be required to include these mechanisms to the reaction topology of the current model. However, even in the absence of explicit consideration of surface reactions and additional mechanisms of FXI, the ext.HM model can be useful in predicting qualitative changes on thrombin generation profiles in response to changes induced by stimulus as observed *in vitro*.

In conclusion, we observed a threshold behavior for the involvement of FXI in thrombin generation based on the initial rate of thrombin generation determined by the concentrations of TF or FXa used to initiate coagulation. Experimental data from thrombin generation assays were first used to improve the robustness of the systems biology model of TF pathway, the HM model, followed by extension of the model to include FXI. The ext.HM model was subsequently used to predict the ability of TFPI to influence the importance of FXI on thrombin generation, which was experimentally validated using thrombin generation assays. This demonstrates the utility of computational systems biology approaches to evaluate complex reaction systems with feedback loops.

Chapter 4. The basement membrane protein nidogen-1 supports platelet adhesion and activation

Hari Hara Sudhan Lakshmanan, Alexander R. Melrose, Anna-Liisa I. Sepp, Annachiara Mitrugno, Anh T.P. Ngo, Ayesha Khader, Rachel Thompson, Daniel Sallee, Jiaqing Pang, Pierre H. Mangin, Martine Jandrot-Perrus, Joseph E. Aslan and Owen J.T. McCarty

4.1 Abstract

The core structure of the extracellular basement membrane is made up of self-assembling networks of collagen and laminin which associate with each other through the bridging adapter proteins including the sulfated monomeric glycoprotein nidogen. While collagen and laminin are known to support platelet adhesion and activation via $\beta 1$ integrins and glycoprotein (GP) VI, respectively, whether nidogen contributes to platelet activation and hemostasis is unknown. In this study we demonstrate that recombinant human nidogen-1 supports platelet adhesion and stimulates platelet activation in a phospholipase-C γ -2 (PLC γ 2), Src and Syk kinase-dependent manner downstream. Platelet adhesion to nidogen was inhibited by blocking the platelet receptors GPVI and $\beta 1$ integrins. Platelet adhesion to nidogen activated the I κ B kinase (IKK) complex, while pharmacological inhibition of IKK blocked platelet spreading on nidogen. Taken together our results suggest that nidogen may play a redundant role in hemostasis by activating platelets downstream of GPVI.

This work was originally published by the

Platelets. 2021; 32:3, 424-428.

Reused with permission

4.2 Introduction

Chapter 3 presented an analysis of the biochemical reactions of the coagulation network responsible for the generation of thrombin. A hemostatic plug is the result of fibrin formation and platelet activation, in part, by the ECM proteins such as collagen and laminin. In addition to activating platelets, ECM proteins also support platelet adhesion to serve as a platform for platelet aggregation. Collagen and laminin are linked together by a globular protein called nidogen. Studies in Chapter 4 were designed to determine if nidogen-1 can activate platelets and play a role in hemostasis. The data presented in the study suggests that nidogen-1 may activate platelets through the glycoprotein receptor GPVI and support platelet adhesion through integrin $\beta 1$. The results of this study suggest that nidogen-1 may play a redundant role in hemostasis alongside collagen and laminin.

4.3 Background

The major constituents of the subendothelial matrix include various variants of collagen and laminin, which assembly to form two independent networks (128). Collagen plays a major role in providing structural stability while laminin is essential for the initial assembly of the basement membrane. As these networks have only a weak affinity for each other, the matrix protein nidogen acts as an integrating element

for basement membrane assembly by promoting noncovalent molecular connections between laminin and collagen IV (48). Indeed, in mice, nidogen deficiency causes impaired lung and heart development leading to perinatal lethality (49). Studies including those in *C. elegans* revealed that nidogen may play other nonstructural roles including synaptic transmission and axonal pathfinding (129,130). As collagen and laminin are known to play nonstructural roles in hemostasis through activation of blood platelets and coagulation factors, we designed the current study to investigate whether nidogen likewise contributes to hemostasis by supporting platelet activation.

Hemostasis is dependent upon concomitant activation of the blood coagulation cascade and blood platelet adhesion to and activation by subendothelial extracellular matrix (ECM) proteins at sites of vascular injury (1). The adhesive protein von Willebrand factor (VWF) binds to collagen to facilitate recruitment of platelets from the blood stream in a glycoprotein (GP) Ib-dependent manner (19). β 1 integrin-dependent adhesion to collagen mediates firm adhesion while platelets are rapidly activated by the platelet Immunoglobulin superfamily receptor, GPVI. Crosslinking of GPVI induces Src kinase-dependent tyrosine phosphorylation of the FcR γ -chain immunoreceptor tyrosine-based activation motif (ITAM) (131,132). This initiates a Syk-dependent signaling cascade that leads to formation of the LAT signalosome and activation of one of the major effector enzymes in the GPVI signaling cascade, phospholipase C (PLC) γ 2, which triggers intracellular calcium mobilization, liberation of the second messengers 1,2-diacylglycerol and inositol 1,4,5 trisphosphate and granule release (26). Activated platelets subsequently flip their

membrane to expose phosphatidylserine and catalyze local thrombin generation and fibrin formation to rapidly form a hemostatic plug (133).

The discovery that the ECM protein laminin likewise binds and activates platelets in a GPVI-dependent manner to support thrombus formation under flow brought to light GPVI as more than a faithful platelet receptor for collagen (29). Rather, GPVI is a promiscuous receptor for a growing number of ligands including adhesive proteins (fibrin)ogen, fibronectin and vitronectin acting in concert to support thrombus growth and stabilization (28,29,134-136). Herein this study adds nidogen to the growing list of ligands that bind and activate GPVI to ensure thrombus formation under flow, providing further evidence that a cacophony of redundant mechanisms have evolved to activate GPVI to maintain hemostasis (137).

4.4 Materials and Methods

4.4.1 Reagents

Reagents were purchased from Sigma-Aldrich (St Louis, MO, USA) unless specified otherwise. Recombinant human nidogen-1 was obtained from R&D Systems (Minneapolis, MN, USA), soluble collagen from Corning (Corning, NY, USA), fibrillar collagen from Chrono-Log (Havertown, PA, USA) and human fibrinogen from Enzyme Research (South Bend, IN, USA). U73122 and U73343 were obtained from Tocris (Bristol, UK). Anti-GPVI ACT017 blocking antibody was donated by Acticor Biotech (Paris, France). Anti- β 1 (clone: AIB2) blocking antibody was purchased from Millipore (Burlington, MA, USA).

4.4.2 *Isolation of human platelets*

Platelets were isolated from human venous blood drawn from healthy volunteers as described in Chapter 2 of the dissertation.

4.4.3 *Static platelet adhesion and spreading assay*

Platelet adhesion and spreading assay was carried out as previously described. Briefly, glass coverslips were coated with human fibrinogen (50 µg/mL), soluble collagen (50 µg/mL) or recombinant nidogen-1 (50 µg/mL), followed by surface blocking with bovine serum albumin (BSA) (5 mg/mL). Inhibitors or vehicle were added to platelets in solution (5×10^7 /mL) for 15 minutes before exposure to indicated immobilized surfaces. After 45 minutes, nonadherent platelets were discarded and surface-bound platelets were washed 3 times with PBS. Platelets were imaged using Kohler illuminated Nomarski differential interference contrast (DIC) optics with a Zeiss 63x oil immersion 1.40 NA plan-apochromat lens on a Zeiss Axio Imager M2 microscope.

4.4.4 *Statistical Analysis*

Data were analyzed using GraphPad PRISM 5.0 software (San Diego, CA, USA). To determine statistical significance, Student's paired t-test was used for comparison between treatment and control, while one way-ANOVA was performed with Dunnet's multiple comparison test for experiments with multiple treatments. Results are expressed as the mean \pm standard error of the mean (SEM). Differences were considered significant at $P < 0.05$.

4.5 Results

4.5.1 *Nidogen supports platelet adhesion and activation*

We initially investigated the ability of immobilized recombinant nidogen-1 to support platelet adhesion and spreading as compared to fibrinogen and collagen. As shown in **Figure 4.1A-B**, an increasing degree of platelet binding was observed on surfaces coated with an increasing concentration of recombinant human nidogen-1, fibrinogen or soluble collagen. Moreover, platelets fully spread to form lamellipodia on immobilized nidogen-1, fibrinogen and soluble collagen. In contrast, a minimal number of platelets bound to a BSA-coated surface which served as a negative control.

We investigated the intracellular signaling cascades activated in platelets following adhesion to nidogen relative to adhesion fibrinogen and the GPVI-agonist collagen-related peptide (CRP-XL). Platelet adhesion on nidogen promoted the activation of tyrosine kinase signaling events, as determined by Western blotting for tyrosine phosphorylated proteins with 4G10 antisera, phosphorylated Syk and protein kinase C (PKC) activation, as determined by phosphorylation of PKC substrates, similar to adhesion to fibrinogen and CRP-XL (**Figure 4.1C**). Relative to CRP-XL adherent platelets, platelets adherent to nidogen showed less phosphorylation of PLC γ 2, a critical regulator of secretion and activation. Other critical mediators of platelet secretion in the NF- κ B system were phosphorylated at levels comparable to CRP-XL(138). Interestingly, we detected phosphorylated IKK in platelets adherent on nidogen, suggesting consistent with our pharmacological data showing that the IKK

inhibitor IKK-16 blocked platelet spreading on nidogen, suggesting that the nongenomic role of IKK in platelets may extend to regulating platelet signaling and activation.

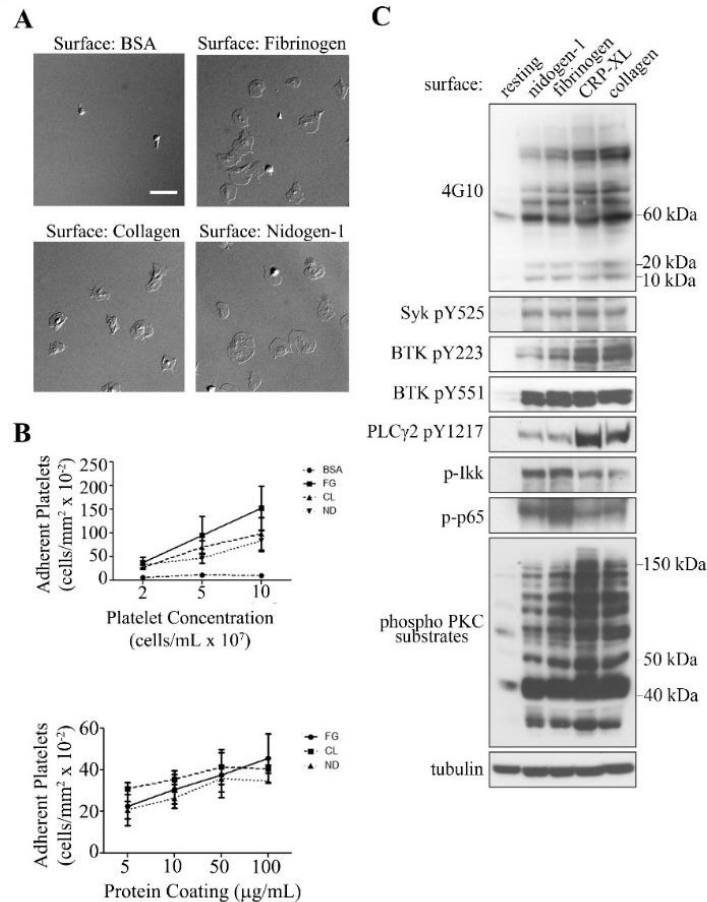


Figure 4.1. Adhesion and spreading of human platelets on nidogen-1. (A) Human washed platelets (2×10^7 /mL) were placed on coverslips coated with fibrinogen ($100 \mu\text{g/mL}$), soluble collagen ($50 \mu\text{g/mL}$), recombinant nidogen-1 ($100 \mu\text{g/mL}$) or BSA (5 mg/mL) for 45 min at 37°C and imaged using differential interference contrast (DIC) microscopy. Images are representative of three independent experiments. Scale bar, $10 \mu\text{m}$. (B) The number of adherent platelets on BSA, fibrinogen (FG), soluble collagen (CL) and nidogen-1 (ND) for increasing platelet concentrations and increasing protein concentrations were recorded for 3 fields of view and expressed as mean \pm SEM from at least 3 different experiments. (C) Lysates from washed human platelets seeded on coverslips coated with fibrinogen, CRP-XL (collagen related peptide), recombinant nidogen-1 or quiescent solution were analyzed for phosphorylation of Syk, PKC (protein kinase C) activation, IKK activation, NF- κ B activation and PLC γ 2 activation by western blotting (WB). Blots are representative of three experiments.

Next, we sought to investigate mechanisms of platelet adherence and spreading on nidogen surfaces using pharmacological inhibitors of key signaling proteins in platelet activation programs. As shown in **Figure 4.2A-B**, platelet spreading on nidogen was significantly reduced in the presence of a Src family kinase inhibitor (PP2), a Syk-specific inhibitor (BAY 61-3606), or the PI3K inhibitor wortmannin. Inhibition of PLC γ 2 with the broad-spectrum PLC inhibitor U73122 but not the inactive analog U73343 dramatically reduced both platelet adhesion and spreading on nidogen (**Figure 4.2C-D**). In parallel experiments and in accord with previous reports, we found that PP2, BAY 61-3606 and wortmannin significantly decreased platelet spreading on fibrinogen- and soluble collagen-coated surfaces (data not shown) (139). We next examined the role of the transcription factor NF- κ B, which has recently been demonstrated to play non-genomic roles in platelet activation, secretion and aggregation (138). Inhibition of I κ B kinase (IKK), an activator of NF- κ B, with IKK-16 decreased the number of adherent platelets and significantly reduced platelet spreading (**Figure 4.2C-D**). Additionally, inhibition of IKK decreased platelet adhesion and prevented platelet spreading on fibrinogen and soluble collagen (data not shown).

Together, Western blot and inhibitor studies suggest that both nidogen-1 and collagen share a common platelet receptor and the sequence of signaling events consistent with an ITAM-based signaling cascade. We therefore next tested the hypothesis that platelet activation by nidogen-1 was mediated by the ITAM receptor GPVI. Our results show that inhibition of GPVI with ACT017, a blocking antibody specific to GPVI, resulted in a significant decrease in the degree of adhesion of human platelets on nidogen. Consistent with previous studies, blockade of GPVI with ACT017

reduced the ability of platelets to spread on soluble collagen-coated surfaces (data not shown) (140,141). The degree of platelet adhesion and spreading onto nidogen-1 was significantly reduced by the presence of the ADP inhibitor apyrase, α IIB β 3 inhibitor eptifibatide, and AIIB2, a β 1 integrin blocking antibody (**Figure 4.2E-H**). Likewise, platelet spreading was reduced on fibrinogen and soluble collagen by apyrase and eptifibatide, while AIIB2 only reduced platelet adhesion and spreading on soluble collagen (data not shown). Taken together these observations suggest that nidogen is a ligand for GPVI and β 1 integrin which stimulates downstream tyrosine kinase signaling pathways including Src, Syk, PLC and PKC activation.

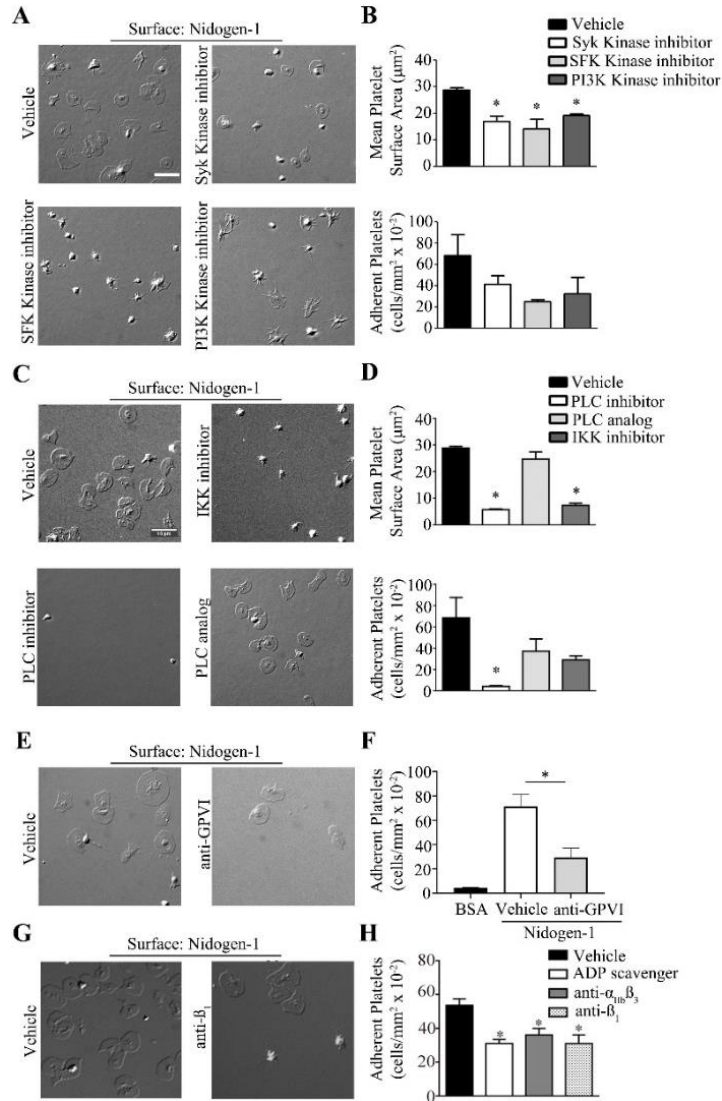


Figure 4.2. Effect of platelet inhibitors on platelet adhesion and spreading on nidogen-1. Human washed platelets ($2 \times 10^7/\text{mL}$) were pre-treated with (A) vehicle (DMSO), Syk inhibitor (Bay-61-3606, $5 \mu\text{M}$), SFK inhibitor (PP2, $10 \mu\text{M}$), PI3K inhibitor (wortmannin, 100 nM), (C) PLC inhibitor (U73122, $10 \mu\text{M}$), PLC inhibitor analog (U73343, $10 \mu\text{M}$) or IKK inhibitor (IKK-16, $10 \mu\text{M}$) (E) vehicle (DMSO) or anti-GPVI (ACT017 GPVI inhibitor, $40 \mu\text{g}/\text{mL}$) (H) vehicle (DMSO), anti- β_1 (AIB2, $20 \mu\text{g}/\text{mL}$), anti- $\alpha_{IIb}\beta_3$ (integrillin, $20 \mu\text{g}/\text{mL}$) (data not shown) or ADP scavenger (apyrase, $2 \text{U}/\text{ml}$) for 15 min prior to seeding on coverslips coated with recombinant nidogen-1 ($100 \mu\text{g}/\text{mL}$) for 45 min at 37°C and imaged using differential interference contrast (DIC) microscopy. Images are representative of at least 3 independent experiments. (B) and (D) Number of adherent platelets and mean surface area of platelet on nidogen-1 were recorded for 3 fields of view for each condition and expressed as mean \pm SEM. (F) and (H) Number of adherent platelets was recorded for 3 fields of view for each condition and expressed as mean \pm SEM. * $P < 0.05$ with respect to platelet adhesion in the absence of inhibitors.

4.6 Discussion

Here we report a potential hemostatic role for the extracellular matrix protein nidogen in supporting platelet adhesion and activation. Moreover, our data adds nidogen to the triumvirate of GPVI ligands present in the ECM including collagen and laminin. Nidogen exhibits a modular structure containing three globular domains, G1-3, separated by a linker region between G1 and G2 and a longer rod-like region located between G2 and G3 (43). Common to other ECM proteins, nidogen contains an epidermal growth factor-like (EGF) module crosslinked to a β -barrel domain within the G2 globule; this complex is responsible for mediating interactions with both perlecan and collagen type IV (128). The rod domain between G2 and G3 contains another four EGF-like repeats, the first of which contains an RGD binding motif known for potentiating integrin interactions. The six LDL receptor LY modules present in the G3 globule of nidogen mediate interactions with laminin via its single laminin γ 1 EGF-like repeat III4. The laminin-nidogen complex and nidogen alone but not laminin alone are known to bind collagen, resulting in ternary complex formation, permitted by the fact that the G2 domain of nidogen contains the binding site for nidogen-collagen interactions (142). The binding site for nidogen is predominantly located within the triple helix region of collagen; it is the triple helical structure of collagen that is thought to promote the dimerization of the platelet receptor GPVI to induce signaling through receptor tyrosine kinases. An alternative mechanism for GPVI-mediated dimerization and activation may be higher-order receptor clustering as a result of increased ligand density (143). This may underlie the mechanism by which the polymers of fibrin and laminin and nidogen dimerize GPVI to induce

platelet activation (144). How these ligands are recognized by GPVI remains to be established. Yet, the fact that soluble laminin and nidogen are incapable of activating platelets via GPVI in solution but rather require immobilization lends credence to the concept that the ECM microenvironment plays a critical role in congregating GPVI ligands to ensure hemostasis at sites of vascular injury (29). Taken together, our study suggests that nidogen-1 should be considered as an addition to the growing list of hemostatic proteins of the ECM.

Chapter 5. Design of a microfluidic bleeding chip to evaluate antithrombotic agents

Hari Hara Sudhan Lakshmanan, Adity A. Pore, Tia C. L. Kohs, Feyza Yazar, Rachel M. Thompson, Patrick L. Journey, Jeevan Maddala, Sven R. Olson, Joseph J. Shatzel, Siva A. Vanapalli, and Owen J. T. McCarty

This work was originally published by

Cellular and Molecular Bioengineering, 2020; 13(4):331-339.

Reused with permission from the publisher.

5.1 Abstract

Medical interventions that could prevent thrombosis without compromising hemostasis are key to improving the standard of care in patients that require anticoagulant and/or antiplatelet therapy. Since limited *in vitro* methods exist for assessing the effects of anticoagulants on hemostasis, the development of novel therapies to safely prevent thrombosis in patients relies on preclinical animal models and early phase human trials. Herein, we present the design of a microfluidic “bleeding chip” to evaluate the effects of antithrombotic therapies on hemostatic plug formation *in vitro*. The design of the microfluidic device consists of two orthogonal channels: an inlet that serves as a model blood vessel, and a bleeding channel to model hemostatic plug formation at sites of compromised endothelial barrier function. This is achieved by placing a series of 3 pillars spaced 10 μm apart at the

intersection of the two channels. The pillars and bleeding channel are coated with the extracellular matrix protein collagen. Perfusion of human whole blood through the microfluidic bleeding chip led to initial platelet adhesion and aggregation at the pillars followed by hemostatic plug formation and occlusion of the bleeding channel. This simple microfluidic device holds potential to be developed into a tool for assessing the effects of anticoagulant therapy on hemostasis.

5.2 Introduction

Hemostasis involves an interplay between the coagulation biochemistry and the platelet biology regulated by the forces of blood flow. While Chapters 3 and 4 investigated the biochemistry and platelet biology, Chapter 5 describes the development of a microfluidic device that integrates the biochemistry and platelet biology together under a physiologically relevant flow environment pertinent to the formation of a hemostatic plug. Our device holds potential to be used as a tool to investigate the bleeding risks associated with novel anticoagulants to prevent thrombosis. Moreover, this device can also be used to design and investigate therapies for bleeding disorders such as hemophilia.

5.3 Background

Patients of respiratory diseases, such as COVID-19 and flu suffer from severe inflammatory and thrombotic complications (145-148). Critically ill patients with the flu are prone to develop thrombotic manifestations including microvascular thrombosis, venous thromboembolism, and acute arterial thrombosis (149). The recent COVID 19 pandemic has increased the importance of understanding the

mechanisms of cross-talk between innate immunity and coagulation, often termed as immunothrombosis (150). While heparin is a convenient and biologically plausible attractive anticoagulant for infectious diseases due to its potential anti-inflammatory, anti-complement, and even direct antiviral effects, the persistently high rate of thromboembolic disease and the risk of hemorrhage associated with routine heparin use implies an urgent unmet need for alternative agents (14,151,152). This has led to significant enthusiasm for mobilizing clinical trials targeting either contact or TF pathway, balancing efficacy with safety. With regards to developing novel anticoagulants for treating thrombosis, this demands that these strategies ensure hemostatic safety, i.e. no abnormal bleeding. While the most clinically relevant conclusions regarding the safety of anticoagulants will ultimately be learned through clinical trials, *in vitro* models hold potential usefulness in revealing early safety and efficacy signals to guide future anticoagulant development of agents to prevent thrombosis in patients with infectious diseases without compromising hemostasis.

The key mechanisms that drive intravascular thrombus formation in diseased vascular beds were elucidated in part due to the creation and use of *in silico*, *in vitro*, *ex vivo* and *in vivo* models of thrombus formation under shear flow (6,81,153). Building upon this knowledge, a number of antithrombotic agents targeting either platelets or the coagulation cascade have been brought to market for use in the prevention or treatment of cardiovascular diseases including heart attack and stroke. Yet, despite advances in identifying targets to improve the efficacy of antithrombotic therapy, *in vitro* models to predict clinical bleeding are limited. This is particularly relevant in COVID-19, as new antithrombotic agents including inhibitors of platelet function, FX, or the contact activation system will likely have to be used in combination with

heparin as a standard-of-care therapy (154). An understanding of any potentially deleterious effects of such drug combinations on hemostasis will have to await the results of ongoing or proposed early phase clinical trials. This is due in part to the fact that the physical biology and rheology underlying hemostatic plug formation are ill-defined relative to our understanding of thrombosis (18).

The events that support hemostasis (extravascular) versus thrombosis (intravascular) are distinct in part due to the rheology of blood flow that differentially distributes blood constituents inside and outside blood vessels. Several elegant microfluidic models of the hemostatic response to a mechanical injury of the microvasculature have recently been developed (155,156). Here we extend these models based on the percolation theory of fluid dynamics to developed a model of blood transport into the tissue space at sites of compromised endothelial cell barrier function, such as in inflamed tissue beds and other forms of microangiopathy (74). To achieve this, we present the design of a microfluidic device with two orthogonal channels: a main channel that serves as a model blood vessel, and a bleeding channel to model hemostatic plug formation. We propose this model could be utilized to identify potential anticoagulant and antithrombotic targets and test agents to mitigate the thrombotic complications associated with COVID-19 whilst preserving hemostasis.

5.4 Materials and Methods

5.4.1 Design and fabrication of microfluidic pillar device

The design consists of two orthogonal channels: a main channel of width 150 μm , length 10 mm and a side channel of width 100 μm , length 3 mm as shown in

Figure 5.1A. We designed 3 circular pillars of diameter 20 μm , placed 10 μm apart at the intersection of two channels. All features have a uniform height of 50 μm . One side of the main channel serves as the inlet for blood, referred to as the *inlet channel* and the side channel with the pillars is termed the *bleeding channel* as indicated in **Figure 5.1A**. Only the bleeding channel is functionalized with fibrillar collagen to represent the subendothelial ECM. This method can be modified to include coating the bleeding channel with tissue factor alone or in combination with extracellular matrix proteins including collagen, nidogen, or laminin (157,158). The gaps in the pillars represent compromised endothelial barrier function as a result of inflammation or vascular injury. The physical parameters of the pillars including number, radius, and spacing could be modified to study the effects of the physical biology of barrier function on the kinetics of hemostatic plug formation.

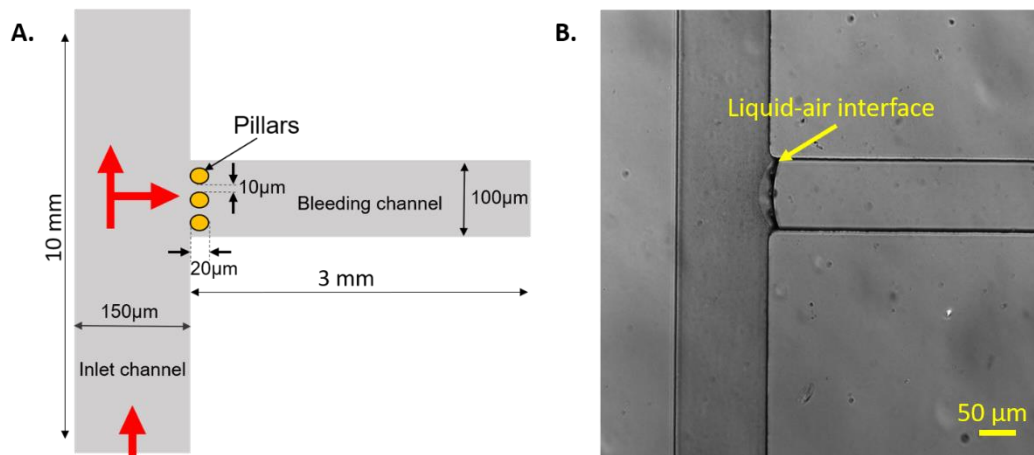


Figure 5.1 Design and development of a polydimethylsiloxane based microfluidic bleed chip. (A) The bleed chip consists of an inlet channel of width 150 μm , length 10 mm and a side channel of width 100 μm , length 3 mm referred to as the *bleeding channel*. At the intersection of channels, there are 3 pillars of 20 μm diameter with a 10 μm gap between them. Red arrows depict the direction of blood flow in the device (Figure not to scale). (B) Differential interference contrast (DIC) 10 \times image of the device where the bleeding channel is coated with fibrillar collagen (100 $\mu\text{g mL}^{-1}$). The arrow indicates the liquid-air interface during coating of the bleeding channel. Scale: 50 μm .

The design for the bleeding chip was drawn in AutoCAD and was printed on photomask (CAD/Art Services Inc., Oregon, USA). Standard soft-lithography techniques were used for making the bleed chip (159,160). The master mold was a single layer design, fabricated using a negative photoresist SU-8 2050 (Kayaku Advanced Materials, USA) with feature height of 50 μm . Microfluidic devices were made by mixing polydimethylsiloxane (PDMS) (Sylgard 184, Dow Corning, USA) monomer and the curing agent in a 10:1 ratio followed by degassing of the solution, pouring it over the master mold and curing it at 70°C for 2 hrs. After curing, the PDMS replicas were cut and peeled from the SU-8 mold. Fluid inlets and outlets were punched using a 1 mm biopsy punch (Miltex, Japan). The PDMS replicas were bonded to a cover glass (Thermo Scientific, USA) of thickness 170 μm , after plasma

treating (Harrick Plasma, Ithaca, New York) the surfaces for 90 s. This assembly was baked at 70°C for 4 mins to strengthen the bonding.

To coat the bleeding channel with fibrillar collagen (100 µg ml⁻¹, Chronolog), a collagen droplet of 2 µL volume was introduced by pipette into the bleeding channel; the leading edge of the droplet meniscus was advanced until the collagen solution reached the pillars as observed with a 10× microscope objective. Capillary forces were sufficient to restrict the collagen solution from entering the orthogonal vessel channel, thus allowing selective coating of the bleeding channel and pillars with collagen as shown in **Figure 5.1B**. After an hour of incubation at room temperature, both channels were washed with phosphate buffer saline (PBS) and blocked with 5 mg/mL denatured bovine serum albumin (BSA) for 1 hr followed by washing with PBS. Relevant controls would include coating the bleeding channel with BSA.

5.4.2 *Experimental setup*

Human venous blood was collected from healthy adult volunteers into a syringe filled with 3.8% sodium citrate (1/10th blood volume) in accordance with the Oregon Health & Science University Institutional Review Board. Citrated blood was recalcified with the addition of (1:9 recalcification buffer: blood) recalcification buffer (75 mmolL⁻¹ CaCl₂ and 37.5 mmolL⁻¹ MgCl₂), to allow for coagulation. This method could be modified for use with reconstituted blood (purified red blood cells, platelets, and plasma) to allow for parameters such as platelet count to be adjusted. Recalcified blood was loaded into a 1 mL syringe and assembled onto a Harvard 2000 syringe pump as shown in **Figure 5.2**. The syringe was connected to the device inlet with a

0.5 mm polyethylene tubing (Braintree scientific, USA) and the blood was perfused at a constant flow rate of $10 \mu\text{L min}^{-1}$, which corresponds to an arterial shear rate of 1000 s^{-1} in the inlet channel. The outlet of the bleeding channel was connected with polyethylene tubing (20 cm length) graduated every 0.5 cm to record the velocity of blood flow in the bleeding channel. The main channel outlet was also connected to PE tubing of similar length for waste collection. Platelet adhesion, aggregation and thrombus formation in the device near the pillars during blood perfusion was recorded using Kohler illuminated Nomarski differential interference contrast (DIC) optics with a Zeiss $10\times$ lens on a Zeiss Axio Imager M2 microscope (Carl Zeiss MicroImaging GmbH, Germany). Graduations in the polyethylene tubing connected to the bleeding channel enabled manual monitoring and recording of blood velocity and volume in the bleeding channel.

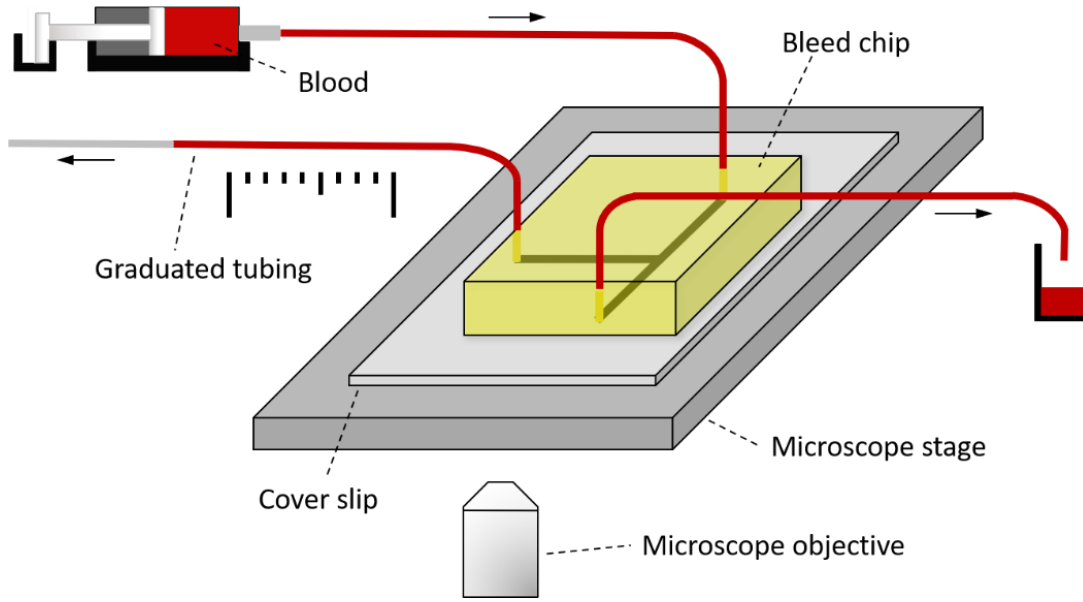


Figure 5.2 Experimental setup for the use of bleed chip with the blood sample.

Device inlet is connected to a syringe pump with a syringe filled with recalcified whole human blood. The bleeding channel is connected to a 0.5 mm polyethylene tube with graduations every 0.5 cm to record the blood flow rate through the bleeding channel. An equal length of polyethylene tubing is connected to the second outlet leading to waste collection. Real time dynamics of blood flow inside the bleed chip is captured with the 10× objective of a DIC Zeiss Axio Imager 2 microscope. Arrows denote the direction of blood flow.

5.5 Results and discussion

5.5.1 Modeling blood flow in the microfluidic pillar device

We performed computational fluid dynamic simulations using a 2D model of the bleeding chip created in COMSOL to predict the hemodynamics at and near the interface created by the pillars. Our model included the constant flow rate of $10 \mu\text{L min}^{-1}$ at the inlet, a constant atmospheric pressure at the main channel outlet and a constant flow rate of $2 \mu\text{L min}^{-1}$ at the bleeding channel outlet. Blood was modeled as a non-Newtonian fluid using power-law of viscosity as described in the literature

(161). Our initial model was based on the average physical parameters of density and viscosity of human whole blood and did not consider changes in these parameters due to the addition of anticoagulants, recalcification buffer, or differences in donor hematocrit. Based on the inlet flow rate, we estimated a Reynold's number (Re) ≈ 0.5 for flow in the device resulting in an assumption of creeping flow inside the device. Microfluidic devices enable the use of low blood volume to simulate physiological shear rates observed in arteries and veins, however due to the inherent small dimensions the Re produced in these devices are < 1 compared to the Re observed in arteries and veins that are in range of 1-4000 (162). Although the low Re flow in the model may not capture the physiology of blood flow, this is a limitation associated with the field of microfluidics in general and there remains a need for scaling approaches that better relate the rheology observed in microfluidic models to the biophysical parameters of veins, capillaries and arteries. The Navier-Stokes equation for creeping flow was solved using COMSOL under steady state conditions to create velocity and shear rate profiles as shown in **Figure 5.3A and B**. Velocity profiles derived from the microfluidic device indicated a series of stagnation points along the pillar surface and the corners at the channel intersection **Figure 5.3A**. Platelet aggregation at stagnation points has been shown to initiate a core and shell thrombus wherein the core consists of procoagulant platelets which facilitates localized thrombin generation whereas the shell is comprised of weakly activated platelets which acts as a rheological shield (66,163). For our bleeding chip model, the shear rate profile shows a change in shear rate from 1000 s^{-1} in the inlet channel to 9000 s^{-1} in the spaces between the pillars of the bleeding channel, thus introducing a shear gradient. This region of increasing shear rate was followed by decreasing shear rates in the bleeding channel downstream of the pillars as shown in **Figure 5.3B**. Rapid

transition of shear rate over short distances has been shown to promote platelet activation and aggregation due to platelet GPIb-von Willebrand factor (vWF) interaction (80). The Péclet number (Pe) $\gg 1$ for the transport of zymogens from bulk flow to the pillar surface at steady state conditions implies a significant dependence on advection as the primary transport mechanism (72,78).

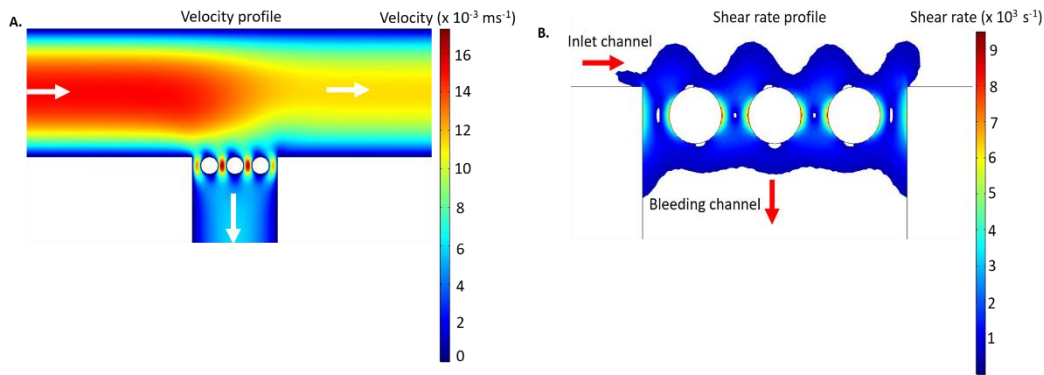


Figure 5.3 Estimation of shear rate and velocity in the bleed chip using numerical modeling. Computational fluid dynamics model of the bleed chip was solved using COMSOL to generate (A) surface plots of velocity and (B) shear rate in the bleed chip at initial steady state conditions. (A) Surface plot of velocity in the bleed chip at steady state conditions. White arrows indicate the direction of flow in the device. Blood is modeled as a non-Newtonian power law fluid and the Navier-Stokes equation is solved using COMSOL to compute the velocity and shear rate in the bleed chip at steady state conditions. (B) Wall shear rate increases from 1000 s^{-1} in the main channel to 9000 s^{-1} on pillar surfaces and then decreases to 1000 s^{-1} distal to the pillars in the bleeding channel.

5.5.2 Hemostatic plug formation in the microfluidic pillar device

We experimentally observed the initiation and propagation of hemostatic plug formation at the sites predicted by our computational model as “locations of shear gradients”. The dynamics of hemostatic plug formation were imaged by DIC microscopy. **Figure 5.4A** shows the progression of platelet aggregation and

coagulation around the pillars at the entrance of bleeding channel at 0 min, 5 min, and 10 min perfusion times. Hemostatic plug formation was observed to initiate at and around the pillars as indicated by the dotted circle in **Figure 5.4A**. The growth of the hemostatic plug continued in the direction of flow inside the bleeding channel over the next 5 min. By 10 min a patent hemostatic plug was formed and blood flow ceased. In contrast, in the absence of coagulation using sodium citrate-anticoagulated whole blood, hemostatic plug formation was incapable of stopping blood flow in the bleeding channel. At present the time to occlusion is a laboratory-based experimental parameter, akin to a clotting time in an APTT assay; future studies are required to relate this parameter to the kinetics of hemostatic plug formation at sites of vascular injury or compromised barrier function and relevant scaling of the model to vascular beds, veins and arteries.

The velocity of blood in the bleeding channel was recorded by quantifying the rate of blood flow within a graduated polyethylene tubing connected to the distal end of bleeding channel. We report the scaled velocity $(\bar{u}) = \frac{u_i}{u_0}$ in **Figure 5.4B** where u_i is the velocity of blood measured at a given time point and u_0 is the initial velocity of blood measured in the tubing connected to the bleeding channel. Our pilot data show a reduction in blood flow velocity as a function of time. Of note, we observed fluctuations in scaled velocity due to ‘rebleeding’ wherein a portion of the hemostatic plug would become unstable and erode in a similar manner as has been observed in animal models of hemostatic plug formation (164,165). Our current technique to measure velocity of blood in the bleeding channel is limited to the granularity of measuring discrete time intervals associated with 1.3 μ L gradations in blood volume; continuous monitoring of the blood volume and velocity with techniques including

gravimetric or doppler measurements of volumetric flow rate would improve the precision of this platform, albeit at an increased cost of design.

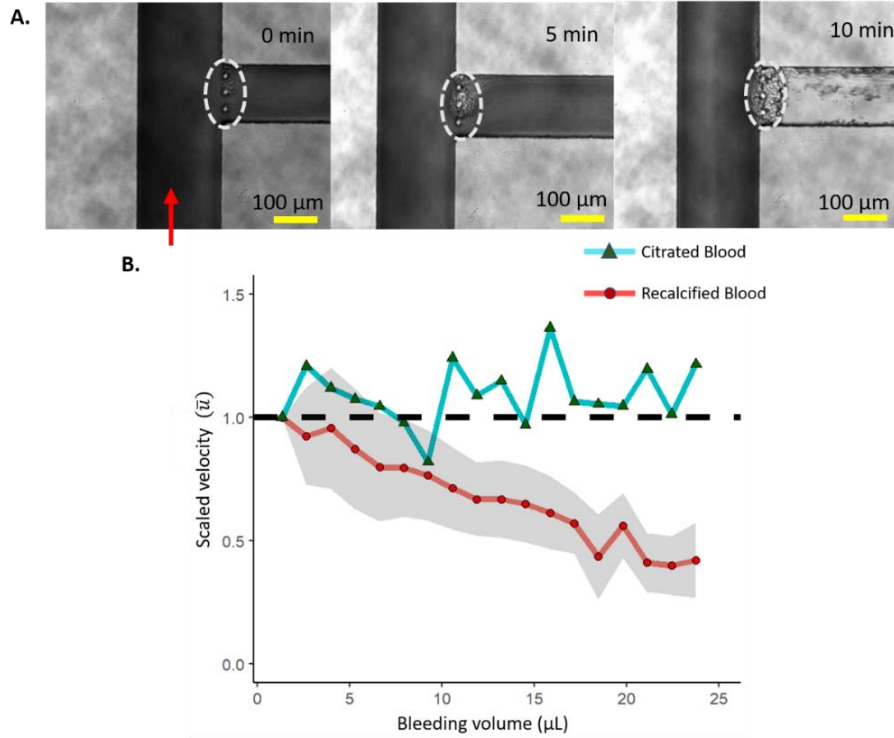


Figure 5.4 Dynamics of blood flow and hemostatic plug formation in the bleed chip.

Human whole blood, with or without recalcification, was perfused through the bleed chip at a constant flow rate of $10 \mu\text{L min}^{-1}$ using syringe pump. The dynamics of hemostatic plug formation in the pillar region was recorded through $10\times$ DIC microscope and the velocity of blood in the bleeding channel was recorded through a graduated tubing connected to the bleeding channel outlet and transformed into scaled velocity. **(A)** $10\times$ DIC images of the pillar region of the bleed chip at 0, 5 and 10 mins after perfusion of recalcified whole human blood at a constant inlet flow rate of $10 \mu\text{L min}^{-1}$. Red arrow depicts the direction of blood flow in the device and the white ellipse with broken lines indicates the pillar region. Scale: $100 \mu\text{m}$. **(B)** Scaled velocity of blood (\bar{u}) as a function of volume of blood in the bleeding channel. Scaled velocity ($\bar{u} = \frac{u_i}{u_0}$) is the ratio of blood velocity at a given time point (u_i) to the initial blood velocity (u_0) measured in the bleeding channel. Dashed line indicates a scaled velocity (\bar{u}) of 1.0. Errors are \pm standard error of means (SEM) for four trials.

Microthrombi can cause death in infectious diseases such as COVID-19, sometimes despite the administration of low molecular weight heparin (LMWH) (166-168). This

warrants the need for novel safe and effective antithrombotic strategies to combat thrombosis in patients with infectious diseases, as well as our lack of understanding of the pathology of thrombosis during infection. Novel anticoagulant strategies such as inhibitors of the contact activation system (CAS) of coagulation and stimulators of the protein C pathway will likely see introduction into clinical trials in combination with heparin products (154). As LMWH is known to compromise hemostasis, combinations of novel anticoagulants with LMWH will require careful study to ensure no compounding effects on hemostasis. The development of *in vitro* or *ex vivo* models of hemostasis may be useful in predicting the potential for adverse major bleeding events for the use of novel anticoagulants as monotherapy or in combination with LMWH prior to evaluation in clinical trials. Herein, we describe the development of a simple microfluidic-based assay to model hemostasis. We aim to use this model for evaluation and dose selection of CAS inhibitors for use in clinical trials to evaluate their safety and efficacy in mitigating thrombosis associated with infectious diseases.

Chapter 6. Modeling the effect of blood vessel bifurcation ratio on occlusive thrombus formation

Hari Hara Sudhan Lakshmanan, Joseph J. Shatzel, Sven R. Olson, Owen J.T.

McCarty, Jeevan Maddala

This work was originally published by the journal of
Computer Methods in Biomechanics and Biomedical Engineering, 2019;
22(11):972-980.

Reused with permission from the publisher.

6.1 Abstract

Vascular geometry is a major determinant of the hemodynamics that promote or prevent unnecessary vessel occlusion from thrombus formation. Bifurcations in the vascular geometry are repeating structures that introduce flow separation between parent and daughter vessels. We modelled the blood flow and shear rate in a bifurcation during thrombus formation and show that blood vessel bifurcation ratios determine the maximum shear rate on the surface of a growing thrombus. We built an analytical model that may aid in predicting microvascular bifurcation ratios that are prone to occlusive thrombus formation. We also observed that bifurcation ratios that adhere to Murray's law of bifurcation may be protected from occlusive thrombus formation. These results may be useful in the rational design of diagnostic microfluidic devices and microfluidic blood oxygenators.

6.2 Introduction

Studies in Chapters 3, 4 and 5 focused on the role of biochemical reactions, platelets and flow in hemostasis. Studies in Chapter 6 focus on thrombosis, in particular the effect of microvascular geometry on determining the potential for a thrombus to grow and completely block the vessel. A first principles-based analytical mathematical model was developed to correlate the microvascular bifurcations to the shear rates inside the vessel. This model was used to analyze the effect of the diameter-ratios of the vessels in a bifurcation on the dynamics of shear rate during thrombus growth. The model developed in this study could be useful for the design and analysis of microfluidic networks for research and the clinic.

6.3 Background

Blood vessel injury provokes the process of hemostasis which stops the extravasation of blood into the extravascular space. Hemostasis involves the aggregation of platelets under flow in conjunction with fibrin formation following activation of the coagulation cascade. The growth of this aggregate of platelets bound together by fibrin – a thrombus – is ideally stymied as the injury is sealed. However, in pathologic situations normal clot formation can go unchecked, leading to progressive thrombus growth and ultimately blood vessel occlusion and damage. Clinically this process – thrombosis – can incur substantial patient morbidity, medical resources and costs (2). Examples of pathologic thrombosis include coronary artery thrombosis, venous thromboembolic disease (VTE), including deep vein thrombosis, and pulmonary embolism.

Thrombosis in larger arteries and veins leads to significant clinical symptoms including mortality and morbidity. Angiography and duplex imaging can be used to identify large vessel thrombosis; however currently available imaging techniques lack requisite sensitivity to evaluate smaller vessels such as arterioles and venules, despite the fact that altered blood flow and thrombi in the microvasculature is associated with cardiovascular disease (75).

Clinical decision making when it comes to anticoagulation is often dichotomous; for example, duration of anticoagulation for VTE is primarily dependent on whether the event was provoked by a transient risk factor or not, with “unprovoked” VTE carrying a high risk of recurrent thrombosis and typically mandating lifelong anticoagulation (169). Arterial thrombosis can be treated with antiplatelet agents or anticoagulants depending on the thrombus location and etiology (170). While select therapies may improve outcomes in a subset of patients with thrombosis, there remains an unmet need to better stratify patients who will benefit from the available therapies, balancing safety with efficacy. More granular risk stratification could conceivably be aided by mathematical models that could predict occlusion in microvessels and imaging to visualize microvascular thrombi (171). Vessel geometry and local hemodynamics are factors that contribute to initiation of thrombus formation leading to vessel occlusion. Bifurcations present a complex hemodynamic environment with unique properties that may specifically predispose these regions to thrombosis (172). Results from microfluidic studies that involve multiple bifurcations demonstrate the importance of geometry in the kinetics of thrombus formation (161). Clinically, large vessel bifurcations are common sites of arterial plaques and

thrombosis, predisposing patients to stroke in the case of carotid artery bifurcation (173).

Hemostasis is initiated by platelets, and platelet transport is itself dependent on hematocrit, shear rate and geometry. Mathematical models that describe the thrombus growth rate predict the transport of platelets to the site of injury and the activation of platelets (1). Platelets act as catalysts for the recruitment and activation of coagulation factors and additional platelets, both of which sustain thrombus growth and restrict it to the site of injury. Convective transport of platelets to the site of thrombus formation and reactions of select coagulation factors define the growth rate of the thrombus. The thrombus structure and the growth rate is a dynamical process which varies due to constant changes in hemodynamics within and around the forming thrombus.

Recent observations have established the 'core and shell' structure theory of thrombus formation (66,163,174,175). The core of the thrombus contains fully activated platelets bound together by fibrin, while the shell contains weakly activated platelets that are subject to increased shear forces due to blood flow. Platelets upstream of the thrombus adhere to the shell, while the weakly bound platelets on the downstream surface of the thrombus leave the shell due to shear forces. Biophysical studies based on insights from the 'core and shell' structure describe thrombus growth under flow based on local shear rates (176,177). Experimental studies and mathematical models suggest that the platelet aggregation rate under flow is non-linearly dependent on shear rate (178).

Belyaev et al. built on the previous theories of thrombus growth rate and proposed a critical shear rate ($\dot{\gamma}_{cr}$) of 3400 s^{-1} at which the rate of platelet attachment to the shell equals the detachment rate of platelets from the shell due to flow (176). As the shear rate on the thrombus surface reaches the critical shear rate the growth rate becomes zero. The theory of critical shear rate is built on the flow dependence of platelet aggregation on the thrombus shell. Recent studies have shown the importance of vascular geometry and boundary conditions in thrombus formation and evolution of shear rate (79,179).

Blood vessels narrow and bifurcate into smaller vessels to perfuse tissues as capillaries. Murray theorized the optimum branching of blood vessels based on a minimum work principle and showed that the sum of the cubes of daughter vessel diameters should equal the cube of the parent vessel diameter (180); this has been supported by *in vivo* evidence (181-183). Zamir stated that a vessel bifurcates in a way that minimizes the total drag on the parent and daughter vessels in the bifurcation (184). While these theories have provided insights into the selection principles behind bifurcations in the vasculature from a hemodynamics perspective, in this report we analyzed bifurcation ratios in terms of thrombus growth and vessel occlusion.

6.4 Materials and methods

6.4.1 Modeling the circulatory system as a hydraulic circuit

A vascular bifurcation is composed of a parent vessel and two daughter vessels that diverge from the parent vessel. Diameters of the vessels are given by D , D_1 and D_2

for the parent, daughter 1 and daughter 2, respectively as shown in Figure 1.

Bifurcation ratios are defined as ratios of daughter vessel diameters to the parent vessel diameter, i.e. $r_1 = D_1/D$ and $r_2 = D_2/D$. Given the fluid properties, shear rate in this geometry is a function of boundary conditions of the geometry and the hydraulic resistances of the branches. In this work, we assume a constant pressure boundary condition for a given bifurcation geometry (176).

The heart is modeled as a pump of constant flow rate (averaged over systole and diastole) and the vascular network is modeled as a series of blood vessels of varying sizes interconnected together. The smallest vessels (diameters $< 100 \mu\text{m}$) in the vascular network offer the highest resistance to the network. These resistances further increase as a result of plaque or thrombus formation. Importantly, single microvasculature bifurcation of small vessels is modeled as a parallel resistance with the rest of the vascular network as shown in **Figure 6.1**, justifying our constant pressure boundary condition. The overall resistance offered by the remaining vascular network is defined as systematic vascular resistance (SVR). **Figure 6.1B** illustrates the nomenclature used in the modeling the inlet diameters of vessels (D , D_1 and D_2), thrombus length (L_{12}), vessel lengths (L , L_1 and L_2) and the open diameter of the thrombotic region (D_{12}). The daughter vessel with the thrombus is modeled as a series of three resistances – R_{11} (portion of the vessel upstream of thrombus), R_{12} (thrombus), and R_{13} (portion of the vessel downstream of thrombus). **Figure 6.1C** depicts the bifurcation modeled as resistances connected to a common source – heart.

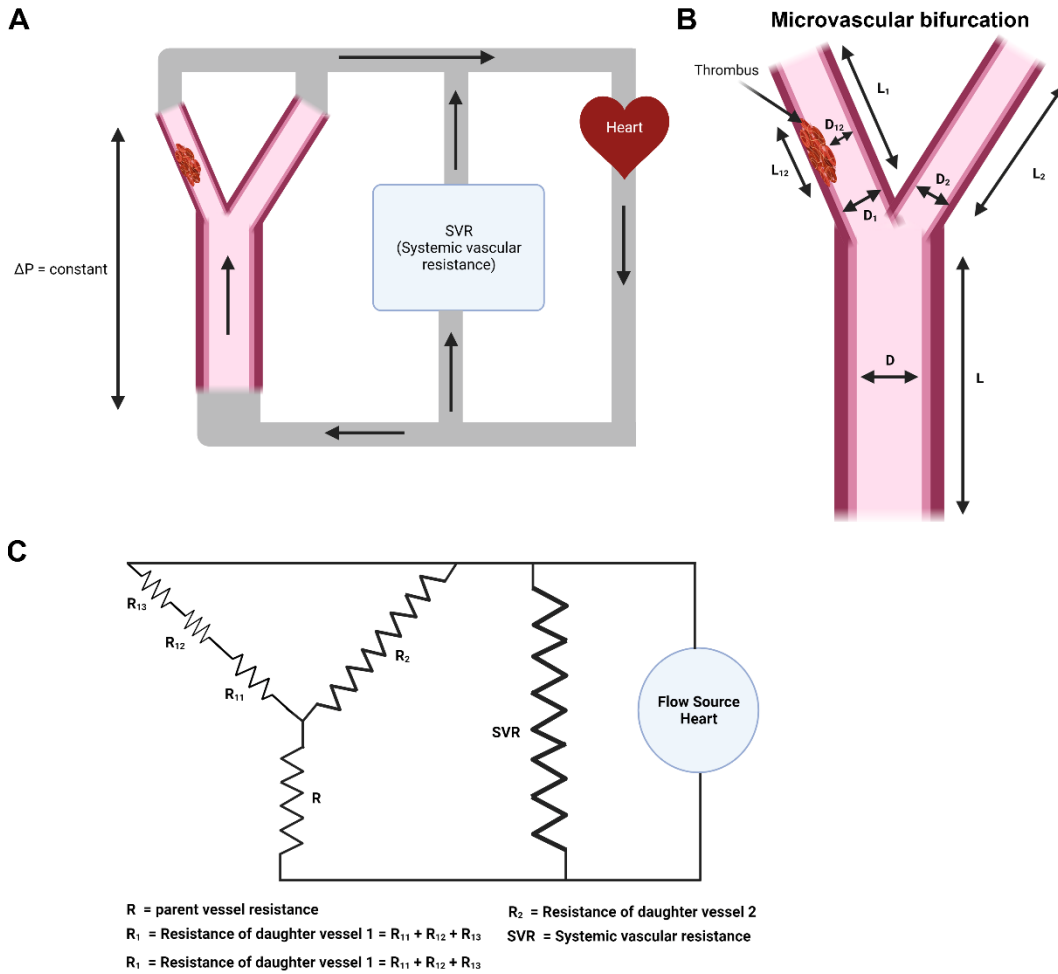


Figure 6.1 Modeling a microvasculature bifurcation with a thrombus as a series of resistances. (A) Sketch of a vessel bifurcation with a thrombus in one of the daughter vessels modeled in parallel with the rest of the vessels as the systemic vascular resistance (SVR) fed by the heart. (B) Vessel bifurcation sketch with the parameters considered in the model. D – Diameter of the parent vessel, D_1 and D_2 original diameters of the daughter vessels. L – length of the parent vessel, L_{12} – Thrombus length, D_{12} – Diameter of the vessel region available for thrombus growth, L_1, L_2 – Total lengths of daughter vessels. (C) The system of a bifurcation along with larger vessels modeled as a hydraulic circuit with the vessels as the resistance to the flow of blood from the source – heart. R – Hydraulic resistance of the parent vessel of a bifurcation, R_{12} – Hydraulic resistance of the thrombotic region in daughter 1 as a function of time, R_{11} and R_{13} – Resistance of non-thrombotic regions of daughter 1. R_2 – hydraulic resistance of daughter 2. Flow source denotes the heart.

6.4.2 *Mathematical modeling of flow and shear rate in microvascular bifurcations*

Flow rate, Q , through a cylindrical vessel is given as the ratio of pressure drop (ΔP) to hydraulic resistance (R_H) based on the Hagen Poiseuille relation,

$$Q = \frac{\Delta P}{R_H} \quad (1)$$

The hydraulic resistance, R_H , is defined as a function of fluid viscosity (μ), length (L_i) and diameter of the vessel (D_i), where, $R_H = \frac{128\mu L_i}{\pi D_i^4}$. In our case, ΔP is the pressure drop across the entire bifurcation while R_H is the total hydraulic resistance of the bifurcation. A change in the diameter of the vessel available for blood flow due to the formation of an occlusive thrombus changes the overall hydraulic resistance. Occlusion ratio (x) is the ratio of thrombus height to the vessel diameter with 100 multiplied by occlusion ratio defined as the percentage of occlusion. In our case, the difference in D_1 and D_{12} gives the thrombus height while D_1 the initial diameter of the vessel.

$$x = \left(1 - \frac{D_{12}}{D_1}\right) \quad (2)$$

The hydraulic network is analogous to an electrical network. Kirchhoff's circuit laws are applied to the vascular bifurcation to obtain overall resistance. Total resistance of the bifurcation (R_t) is the sum of the resistance due to the parent vessel (R) and the daughter vessels (R_1 and R_2). The resistances R_1 and R_2 are parallel to each other and

together they are in series with the parent vessel resistance; the total resistance is given by:

$$R_t = R + \frac{R_1 * R_2}{R_1 + R_2} = \frac{128\mu}{\pi} \left(\lambda + \frac{\lambda_1 * \lambda_2}{\lambda_1 + \lambda_2} \right) \quad (3)$$

$$\text{where } \lambda_1 = \frac{L_{11}}{(D * r_1)^4} + \frac{L_{12}}{(D * r_1 * (1 - x))^4} + \frac{L_{13}}{(D * r_1)^4}, \lambda_2 = \frac{L_2}{(D * r_2)^4}$$

The above relation captures the hydraulic resistance of the bifurcation for any stage of thrombus growth, defined using occlusion percentage. The overall shear rate on the thrombus is estimated using the hydraulic resistance equation along with the given pressure drop boundary condition.

We assume blood to be a Newtonian fluid and the flow to be in the steady state laminar region. As stated in the introduction of the thesis, under high shear rates blood behaves as a Newtonian fluid. Therefore, we expect this to be a reasonable and valid assumption for the high shear blood flow observed in capillaries, arterioles and venules that forms the focus of the current study. Wall shear rate for laminar flow is given by $\dot{\gamma} = 32Q/\pi D^3$. Solving for flow rate in the vessel with the thrombus, we obtain equation (4) that describes the shear rate on the surface of the thrombus ($\dot{\gamma}_{th}$) at an occlusion ratio of 'x'.

$$\dot{\gamma}_{th} = \frac{\lambda_2 \dot{\gamma}}{(r_1^3 (1 - x_1)^3) (\lambda_1 + \lambda_2)} \quad (4)$$

$$\dot{\gamma} = \frac{32\Delta P}{\pi D^3 R_t}$$

Where $\dot{\gamma}$ is the wall shear rate in the parent vessel and r_1 is the bifurcation ratio of the daughter vessel with the thrombus. The derivation for $\dot{\gamma}_{th}$ is detailed in **Appendix A**. In order to simplify the analysis in terms of thrombus length, we introduce the dimensionless parameter ' ϕ ', which is thrombus length ratio defined as the ratio of length of the thrombus to length of the vessel $\phi = L_{12}/L_1$. Introduction of ' ϕ ' transforms the parameter λ_1 into $\lambda_1 = (L_1/r_1^4 D^4) [(1 - \phi) + \phi/(1 - x_1)^4]$. Equation (4) is a valid relation to estimate shear rate for any boundary condition and any configuration of a bifurcation.

6.5 Results

Dynamics of shear rate as function of geometry change due to thrombus growth was simulated in COMSOL using a two-dimensional (2D) bifurcation model. The Navier-Stokes equation was solved at every node of the finely meshed model until convergence (tolerance of 1e-6). Steady state simulations were performed at each stage of occlusion from 0 to 100% in steps of 10% increase. Constant pressure drop across the bifurcation was employed as the boundary condition. **Figure 6.2A** shows the surface plot of shear rate in a bifurcation with a thrombus at 70% occlusion. We assumed a rectangular shape for the thrombus and increased only the height of the thrombus to correspond with various percentages of occlusion. Studies in the literature suggest that the length of thrombus remains relatively constant during its growth especially in the microvasculature (185). We also considered blood to be a Newtonian fluid with a constant viscosity. **Figure 6.2B** shows the scaled shear rate

which is the ratio of maximum shear rate to the initial shear rate in the thrombus region plotted against the percentage of occlusion in the bifurcation. We employed a 2D COMSOL model of the bifurcation to validate the non-linearity in shear rate on the thrombus surface in a bifurcation. We observed the scaled shear rate (ratio of instantaneous shear rate to initial shear rate on thrombus surface) increase until 60% occlusion and then fall to zero at 100% occlusion. This non-linearity in shear rate observed in our COMSOL model agrees well with the previous computational and experimental reports that used pressure driven flow (179).

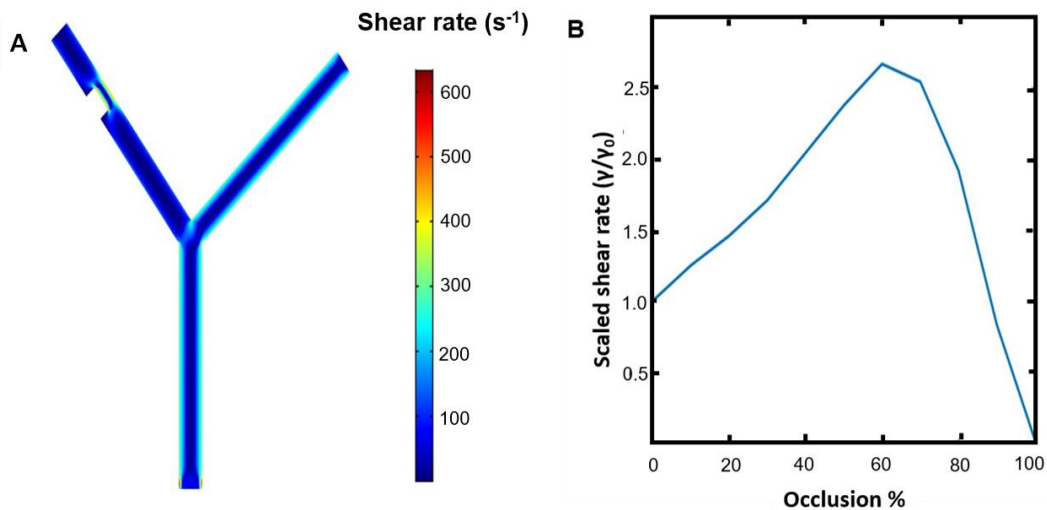


Figure 6.2 Estimation of the shear rate on thrombus surface in a microvascular bifurcation. 2-dimensional (2-D) finite element model of a microvascular bifurcation with a thrombus was setup and solved in COMSOL to estimate the shear rate on the thrombus in one of the daughter vessels of a bifurcation (A) 2-D surface plot of shear rate in a bifurcation under a constant pressure drop (ΔP) of 100 Pa. The thrombus is modeled as a rectangular obstruction in the daughter vessel. (B) Scaled shear rate ($\frac{\gamma}{\gamma_0}$) on the thrombus estimated for 0 to 100% occlusion of the daughter vessel.

We next analytically examined the shear rate around a thrombus of constant length, without any local turbulence, for different parameters and boundary conditions. The shear rate was estimated using the Hagen Poiseuille relation and laminar flow shear

rate model. Solving equation (4) in MATLAB for different occlusion percentages under constant flow rate and constant pressure drop boundary conditions allows us to examine the effect of boundary conditions on the shear rate behavior. **Figure 6.3** compares the scaled shear rate against the occlusion percentage for constant pressure drop and constant flow rate conditions. Equation (4) is used to estimate the shear rates on the thrombus surface for constant pressure drop and constant flow rate boundary condition by updating the $\dot{\gamma}$, wall shear rate in the parent vessel through updating the total resistance of the bifurcation with either a constant flow rate (Q) or a constant pressure drop (ΔP). We see that progression of shear rate is non-linear as the vessel occludes and this non-linearity agrees with the results from our COMSOL model. Unlike a straight channel, in a bifurcation both the boundary conditions yield non-linear shear rate curves. Under constant flow rate, as the occlusion percentage increases in one of the daughter vessels the flow gets diverted to the other daughter without the thrombus while the total flow into the bifurcation remains constant. However, the velocity around the stenotic region increases due to a decrease in diameter until a significant reduction in flow rate occurs.

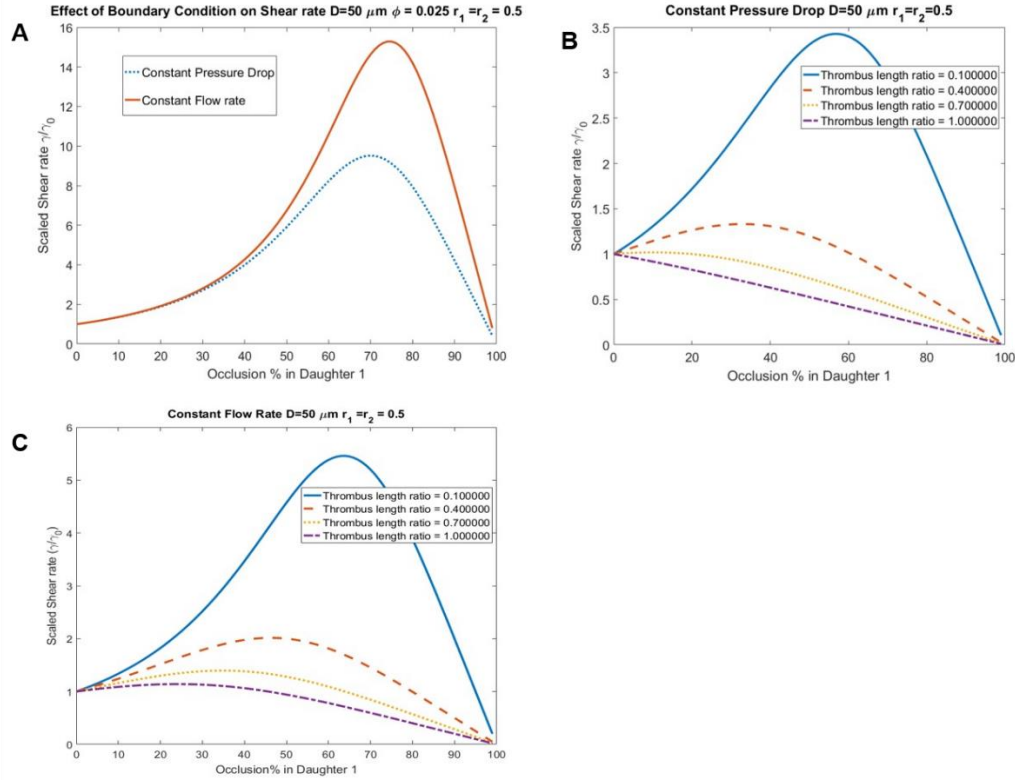


Figure 6.3 Effect of boundary conditions and thrombus length ratio (ϕ) on the dynamics of shear rate in a bifurcation. Equation (4) was solved with either a constant pressure drop or a constant flow rate across the bifurcation to estimate the shear rates on the surface of thrombus in the daughter vessel. **(A)** Shear rate dynamics for the thrombus growing in a daughter vessel of the bifurcation for constant pressure drop across the bifurcation and constant inlet flow rate to the bifurcation boundary conditions. Occlusion % denotes the percentage of vessel occlusion by thrombus. **(B)** Shear rate dynamics on a thrombus in a bifurcation under constant inlet flow rate for different thrombus length ratios (ϕ). **(C)** Shear rate dynamics on a thrombus in a bifurcation under constant pressure drop for different thrombus length ratios (ϕ).

Figure 6.3B and C show the scaled shear rate profiles for different injury length ratios (ϕ) under constant flow rate and pressure drop boundary conditions respectively; a bifurcation with an inlet diameter of $38 \mu\text{m}$ with a bifurcation ratio of $r_1 = r_2 = 0.5$ was used in these results. With an increase in ϕ , the maximum shear rate on the thrombus decreases under both constant flow rate and pressure drop

conditions suggesting that the degree of shear force experienced by the surface of a thrombus decreases with thrombus length. The shear rate behaves linearly for $\phi > 0.7$ under constant pressure boundary conditions while under constant flow rate the shear rate continues to behave in a non-linear manner even for $\phi = 1$.

Belyaev et al. examined the effect of thrombus length on the maximum shear rate during thrombus growth in a straight vessel (176). In our work we looked at the effect of lateral flow in an adjacent vessel on the thrombus under select configurations. Specifically, we studied the impact of bifurcation ratios on the maximum shear rate around the thrombus and identified the bifurcation ratios predicted to prevent occlusion.

An estimate of maximum possible shear rate during thrombus growth is crucial to determine the occlusivity of the thrombus. Maximum shear rate during thrombus growth is a function of thrombus length ratio, bifurcation ratio and the length of the blood vessel. We used the MATLAB symbolic toolbox to solve equation (4) for the occlusion ratio (x_1) at which the shear rate reaches maximum

$$x_1 = 1 - \left(\frac{l_1 L \phi r_2^4 + \phi l_1 l_2}{l_1 l_2 (1 - \phi) + L l_1 (1 - \phi) r_2^4 + L l_2 r_1^4} \right)^{\frac{1}{4}} \quad (5)$$

where l_1, l_2 are the lengths of daughters 1 and 2, L is the parent vessel length, ϕ is thrombus length ratio and r_1, r_2 are the bifurcation ratios. The occlusion ration at which the shear rate will reach its maximum during thrombus growth can be estimated using equation (5) for various bifurcation ratios r_1, r_2 and can be compared to the critical shear rate ($\dot{\gamma}_{cr}$) to determine the occlusivity of a thrombus.

6.5.1 Complete occlusion and partial occlusion in terms of bifurcation ratios

In order to make the comparison more convenient we introduce a dimensionless quantity that we call ‘critical shear ratio’, defined as the ratio of maximum shear rate around a thrombus to the critical shear rate ($\dot{\gamma}_{max}/\dot{\gamma}_{cr}$). If a thrombus has a critical shear ratio of more than 1, it means that the shear forces around the thrombus are strong enough to disrupt the platelet attachment and stop its growth. For all bifurcation configurations with critical shear ratio > 1 , the thrombus is defined as non-occlusive.

In **Figure 6.4**, on the ‘y’ axis is the ratio of maximum shear rate during thrombus growth to the critical shear rate, ‘critical shear ratio’ and on the ‘x’ axis is the bifurcation ratio r_1 . Each curve in the plot is for a r_2 value as given in the legend. The red dotted horizontal line that separates the plot into two regions is the line at which $\dot{\gamma}_{max} = \dot{\gamma}_{cr}$ or critical shear ratio = 1. We consider bifurcation ratios only in the range of 0.1 to 0.9 as the bifurcation ratios observed in vasculature lie in that range (181). The region of the curve that lies above the red dotted line denote the bifurcation ratios where the maximum shear rate on the thrombus surface exceeds the critical shear rate. The region of the curve below the red dotted horizontal line denotes the bifurcation ratios that do not disrupt the growth of thrombus to occlusion as the maximum shear rate is less than the critical shear rate. When the maximum shear rate is less than the critical shear rate, it means that the hydrodynamic forces are not strong enough to disrupt the thrombus growth leading it to complete occlusion. These data suggest that the biophysical properties of bifurcation ratios regulate thrombus growth. Specifically, for a bifurcation with a parent vessel diameter of $38 \mu m$ with ϕ

of 0.02, all combinations of bifurcation ratios of r_1 and r_2 that lie above the critical shear ratio of 1 are not predicted to produce an occlusive thrombus. Taken together, our data suggest that bifurcation ratios of blood vessels play a significant role in determining the maximum shear rate on a thrombus growing in the daughter vessels. Even though the initial critical shear ratio ($\dot{\gamma}_{max}/\dot{\gamma}_{cr}$) is less than 0.2, it increases rapidly to more than 1 as the thrombus grows due to an increase in velocity in the thrombotic region.

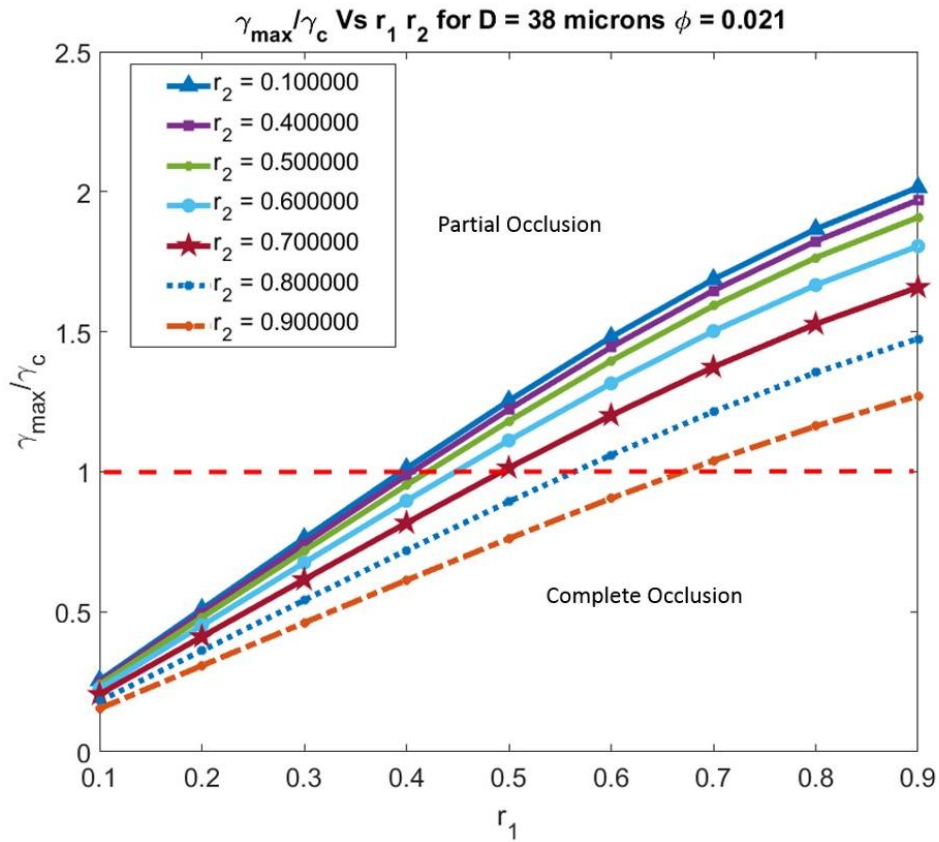


Figure 6.4 Sensitivity of critical shear ratio on bifurcation ratios – Phase plot. A phase plot of r_1 and r_2 values along with their corresponding critical shear ratios for a thrombus of length ratio (ϕ) of 0.02 and a parent vessel diameter (D) of 38 μm .

6.6 Discussion

Thrombi in arterioles and venules increase the overall hydrodynamic resistance of the microvasculature resulting in rapid changes to the local wall shear rate. The magnitude of shear rate change depends on the lateral flow in the vascular network. Specifically, when a thrombus grows in a vessel adjacent to a much larger vessel, the reduction in flow rate into the thrombotic vessel may not be significant. However, in symmetric bifurcations, when both the daughters have nearly identical initial flow rates, the impact of thrombus growth in one daughter vessel on the dynamics of shear rate is substantial. Our results suggest that a comprehensive survey of the microvasculature to gather location-specific pressure drops may yield a vascular map with zones of probable occlusion.

Microfluidic extracorporeal membrane oxygenators are used for patients with a need for pulmonary rehabilitation (186,187). Our analytical model could be used in designing and testing microfluidic oxygenators. We take into account the key design principles involved in designing microfluidic oxygenators such as flow resistance and shear rates in microfluidic bifurcations (188). We believe our model would also find application in the design of microfluidic devices that can precisely perturb hemodynamic parameter space to diagnose bleeding or clotting disorders. We believe our model could also aid the optimization of current Organs-on-chip devices to generate fully occluding thrombus. These devices are currently used to optimize drug dosage for thrombolysis (156,189,190).

Our model evaluates the critical shear ratio ($\dot{\gamma}_{max}/\dot{\gamma}_{cr}$) on the thrombus surface for select bifurcation ratios. The phase plot represents the critical shear ratio for all combinations of r_1, r_2 values in the range of 0.1 to 0.9. Among these bifurcation ratios only a subset of them satisfy Murray's law. Interestingly almost all the pairs of bifurcation ratios that satisfy Murray's law lay above the red-dotted line in **Figure 6.4**, i.e. in the region of partial occlusion. This means that for these cases the thrombus growing in a bifurcation that fits the definition of Murray's law would not occlude the vessel. In order to signify such events, we overlaid the bifurcation ratios that obey Murray's law on top of the critical bifurcation ratios that are predicted by our model to determine if these bifurcation ratios are susceptible to occlusive thrombus formation.

In **Figure 6.5**, we evaluate the bifurcation ratios predicted by our model for critical shear ratios of 0.8, 1.0 and 1.2 against the bifurcation ratios that obey Murray's law. Bifurcation ratios that lie below the dotted line corresponding to a critical shear ratio of 1.0 promote complete occlusion as the shear rate in those vessels would never reach the critical shear rate to stop thrombus growth. The *circles* denote the bifurcation ratios that fit the Murray's law. Only one pair of bifurcation ratio ($r_1 = 0.65, r_2 = 0.9$) falls under the region of complete occlusion. In the setting of the constricted daughter vessels, we observed an increase in the number of bifurcation ratios under the region of complete occlusion. The curve consisting of '*pluses*' in the plot denotes the modified bifurcation ratios with 30% occlusion, and shows a larger portion of bifurcation ratios under the complete occlusion region.

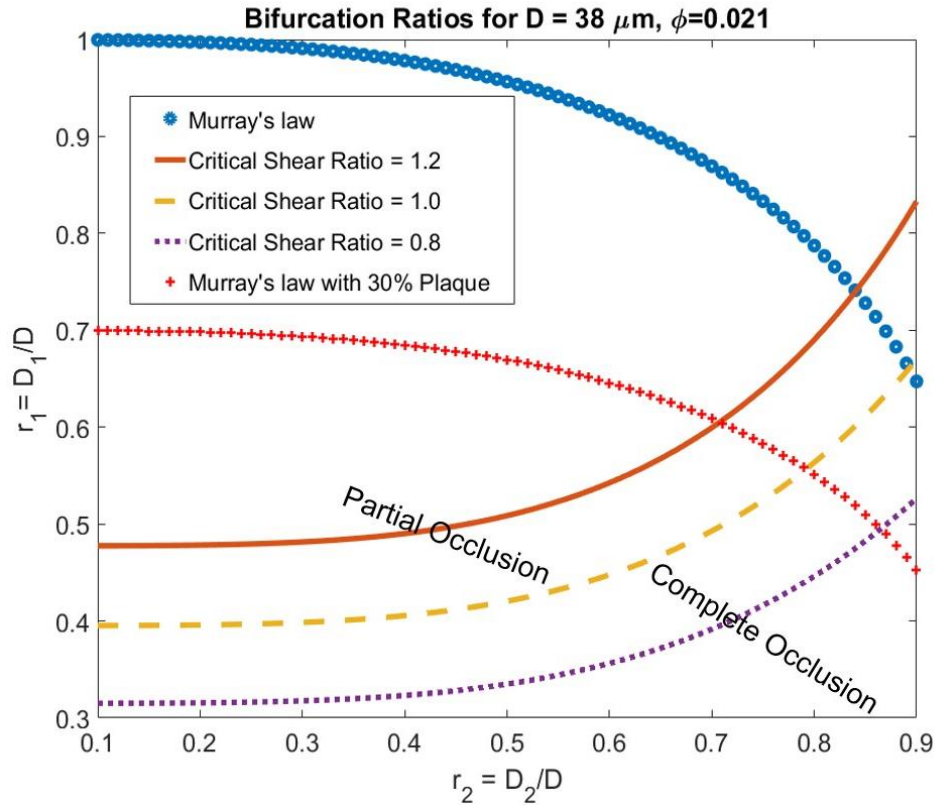


Figure 6.5 Effect of microvascular plaque on occlusive thrombus formation. r_1 and r_2 values predicted from Murray's law for bifurcations with no plaque and 30% plaque with the r_1 and r_2 values for critical shear ratios of 0.8, 1.0 and 1.2 on a thrombus of length ratio (ϕ) 0.02 in a bifurcation with a parent vessel diameter (D) of $38 \mu\text{m}$.

Limitations of this model include the specificity of the results in terms of bifurcation ratios. Our model solves for dependence of maximum shear rate on bifurcation ratios by holding the other variables such as thrombus length ratio, parent vessel diameter and the length of the vessels as fixed parameters. We show that maximum shear rate on the thrombus depends on its length; however, the phase plots are for a fixed thrombus length ratio (0.02). The quantitative nature of the phase plot would likely change for different values of these parameters while the qualitative nature of results would remain unchanged. Change in injury length would alter the maximum shear

rate on the thrombus surface and in addition change the non-linearity of shear rate dynamics to linearly decrease when the thrombus is longer than the critical length (176). However, in case of a constant flow rate boundary condition, non-linearity of shear rate remains unchanged even for a thrombus as long as the vessel. The diameter of the vessels contributes to the vascular resistance to the power of 4, while the length of the vessels contributes to the vascular resistance to the power of 1; thus, the sensitivity of the model to vessel length is much lower as compared to the vessel diameter. However, the extent of bifurcation ratios under the complete occlusion region would change as it should for different thrombus length ratios. Longer thrombus lengths mean higher resistance to flow and as a result would result in decreased maximum shear rates on the thrombus surface for both constant flow rate and constant pressure drop boundary conditions in a bifurcation. Our model also does not consider the curvature of blood vessels, which could affect the local shear rate magnitude. The role of bifurcation geometry is more prominent when we assume blood as a discrete phase flow and this is outside the scope of our current work as modelling blood as a discrete phase fluid will need a multiscale simulation and an analytical model may not be possible. The results proposed in the current work are at steady state downstream to the bifurcation and these results are still valid considering a continuum fluid assumption (156,179,191). We also do not consider the effect of bifurcation angle on the flow dynamics as the impact of bifurcation angle on the wall shear stress downstream would likely be negligible in the case of fully developed steady state flow considered in our model. The COMSOL model has a bifurcation angle of 45° and the analytical model considers bifurcations as resistances to flow which would not be affected by the change in bifurcation angle. Bifurcation angle may have a significant impact on shear stress on thrombus if cells are recruited at the

site of bifurcation. This is not the case in our present model as we assume the clot to form in one of the daughter vessels, downstream of the site of bifurcation. The extension of our model to accommodate larger vessels would require considerations of pulsatile flow and a hybrid boundary condition that would reflect the biophysics of blood flow during thrombus growth. In larger bifurcations such as carotid arteries the presence of recirculation zones would challenge the laminar flow conditions in our current model.

Chapter 7. Conclusions and Future Directions

7.1 Conclusions

The studies outlined in this dissertation have investigated the role of coagulation biochemistry, platelet biology, blood rheology and vascular geometry in hemostasis and thrombosis. The ultimate goal of the research presented in this dissertation is to improve our understanding of hemostasis and thrombosis so that the anticoagulation strategies and drugs implemented in a clinical setting will effectively mitigate thrombosis in diseases while preserving the hemostatic safety. In this chapter, I will summarize the major findings and conclusions drawn from these studies and describe future work to interrogate the interplay between coagulation, platelets and flow.

In Chapter 3, we developed a systems biology model of thrombin generation starting with the HM model as the basis. As these experiments indicated, a threshold effect of FXI on thrombin generation and the fact that the HM model did not include FXI prompted the need to expand the utility of the HM model with the inclusion of FXI. Using the experimental thrombin generation data obtained from PPP, we improved the HM model before expansion to include FXI. The ext.HM model along with the experimental measurements of TF-mediated thrombin generation were utilized to identify that the threshold effect of FXI on thrombin generation was absolutely dependent on the inhibitory role of TFPI under low concentrations of TF. The study highlights the role of feedback and inhibitory mechanisms relevant to hemostasis. In addition, the use of the model in combination with *in vitro* experimental data experiments could be a clinical tool to evaluate coagulation disorders. It is

noteworthy that the field is developing FXI antibodies and small molecule inhibitors to safely mitigate thrombosis without affecting hemostasis.

Experimental studies conducted in Chapter 4, investigated the capacity of the dumb-bell shaped ECM protein nidogen-1 to activate platelets and support platelet adhesion. Functional studies revealed that nidogen-1 activates platelets possibly through the transmembrane receptor GPVI and integrin $\beta 1$. Furthermore, the experiments conducted with apyrase suggested that nidogen-1 is a weak agonist of platelet GPVI that requires feedback activation by ADP secreted by platelets. Based on the results of this study and due to the structural similarity between nidogen-1 and nidogen-2, we can hypothesize that nidogen-2 will have a similar capacity to activate platelets. This study highlights the multifunctional roles of the dynamic ECM microenvironment that go beyond providing structural stability to the matrix.

Studies in Chapter 5 described the development of a microfluidic flow chamber that allows for the evaluation of platelets and coagulation simultaneously under physiologically relevant flow conditions in human whole blood. The 'T' shaped microfluidic device developed in this dissertation is the simplest way of recapitulating an injury-sealing process in a microvessel. Moreover, by modifying the space between the microfluidic pillars one can investigate the interplay between coagulation and vascular permeability. One of the limitations of the current system is the constant inlet blood flow rate used to operate the device which could be modified to a constant pressure-based inlet flow to reflect physiology in future experiments.

Chapter 6 focused on developing an analytical mathematical model that correlates the microvascular bifurcations to thrombus growth through the estimation of shear rate dynamics during thrombus development. Using the model, we analyzed the effect of constant pressure and constant flow boundary conditions on thrombus formation inside the microvessels. A thrombus growing in one of the vessels of the bifurcations experiences a non-linear shear rate that increases with the growth of the thrombus due to increase in velocity in the thrombotic region before falling to zero due to lack of flow at 100% occlusion. Furthermore, the model can be used to design microfluidic networks that are protected from occlusive thrombus formation by optimizing the shear rate in the channels. Our model holds potential to be a valuable tool in analyzing the principles of selection in the physiological design of microvascular networks.

7.2 Future directions

Mathematical modeling of biological networks such as the coagulation system has important implications in the quest for both understanding and predicting biological systems. A biological system such as coagulation can be defined as a network of proteins as the ‘nodes’ with their relationship to each other as the ‘edges’. While molecular biology enables the discovery of new ‘nodes’ and ‘edges’, systems biology can use this knowledge to derive an understanding of these complex biological networks as well as predicting experimental outcomes. The validation of the ext.HM model presented in this dissertation falls into the category of using a model to understand the correlations between existing edges rather than the prediction of new edges (mechanisms). Thus, the work presented in this dissertation is an example of

how mathematical models can be useful even when they are not predicting new mechanisms.

The current mathematical models of thrombin generation rely on experimental systems that measure only the concentration of thrombin over time as the output. While the development of fluorogenic substrate-based thrombin generation assays have greatly advanced our knowledge of coagulation, further research into developing more sophisticated assays are essential to the next big leap. As described in Chapter 1 and Chapter 3, multiple enzymes are generated and inhibited during the generation of thrombin in coagulation. Fluorogenic assays that can record the concentration of other enzymes such as FXa, FIXa and/or FXIa during thrombin generation can provide more boundary conditions to improve the accuracy of the kinetic parameters estimated using the mathematical model. A fluorogenic substrate-based FXa generation assay being developed by Harris et al. shows promise in this regard (192).

7.2.1 Analyze the role of TFPI in modifying the contribution of FXI to TF-mediated fibrin generation under flow

Results from the computational model and thrombin generation experiments in Chapter 3 suggest that the role of FXI in coagulation driven by low concentrations of TF may be eliminated by blocking the inhibitory role of TFPI. Based on this, I hypothesize that the contribution of FXI to TF-mediated fibrin generation and thrombus formation under physiologically relevant flow conditions (arterial and venous) would also be dependent on the inhibitory role of TFPI. I will test my

hypothesis using microfluidic flow chambers as shown in **Figure 7.1**. Experiments will be conducted using FXI-depleted platelet poor plasma (PPP) with or without 30 nM FXI. In select experiments, TFPI function will be blocked using antibodies against its K-1 and K-2 domains. The flow chamber will be coated with TF concentrations in the range of 0.1-1 pM and blocked with BSA. All plasmas will be incubated with CTI to block FXIIa-mediated activation of FXI. Fluorescently tagged fibrinogen will be added to the plasma prior to the experiment and fibrin formation in the flow chamber will be recorded in real-time by measuring the fluorescence intensity of fibrin(ogen) deposited in the chamber. Experiments will be performed under shear rates of 300 s^{-1} and 1000 s^{-1} to determine the role of venous and arterial conditions on fibrin generation.

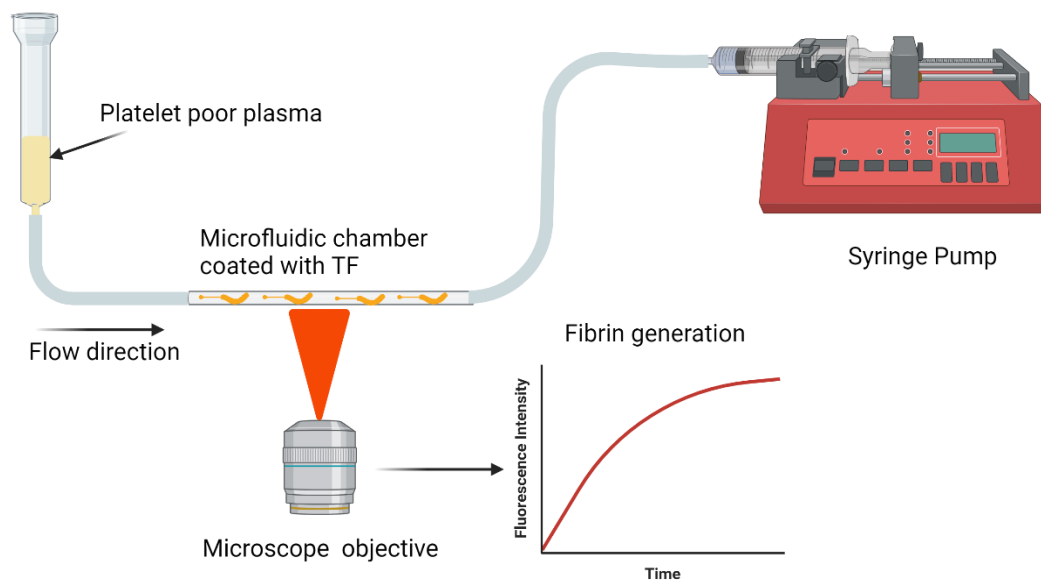


Figure 7.1 Schematic of flow chamber setup to assess fibrin generation under flow. Figure was created using Biorender.com ©Hari hara sudhan Lakshmanan.

7.2.2 Sensitivity analysis of the kinetic parameters of the ext. HM model

The ext. HM model contains 51 kinetic constants that describe the network of thrombin generation (**Table 3.2**). Estimating the parameters of a systems biology model is a necessary challenge as the rate constants derived from experiments typically vary between laboratories. The variations can be attributed to the protein source – recombinant vs plasma derived proteins, buffers, stability of species and the concentration of phospholipids. For example, the kinetic constants for FXa inhibition by anti-thrombin (ATIII) reported in the literature vary over a 3-fold range (193). Thus, future work will involve analyzing the effect of uncertainties in parameters on the thrombin generation outputs, ETP, lag time, peak thrombin and peak time. This can be achieved through local and global sensitivity analysis of kinetic constants of the ext.HM model.

Local sensitivity analysis of the model will be performed using one-at-a-time method, where the change in thrombin generation for a change in the value of each kinetic constant will be recorded without altering other kinetic constants. For example, if Y is a function of X_1 , X_2 and X_3 then the sensitivity of Y to X_1 would be,

$$\text{Sensitivity of } Y \text{ to } X_1 = \left. \frac{\partial Y}{\partial X_1} \right|_{X_2, X_3 = \text{constant}}$$

I propose to analyze the sensitivity of thrombin generation to the kinetic parameters at a high (1 pM) and low (0.1 pM) initial concentration of TF to possibly identify more mechanisms like the feedback activation of FXI by thrombin which may exhibit a threshold behavior based on the initial TF concentrations. Results from the local

sensitivity analysis can aid in the identification of parameters that require the most precise measurement and guide experimental design for the same.

Global sensitivity analysis (GSA) involves varying multiple parameters simultaneously within a 10-fold range to determine the presence of interactions between different parameters and the effect of those interactions on thrombin generation (194). GSA is essential for non-linear models such as the coagulation network as the kinetic parameters will not only affect the system individually but also through the interactions between them. I will use sobol method to perform global sensitivity analysis for a high (1 pM) and low (0.1 pM) initial concentration of TF as previous analyses have been restricted to a relatively higher concentration of TF (108,193). Two different sobol indices are estimated for each parameter, the first-order index and the total-order index (195). The first-order index for a parameter, say k_1 , tells you the ratio of the variance in output due to k_1 to the total variance in output, in other words the contribution of k_1 just by itself to the overall variance of the model output. Total-order index for k_1 will be the sum of contribution of k_1 by itself and the contribution of k_1 due to its interaction with other parameters to the variance of the model output. Let's say there are three parameters, k_1 , k_2 and k_3 , then the total-order index for k_1 will be the sum of, variance due to k_1 alone, variance due to interaction between k_1 and k_2 , variance due to interaction between k_1 and k_3 and the variance due to interaction between k_1 , k_2 and k_3 . An example plot of first and total-order sobol indices for a model with six parameters, k_1 to k_6 , is shown in **Figure 7.2.**

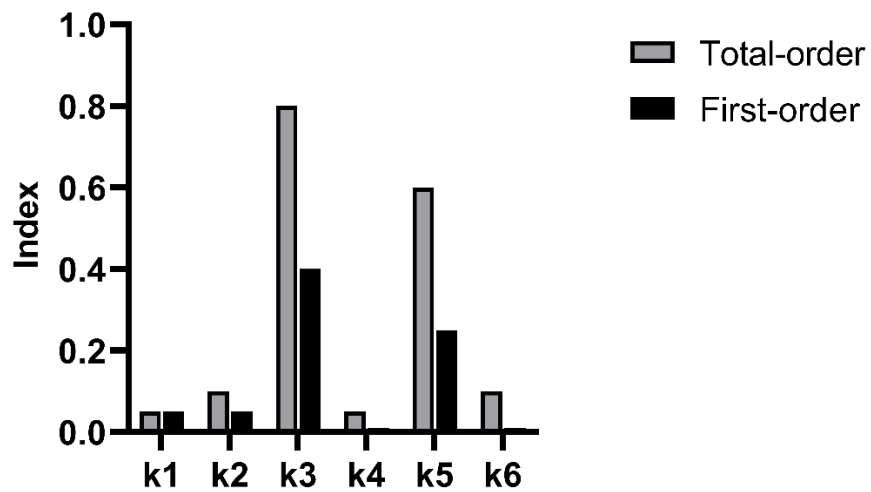


Figure 7.2 Example sobol indices plot for a six-parameter system.

Interpreting the plot shown in **Figure 7.2**, we can see that parameters k3 and k5 are the most critical parameters of the model. Among the two, k3 interacts strongly with other parameters as evidenced by the total-order index of 0.8. Next to k3, parameter k5 has stronger effects on model output due to its interaction with other parameters than by itself. Thus, the sobol indices can help gain deeper insights into the parameters of the model and also aid in the design of *in vitro* experiments to estimate parameters with more accuracy.

7.2.3 Role of polyphosphates in thrombin generation

Chapter 3 focused on evaluating the role of feedback activation of FXI by thrombin in TF-mediated thrombin generation. One of the reasons it was somewhat controversial that FXI activation by thrombin occurs in plasma was because it is rather slow by itself in solution. However, the presence of cofactors such as inorganic

polyphosphates can accelerate this mechanism to potentially increasing the contribution of FXI towards thrombin generation. Inorganic polyphosphates are found to accumulate in microorganisms and are also secreted by activated platelets. My preliminary data indicate that the model can be used in combination with the experiments to gain a mechanistic understanding of the role of polyphosphates in coagulation.

The ext. HM model was simulated with an initial concentration of 30 nM FXI and 0.125 pM TF while keeping the concentrations of other plasma enzymes in their normal values as described in **Table 3.1**. In select simulations, the kinetic constants of FXI and FV activation by thrombin were increased to simulate the effect of PolyP on these reactions. Thrombin generation curves from the simulations of the ext.HM model are shown in **Figure 7.3A**. A two-fold increase in the kinetic constant of FXI activation by thrombin increased only the peak thrombin concentration (grey dashed line) compared to the control (black dashed line). Control refers to the original kinetic constants of the ext. HM model. Even a 10-fold increase in the rate of FXI activation by thrombin increased only the peak thrombin compared to the control without altering the lag phase of thrombin generation (black solid line), as observed through the time taken for the burst in thrombin generation. However, a 2-fold increase in the kinetics of both FXI and FV activation by thrombin resulted in a dramatic decrease in lag time (faster thrombin burst) as well as an increase in peak thrombin concentration compared to the control. The data suggests that if PolyP enhanced only the activation of FXI by thrombin, it would have resulted in the amplification of the peak thrombin rather than hastening the lag phase.

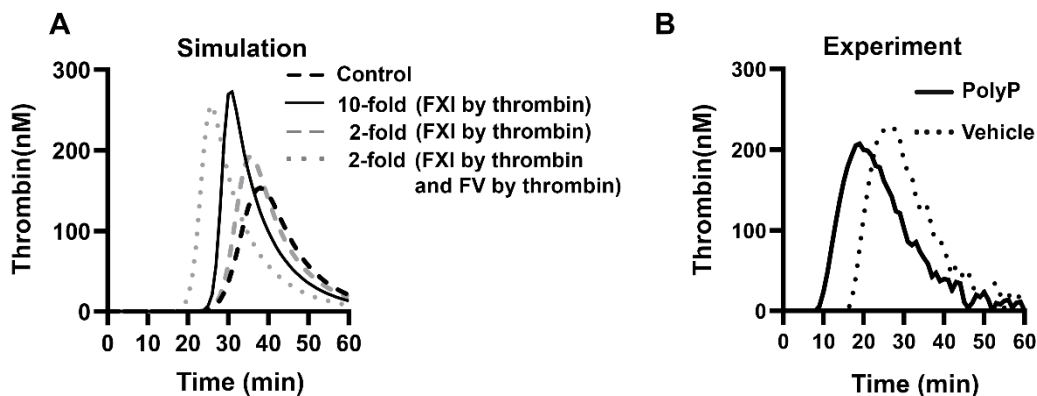


Figure 7.3 Polyphosphates enhance TF-mediated thrombin generation. The effect of PolyP on TF-initiated thrombin generation is analyzed using the extended (ext.) HM model and verified using experiments. **(A)** Thrombin generation curves from simulations of the ext. HM model initiated with 0.125 pM TF and 30 nM FXI. In select simulations, the kinetic constants of FXI activation by thrombin (IIa) was increased by 10-fold or 2-fold with or without increasing the kinetic constant of FV activation by thrombin (IIa) by 2-fold. **(B)** Thrombin generation was initiated with 0.125 pM TF in FXI-depleted plasma supplemented with 30 nM FXI in the presence or absence of 10 μ M PolyP. Data from experiments are representative of $n = 2$ independent experiments.

Preliminary data from the thrombin generation experiments indicate that the presence of PolyP decreases the lag time from around 18 minutes to 8 minutes without considerably altering the peak thrombin concentration (**Figure 7.3B**). While the model predicted the decrease in lag time correctly, it also predicted more than 1.5-fold increase in peak thrombin in contrast to the experiments, warranting the need to include other mechanisms possibly affected by PolyP.

To delineate the contribution of PolyP towards TF-mediated thrombin generation, future studies will involve measuring thrombin generation in FV and/or FXI-depleted plasma with the exogenous addition FV (0-20 nM) or FXI (0-30 nM) in the presence of a range of polyphosphate concentrations (0-20 μ M). In addition, anti-FXI antibody 1A6 will be used in combination with FXI in select experiments to assess the role of

FXIa-mediated FIX activation in thrombin generation in the presence of polyphosphates. The results from these studies can aid in the quantification of the relative contribution of FXI and FV towards TF-mediated thrombin generation with implications in pathology.

References

1. Versteeg, H. H., Heemskerk, J. W., Levi, M., and Reitsma, P. H. (2013) New fundamentals in hemostasis. *Physiol Rev* **93**, 327-358
2. Raskob, G. E., Angchaisuksiri, P., Blanco, A. N., Buller, H., Gallus, A., Hunt, B. J., Hylek, E. M., Kakkar, A., Konstantinides, S. V., McCumber, M., Ozaki, Y., Wendelboe, A., Weitz, J. I., and Day, I. S. C. f. W. T. (2014) Thrombosis: a major contributor to global disease burden. *Arterioscler Thromb Vasc Biol* **34**, 2363-2371
3. Lozano, R., Naghavi, M., Foreman, K., Lim, S., Shibuya, K., Aboyans, V., Abraham, J., Adair, T., Aggarwal, R., Ahn, S. Y., Alvarado, M., Anderson, H. R., Anderson, L. M., Andrews, K. G., Atkinson, C., Baddour, L. M., Barker-Collo, S., Bartels, D. H., Bell, M. L., Benjamin, E. J., Bennett, D., Bhalla, K., Bikbov, B., Bin Abdulhak, A., Birbeck, G., Blyth, F., Bolliger, I., Boufous, S., Bucello, C., Burch, M., Burney, P., Carapetis, J., Chen, H., Chou, D., Chugh, S. S., Coffeng, L. E., Colan, S. D., Colquhoun, S., Colson, K. E., Condon, J., Connor, M. D., Cooper, L. T., Corriere, M., Cortinovis, M., de Vaccaro, K. C., Couser, W., Cowie, B. C., Criqui, M. H., Cross, M., Dabhadkar, K. C., Dahodwala, N., De Leo, D., Degenhardt, L., Delossantos, A., Denenberg, J., Des Jarlais, D. C., Dharmaratne, S. D., Dorsey, E. R., Driscoll, T., Duber, H., Ebel, B., Erwin, P. J., Espindola, P., Ezzati, M., Feigin, V., Flaxman, A. D., Forouzanfar, M. H., Fowkes, F. G., Franklin, R., Fransen, M., Freeman, M. K., Gabriel, S. E., Gakidou, E., Gaspari, F., Gillum, R. F., Gonzalez-Medina, D., Halasa, Y. A., Haring, D., Harrison, J. E., Havmoeller, R., Hay, R. J., Hoen, B., Hotez, P. J., Hoy, D., Jacobsen, K. H., James, S. L., Jasrasaria, R., Jayaraman, S., Johns, N., Karthikeyan, G., Kassebaum, N., Keren, A., Khoo, J. P., Knowlton, L. M., Kobusingye, O., Koranteng, A., Krishnamurthi, R., Lipnick, M., Lipshultz, S. E., Ohno, S. L., Mabwejjano, J., MacIntyre, M. F., Mallinger, L., March, L., Marks, G. B., Marks, R., Matsumori, A., Matzopoulos, R., Mayosi, B. M., McAnulty, J. H., McDermott, M. M., McGrath, J., Mensah, G. A., Merriman, T. R., Michaud, C., Miller, M., Miller, T. R., Mock, C., Mocumbi, A. O., Mokdad, A. A., Moran, A., Mulholland, K., Nair, M. N., Naldi, L., Narayan, K. M., Nasser, K., Norman, P., O'Donnell, M., Omer, S. B., Ortblad, K., Osborne, R., Ozgediz, D., Pahari, B., Pandian, J. D., Rivero, A. P., Padilla, R. P., Perez-Ruiz, F., Perico, N., Phillips, D., Pierce, K., Pope, C. A., 3rd, Porrini, E., Pourmalek, F., Raju, M., Ranganathan, D., Rehm, J. T., Rein, D. B., Remuzzi, G., Rivara, F. P., Roberts, T., De Leon, F. R., Rosenfeld, L. C., Rushton, L., Sacco, R. L., Salomon, J. A., Sampson, U., Sanman, E., Schwebel, D. C., Segui-Gomez, M., Shepard, D. S., Singh, D., Singleton, J., Sliwa, K., Smith, E., Steer, A., Taylor, J. A., Thomas, B., Tleyjeh, I. M., Towbin, J. A., Truelsen, T., Undurraga, E. A., Venketasubramanian, N., Vijayakumar, L., Vos, T., Wagner, G. R., Wang, M., Wang, W., Watt, K., Weinstock, M. A., Weintraub, R., Wilkinson, J. D., Woolf, A. D., Wulf, S., Yeh, P. H., Yip, P., Zabetian, A., Zheng, Z. J., Lopez, A. D., Murray, C. J., AlMazroa, M. A., and Memish, Z. A. (2012) Global and regional mortality from 235 causes of death for 20 age groups in 1990 and 2010: a systematic analysis for the Global Burden of Disease Study 2010. *Lancet* **380**, 2095-2128

4. Wendelboe, A. M., and Raskob, G. E. (2016) Global Burden of Thrombosis. *Circulation Research* **118**, 1340-1347
5. Kalathottukaren, M. T., Haynes, C. A., and Kizhakkedathu, J. N. (2018) Approaches to prevent bleeding associated with anticoagulants: current status and recent developments. *Drug Deliv Transl Res* **8**, 928-944
6. Diamond, S. L. (2016) Systems Analysis of Thrombus Formation. *Circ Res* **118**, 1348-1362
7. Wu, Y. (2015) Contact pathway of coagulation and inflammation. *Thrombosis Journal* **13**, 17
8. Morrissey, J. H., Macik, B. G., Neuenschwander, P. F., and Comp, P. C. (1993) Quantitation of Activated Factor VII Levels in Plasma Using a Tissue Factor Mutant Selectively Deficient in Promoting Factor VII Activation. *Blood* **81**, 734-744
9. Spiess, B. D., Armour, S., Horrow, J., Kaplan, J. A., Koch, C. G., Karkouti, K., and Body, S. C. (2018) Chapter 27 - Transfusion Medicine and Coagulation Disorders. in *Kaplan's Essentials of Cardiac Anesthesia (Second Edition)* (Kaplan, J. A. ed.), Elsevier, Philadelphia. pp 685-714
10. Mann, K. G., Brummel, K., and Butenas, S. (2003) What is all that thrombin for? *Journal of Thrombosis and Haemostasis* **1**, 1504-1514
11. Ofosu, F. A., Liu, L., and Freedman, J. (1996) Control mechanisms in thrombin generation. *Semin Thromb Hemost* **22**, 303-308
12. Sandset, P. M. (1996) Tissue factor pathway inhibitor (TFPI)--an update. *Haemostasis* **26 Suppl 4**, 154-165
13. Rezaie, A. R., and Giri, H. (2020) Anticoagulant and signaling functions of antithrombin. *J Thromb Haemost* **18**, 3142-3153
14. Onishi, A., St Ange, K., Dordick, J. S., and Linhardt, R. J. (2016) Heparin and anticoagulation. *Front Biosci (Landmark Ed)* **21**, 1372-1392
15. Esmon, C. T. (2003) The protein C pathway. *Chest* **124**, 26S-32S
16. Kuter, D. J. (1996) The physiology of platelet production. *Stem Cells* **14 Suppl 1**, 88-101
17. Neunert, C., Noroozi, N., Norman, G., Buchanan, G. R., Goy, J., Nazi, I., Kelton, J. G., and Arnold, D. M. (2015) Severe bleeding events in adults and children with

- primary immune thrombocytopenia: a systematic review. *J Thromb Haemost* **13**, 457-464
18. Fogelson, A. L., and Neeves, K. B. (2015) Fluid Mechanics of Blood Clot Formation. *Annu Rev Fluid Mech* **47**, 377-403
 19. Naimushin, Y. A., and Mazurov, A. V. (2004) Von Willebrand factor can support platelet aggregation via interaction with activated GPIIb-IIIa and GPIb. *Platelets* **15**, 419-425
 20. Ozaki, Y., Asazuma, N., Suzuki-Inoue, K., and Berndt, M. C. (2005) Platelet GPIb-IX-V-dependent signaling. *J Thromb Haemost* **3**, 1745-1751
 21. Stalker, T. J., Newman, D. K., Ma, P., Wannemacher, K. M., and Brass, L. F. (2012) Platelet signaling. *Handb Exp Pharmacol*, 59-85
 22. Almomani, M. H., and Mangla, A. (2021) Bernard Soulier Syndrome. in *StatPearls*, Treasure Island (FL). pp
 23. Li, Z., Delaney, M. K., O'Brien, K. A., and Du, X. (2010) Signaling during platelet adhesion and activation. *Arterioscler Thromb Vasc Biol* **30**, 2341-2349
 24. Bonnefoy, A., and Hoylaerts, M. F. (2008) Thrombospondin-1 in von Willebrand factor function. *Curr Drug Targets* **9**, 822-832
 25. Berndt, M. C., Shen, Y., Dopheide, S. M., Gardiner, E. E., and Andrews, R. K. (2001) The vascular biology of the glycoprotein Ib-IX-V complex. *Thromb Haemost* **86**, 178-188
 26. Watson, S. P., Auger, J. M., McCarty, O. J., and Pearce, A. C. (2005) GPVI and integrin alphaIIb beta3 signaling in platelets. *J Thromb Haemost* **3**, 1752-1762
 27. Lakshmanan, H. H. S., Melrose, A. R., Sepp, A. I., Mitrugno, A., Ngo, A. T. P., Khader, A., Thompson, R., Sallee, D., Pang, J., Mangin, P. H., Jandrot-Perrus, M., Aslan, J. E., and McCarty, O. J. T. (2021) The basement membrane protein nidogen-1 supports platelet adhesion and activation. *Platelets* **32**, 424-428
 28. Alshehri, O. M., Hughes, C. E., Montague, S., Watson, S. K., Frampton, J., Bender, M., and Watson, S. P. (2015) Fibrin activates GPVI in human and mouse platelets. *Blood* **126**, 1601-1608
 29. Inoue, O., Suzuki-Inoue, K., McCarty, O. J., Moroi, M., Ruggeri, Z. M., Kunicki, T. J., Ozaki, Y., and Watson, S. P. (2006) Laminin stimulates spreading of platelets through integrin alpha6beta1-dependent activation of GPVI. *Blood* **107**, 1405-1412

30. Lundblad, R. L., and White, G. C., 2nd. (2005) The interaction of thrombin with blood platelets. *Platelets* **16**, 373-385
31. Quinton, T. M., Kim, S., Derian, C. K., Jin, J., and Kunapuli, S. P. (2004) Plasmin-mediated activation of platelets occurs by cleavage of protease-activated receptor 4. *J Biol Chem* **279**, 18434-18439
32. Petzold, T., Thienel, M., Dannenberg, L., Mourikis, P., Helten, C., Ayhan, A., MPembele, R., Achilles, A., Trojovky, K., Konsek, D., Zhang, Z., Regenauer, R., Pircher, J., Ehrlich, A., Lusebrink, E., Nicolai, L., Stocker, T. J., Brandl, R., Roschenthaler, F., Strecker, J., Saleh, I., Spannagl, M., Mayr, C. H., Schiller, H. B., Jung, C., Gerdes, N., Hoffmann, T., Levkau, B., Hohlfeld, T., Zeus, T., Schulz, C., Kelm, M., and Polzin, A. (2020) Rivaroxaban Reduces Arterial Thrombosis by Inhibition of FXa-Driven Platelet Activation via Protease Activated Receptor-1. *Circ Res* **126**, 486-500
33. Morrow, D. A., Braunwald, E., Bonaca, M. P., Ameriso, S. F., Dalby, A. J., Fish, M. P., Fox, K. A., Lipka, L. J., Liu, X., Nicolau, J. C., Ophuis, A. J., Paolasso, E., Scirica, B. M., Spinar, J., Theroux, P., Wiviott, S. D., Strony, J., Murphy, S. A., Committee, T. P. T. S., and Investigators. (2012) Vorapaxar in the secondary prevention of atherothrombotic events. *N Engl J Med* **366**, 1404-1413
34. Durrant, T. N., van den Bosch, M. T., and Hers, I. (2017) Integrin alphaIIb beta3 outside-in signaling. *Blood* **130**, 1607-1619
35. Usta, C., Turgut, N. T., and Bedel, A. (2016) How abciximab might be clinically useful. *Int J Cardiol* **222**, 1074-1078
36. Scarborough, R. M. (1999) Development of eptifibatide. *Am Heart J* **138**, 1093-1104
37. Yang, M., Huo, X., Miao, Z., and Wang, Y. (2019) Platelet Glycoprotein IIb/IIIa Receptor Inhibitor Tirofiban in Acute Ischemic Stroke. *Drugs* **79**, 515-529
38. Jung, S. M., and Moroi, M. (2000) Activation of the platelet collagen receptor integrin alpha(2)beta(1): its mechanism and participation in the physiological functions of platelets. *Trends Cardiovasc Med* **10**, 285-292
39. van der Meijden, P. E. J., and Heemskerk, J. W. M. (2019) Platelet biology and functions: new concepts and clinical perspectives. *Nat Rev Cardiol* **16**, 166-179
40. Ji, T. H., Grossmann, M., and Ji, I. (1998) G protein-coupled receptors. I. Diversity of receptor-ligand interactions. *J Biol Chem* **273**, 17299-17302
41. Cattaneo, M. (2015) P2Y12 receptors: structure and function. *J Thromb Haemost* **13 Suppl 1**, S10-16

42. Michelson, A. D. (2009) New P2Y₁₂ antagonists. *Curr Opin Hematol* **16**, 371-377
43. Pozzi, A., Yurchenco, P. D., and Iozzo, R. V. (2017) The nature and biology of basement membranes. *Matrix Biol* **57-58**, 1-11
44. Ruggeri, Z. M. (2003) Von Willebrand factor. *Curr Opin Hematol* **10**, 142-149
45. Bhandari, S., and Kumar, R. (2019) Thrombotic Thrombocytopenic Purpura. *N Engl J Med* **380**, e23
46. Cruz, M. A., Yuan, H., Lee, J. R., Wise, R. J., and Handin, R. I. (1995) Interaction of the von Willebrand factor (vWF) with collagen. Localization of the primary collagen-binding site by analysis of recombinant vWF a domain polypeptides. *J Biol Chem* **270**, 10822-10827
47. Bella, J., and Hulmes, D. J. (2017) Fibrillar Collagens. *Subcell Biochem* **82**, 457-490
48. Breitzkreutz, D., Koxholt, I., Thiemann, K., and Nischt, R. (2013) Skin basement membrane: the foundation of epidermal integrity--BM functions and diverse roles of bridging molecules nidogen and perlecan. *Biomed Res Int* **2013**, 179784
49. Bader, B. L., Smyth, N., Nedbal, S., Miosge, N., Baranowsky, A., Mokkalapati, S., Murshed, M., and Nischt, R. (2005) Compound genetic ablation of nidogen 1 and 2 causes basement membrane defects and perinatal lethality in mice. *Mol Cell Biol* **25**, 6846-6856
50. McCarty, O. J., Zhao, Y., Andrew, N., Machesky, L. M., Staunton, D., Frampton, J., and Watson, S. P. (2004) Evaluation of the role of platelet integrins in fibronectin-dependent spreading and adhesion. *J Thromb Haemost* **2**, 1823-1833
51. Ni, H., Yuen, P. S., Papalia, J. M., Trevithick, J. E., Sakai, T., Fassler, R., Hynes, R. O., and Wagner, D. D. (2003) Plasma fibronectin promotes thrombus growth and stability in injured arterioles. *Proc Natl Acad Sci U S A* **100**, 2415-2419
52. Leung, L. L. (1984) Role of thrombospondin in platelet aggregation. *J Clin Invest* **74**, 1764-1772
53. Tuszynski, G. P., Rothman, V. L., Murphy, A., Siegler, K., and Knudsen, K. A. (1988) Thrombospondin promotes platelet aggregation. *Blood* **72**, 109-115
54. Silverstein, R. L., Leung, L. L., and Nachman, R. L. (1986) Thrombospondin: a versatile multifunctional glycoprotein. *Arteriosclerosis* **6**, 245-253

55. Rendu, F., and Brohard-Bohn, B. (2001) The platelet release reaction: granules' constituents, secretion and functions. *Platelets* **12**, 261-273
56. Harrison, P., and Cramer, E. M. (1993) Platelet alpha-granules. *Blood Rev* **7**, 52-62
57. Reed, G. L. (2004) Platelet secretory mechanisms. *Semin Thromb Hemost* **30**, 441-450
58. Chen, Y., Yuan, Y., and Li, W. (2018) Sorting machineries: how platelet-dense granules differ from alpha-granules. *Biosci Rep* **38**
59. Puri, R. N., and Colman, R. W. (1997) ADP-induced platelet activation. *Crit Rev Biochem Mol Biol* **32**, 437-502
60. Morrissey, J. H., Choi, S. H., and Smith, S. A. (2012) Polyphosphate: an ancient molecule that links platelets, coagulation, and inflammation. *Blood* **119**, 5972-5979
61. Zhu, S., Travers, R. J., Morrissey, J. H., and Diamond, S. L. (2015) FXIa and platelet polyphosphate as therapeutic targets during human blood clotting on collagen/tissue factor surfaces under flow. *Blood* **126**, 1494-1502
62. Liu, F., Morris, S., Epps, J., and Carroll, R. (2002) Demonstration of an activation regulated NF-kappaB/I-kappaBalpha complex in human platelets. *Thromb Res* **106**, 199-203
63. Spinelli, S. L., Casey, A. E., Pollock, S. J., Gertz, J. M., McMillan, D. H., Narasipura, S. D., Mody, N. A., King, M. R., Maggirwar, S. B., Francis, C. W., Taubman, M. B., Blumberg, N., and Phipps, R. P. (2010) Platelets and megakaryocytes contain functional nuclear factor-kappaB. *Arterioscler Thromb Vasc Biol* **30**, 591-598
64. Hickman, D. A., Pawlowski, C. L., Shevitz, A., Luc, N. F., Kim, A., Girish, A., Marks, J., Ganjoo, S., Huang, S., Niedoba, E., Sekhon, U. D. S., Sun, M., Dyer, M., Neal, M. D., Kashyap, V. S., and Sen Gupta, A. (2018) Intravenous synthetic platelet (SynthoPlate) nanoconstructs reduce bleeding and improve 'golden hour' survival in a porcine model of traumatic arterial hemorrhage. *Sci Rep* **8**, 3118
65. DeCortin, M. E., Brass, L. F., and Diamond, S. L. (2020) Core and shell platelets of a thrombus: A new microfluidic assay to study mechanics and biochemistry. *Res Pract Thromb Haemost* **4**, 1158-1166
66. Herbig, B. A., and Diamond, S. L. (2017) Thrombi produced in stagnation point flows have a core-shell structure. *Cell Mol Bioeng* **10**, 515-521

67. van Geffen, J. P., Swieringa, F., and Heemskerk, J. W. (2016) Platelets and coagulation in thrombus formation: aberrations in the Scott syndrome. *Thromb Res* **141 Suppl 2**, S12-16
68. Reddy, E. C., and Rand, M. L. (2020) Procoagulant Phosphatidylserine-Exposing Platelets in vitro and in vivo. *Front Cardiovasc Med* **7**, 15
69. Reitsma, S. E., Pang, J., Raghunathan, V., Shatzel, J. J., Lorentz, C. U., Tucker, E. I., Gruber, A., Gailani, D., McCarty, O. J. T., and Puy, C. (2021) Role of platelets in regulating activated coagulation factor XI activity. *Am J Physiol Cell Physiol* **320**, C365-C374
70. Wu, W., Li, H., Navaneetham, D., Reichenbach, Z. W., Tuma, R. F., and Walsh, P. N. (2012) The kunitz protease inhibitor domain of protease nexin-2 inhibits factor XIa and murine carotid artery and middle cerebral artery thrombosis. *Blood* **120**, 671-677
71. (1984) *Perry's Chemical engineers' handbook*, Sixth edition / prepared by a staff of specialists under the editorial direction of late editor Robert H. Perry ; editor, Don W. Green ; assistant editor, James O. Maloney. New York : McGraw-Hill, [1984] ©1984
72. Brass, L. F., and Diamond, S. L. (2016) Transport physics and biorheology in the setting of hemostasis and thrombosis. *J Thromb Haemost* **14**, 906-917
73. (1990) *Clinical Methods: The History, Physical, and Laboratory Examinations. 3rd edition*, LexisNexis UK
74. Bird, R. B., Stewart, W. E., and Lightfoot, E. N. (1960) *Transport Phenomena*, Wiley, New York
75. Jones, C. M., Baker-Groberg, S. M., Cianchetti, F. A., Glynn, J. J., Healy, L. D., Lam, W. Y., Nelson, J. W., Parrish, D. C., Phillips, K. G., Scott-Drechsel, D. E., Tagge, I. J., Zelaya, J. E., Hinds, M. T., and McCarty, O. J. (2014) Measurement science in the circulatory system. *Cell Mol Bioeng* **7**, 1-14
76. Bird, R. B. S. W. E. L. E. N. (2014) *Transport Phenomena*,
77. Secomb, T. W. (2016) Hemodynamics. *Compr Physiol* **6**, 975-1003
78. McCarty, O. J., Ku, D., Sugimoto, M., King, M. R., Cosemans, J. M., and Neeves, K. B. (2016) Dimensional analysis and scaling relevant to flow models of thrombus formation: communication from the SSC of the ISTH. *J Thromb Haemost* **14**, 619-622

79. Hathcock, J. J. (2006) Flow effects on coagulation and thrombosis. *Arterioscler Thromb Vasc Biol* **26**, 1729-1737
80. Nesbitt, W. S., Westein, E., Tovar-Lopez, F. J., Tolouei, E., Mitchell, A., Fu, J., Carberry, J., Fouras, A., and Jackson, S. P. (2009) A shear gradient-dependent platelet aggregation mechanism drives thrombus formation. *Nat Med* **15**, 665-673
81. Herbig, B. A., Yu, X., and Diamond, S. L. (2018) Using microfluidic devices to study thrombosis in pathological blood flows. *Biomicrofluidics* **12**, 042201
82. van Rooij, B. J. M., Zavodszky, G., Hoekstra, A. G., and Ku, D. N. (2020) Biorheology of occlusive thrombi formation under high shear: in vitro growth and shrinkage. *Sci Rep* **10**, 18604
83. Yamamoto, M., Nakagaki, T., and Kisiel, W. (1992) Tissue factor-dependent autoactivation of human blood coagulation factor VII. *J Biol Chem* **267**, 19089-19094
84. Giddings, J. C., and Bloom, A. L. (1975) Factor-V activation by thrombin and its role in prothrombin conversion. *Br J Haematol* **29**, 349-364
85. Lawson, J. H., Kalafatis, M., Stram, S., and Mann, K. G. (1994) A model for the tissue factor pathway to thrombin. I. An empirical study. *Journal of Biological Chemistry* **269**, 23357-23366
86. Gailani, D., and Broze, G. J., Jr. (1991) Factor XI activation in a revised model of blood coagulation. *Science* **253**, 909-912
87. Hockin, M. F., Jones, K. C., Everse, S. J., and Mann, K. G. (2002) A model for the stoichiometric regulation of blood coagulation. *J Biol Chem* **277**, 18322-18333
88. Chelle, P., Morin, C., Montmartin, A., Piot, M., Cournil, M., and Tardy-Poncet, B. (2018) Evaluation and Calibration of In Silico Models of Thrombin Generation Using Experimental Data from Healthy and Haemophilic Subjects. *Bull Math Biol* **80**, 1989-2025
89. Chua, H. N., and Roth, F. P. (2011) Discovering the targets of drugs via computational systems biology. *J Biol Chem* **286**, 23653-23658
90. Iyengar, R. (2009) Computational biochemistry: systems biology minireview series. *J Biol Chem* **284**, 5425-5426
91. Liu, B., Zhang, J., Tan, P. Y., Hsu, D., Blom, A. M., Leong, B., Sethi, S., Ho, B., Ding, J. L., and Thiagarajan, P. S. (2011) A computational and experimental study of the regulatory mechanisms of the complement system. *PLoS Comput Biol* **7**, e1001059

92. Chatterjee, M. S., Denney, W. S., Jing, H., and Diamond, S. L. (2010) Systems biology of coagulation initiation: kinetics of thrombin generation in resting and activated human blood. *PLoS Comput Biol* **6**
93. Kuharsky, A. L., and Fogelson, A. L. (2001) Surface-mediated control of blood coagulation: the role of binding site densities and platelet deposition. *Biophys J* **80**, 1050-1074
94. Dydek, E. V., and Chaikof, E. L. (2016) Simulated Thrombin Generation in the Presence of Surface-Bound Heparin and Circulating Tissue Factor. *Ann Biomed Eng* **44**, 1072-1084
95. Jordan, S. W., and Chaikof, E. L. (2011) Simulated surface-induced thrombin generation in a flow field. *Biophys J* **101**, 276-286
96. Pedicord, D. L., Seiffert, D., and Blat, Y. (2007) Feedback activation of factor XI by thrombin does not occur in plasma. *Proc Natl Acad Sci U S A* **104**, 12855-12860
97. Kravtsov, D. V., Matafonov, A., Tucker, E. I., Sun, M. F., Walsh, P. N., Gruber, A., and Gailani, D. (2009) Factor XI contributes to thrombin generation in the absence of factor XII. *Blood* **114**, 452-458
98. Walsh, P. N., Bradford, H., Sinha, D., Piperno, J. R., and Tuszynski, G. P. (1984) Kinetics of the Factor XIa catalyzed activation of human blood coagulation Factor IX. *J Clin Invest* **73**, 1392-1399
99. Wuillemin, W. A., Eldering, E., Citarella, F., de Ruig, C. P., ten Cate, H., and Hack, C. E. (1996) Modulation of contact system proteases by glycosaminoglycans. Selective enhancement of the inhibition of factor XIa. *J Biol Chem* **271**, 12913-12918
100. Ay, L., Thaler, J., Brix, J. M., Scherthaner, G. H., Ay, C., Pabinger, I., and Scherthaner, G. (2016) Decrease in microvesicle-associated tissue factor activity in morbidly obese patients after bariatric surgery. *Int J Obes (Lond)* **40**, 768-772
101. Puy, C., Ngo, A. T. P., Pang, J., Keshari, R. S., Hagen, M. W., Hinds, M. T., Gailani, D., Gruber, A., Lupu, F., and McCarty, O. J. T. (2019) Endothelial PAI-1 (Plasminogen Activator Inhibitor-1) Blocks the Intrinsic Pathway of Coagulation, Inducing the Clearance and Degradation of FXIa (Activated Factor XI). *Arterioscler Thromb Vasc Biol* **39**, 1390-1401
102. Tucker, E. I., Marzec, U. M., White, T. C., Hurst, S., Rugonyi, S., McCarty, O. J., Gailani, D., Gruber, A., and Hanson, S. R. (2009) Prevention of vascular graft occlusion and thrombus-associated thrombin generation by inhibition of factor XI. *Blood* **113**, 936-944

103. Zilberman-Rudenko, J., Itakura, A., Wiesenekker, C. P., Vetter, R., Maas, C., Gailani, D., Tucker, E. I., Gruber, A., Gerdes, C., and McCarty, O. J. (2016) Coagulation Factor XI Promotes Distal Platelet Activation and Single Platelet Consumption in the Bloodstream Under Shear Flow. *Arterioscler Thromb Vasc Biol* **36**, 510-517
104. Cheng, Q., Tucker, E. I., Pine, M. S., Sisler, I., Matafonov, A., Sun, M. F., White-Adams, T. C., Smith, S. A., Hanson, S. R., McCarty, O. J., Renne, T., Gruber, A., and Gailani, D. (2010) A role for factor XIIa-mediated factor XI activation in thrombus formation in vivo. *Blood* **116**, 3981-3989
105. Brunnee, T., La Porta, C., Reddigari, S. R., Salerno, V. M., Kaplan, A. P., and Silverberg, M. (1993) Activation of factor XI in plasma is dependent on factor XII. *Blood* **81**, 580-586
106. Jones, K. C., and Mann, K. G. (1994) A model for the tissue factor pathway to thrombin. II. A mathematical simulation. *Journal of Biological Chemistry* **269**, 23367-23373
107. Link, K. G., Stobb, M. T., Sorrells, M. G., Bortot, M., Ruegg, K., Manco-Johnson, M. J., Di Paola, J. A., Sindi, S. S., Fogelson, A. L., Leiderman, K., and Neeves, K. B. (2020) A mathematical model of coagulation under flow identifies factor V as a modifier of thrombin generation in hemophilia A. *J Thromb Haemost* **18**, 306-317
108. Danforth, C. M., Orfeo, T., Everse, S. J., Mann, K. G., and Brummel-Ziedins, K. E. (2012) Defining the boundaries of normal thrombin generation: investigations into hemostasis. *PLoS One* **7**, e30385
109. Deguchi, H., Elias, D. J., and Griffin, J. H. (2017) Minor Plasma Lipids Modulate Clotting Factor Activities and May Affect Thrombosis Risk. *Res Pract Thromb Haemost* **1**, 93-102
110. Tucker, E. I., Verbout, N. G., Markway, B. D., Wallisch, M., Lorentz, C. U., Hinds, M. T., Shatzel, J. J., Pelc, L. A., Wood, D. C., McCarty, O. J. T., Di Cera, E., and Gruber, A. (2020) The protein C activator AB002 rapidly interrupts thrombus development in baboons. *Blood* **135**, 689-699
111. Hetmanski, J. H., Zindy, E., Schwartz, J. M., and Caswell, P. T. (2016) A MAPK-Driven Feedback Loop Suppresses Rac Activity to Promote RhoA-Driven Cancer Cell Invasion. *PLoS Comput Biol* **12**, e1004909
112. Hwang, S., Hartman, I. Z., Calhoun, L. N., Garland, K., Young, G. A., Mitsche, M. A., McDonald, J., Xu, F., Engelking, L., and DeBose-Boyd, R. A. (2016) Contribution of Accelerated Degradation to Feedback Regulation of 3-Hydroxy-3-methylglutaryl Coenzyme A Reductase and Cholesterol Metabolism in the Liver. *J Biol Chem* **291**, 13479-13494

113. Mao, X. M., Sun, N., Wang, F., Luo, S., Zhou, Z., Feng, W. H., Huang, F. L., and Li, Y. Q. (2013) Dual positive feedback regulation of protein degradation of an extra-cytoplasmic function sigma factor for cell differentiation in *Streptomyces coelicolor*. *J Biol Chem* **288**, 31217-31228
114. Nemeth, T., and Mocsai, A. (2016) Feedback Amplification of Neutrophil Function. *Trends Immunol* **37**, 412-424
115. Mann, K. G., Butenas, S., and Brummel, K. (2003) The dynamics of thrombin formation. *Arterioscler Thromb Vasc Biol* **23**, 17-25
116. Jesty, J., and Beltrami, E. (2005) Positive feedbacks of coagulation: their role in threshold regulation. *Arterioscler Thromb Vasc Biol* **25**, 2463-2469
117. Nayak, S., Lee, D., Patel-Hett, S., Pittman, D. D., Martin, S. W., Heatherington, A. C., Vicini, P., and Hua, F. (2015) Using a Systems Pharmacology Model of the Blood Coagulation Network to Predict the Effects of Various Therapies on Biomarkers. *CPT Pharmacometrics Syst Pharmacol* **4**, 396-405
118. Crosby, J. R., Marzec, U., Revenko, A. S., Zhao, C., Gao, D., Matafonov, A., Gailani, D., MacLeod, A. R., Tucker, E. I., Gruber, A., Hanson, S. R., and Monia, B. P. (2013) Antithrombotic effect of antisense factor XI oligonucleotide treatment in primates. *Arterioscler Thromb Vasc Biol* **33**, 1670-1678
119. Hsu, C., Hutt, E., Bloomfield, D. M., Gailani, D., and Weitz, J. I. (2021) Factor XI Inhibition to Uncouple Thrombosis From Hemostasis: JACC Review Topic of the Week. *J Am Coll Cardiol* **78**, 625-631
120. Chen, J., and Diamond, S. L. (2019) Reduced model to predict thrombin and fibrin during thrombosis on collagen/tissue factor under venous flow: Roles of gamma'-fibrin and factor XIa. *PLoS Comput Biol* **15**, e1007266
121. Puy, C., Rigg, R. A., and McCarty, O. J. (2016) The hemostatic role of factor XI. *Thromb Res* **141 Suppl 2**, S8-S11
122. Baglia, F. A., and Walsh, P. N. (2007) Thrombin-mediated feedback activation of factor XI on the activated platelet surface is preferred over contact activation by factor XIIIa or factor XIa. *J Biol Chem* **282**, 29067
123. Ivanov, I., Shakhawat, R., Sun, M. F., Dickeson, S. K., Puy, C., McCarty, O. J., Gruber, A., Matafonov, A., and Gailani, D. (2017) Nucleic acids as cofactors for factor XI and prekallikrein activation: Different roles for high-molecular-weight kininogen. *Thromb Haemost* **117**, 671-681

124. Mohammed, B. M., Matafonov, A., Ivanov, I., Sun, M. F., Cheng, Q., Dickeson, S. K., Li, C., Sun, D., Verhamme, I. M., Emsley, J., and Gailani, D. (2018) An update on factor XI structure and function. *Thromb Res* **161**, 94-105
125. Puy, C., Tucker, E. I., Matafonov, A., Cheng, Q., Zientek, K. D., Gailani, D., Gruber, A., and McCarty, O. J. (2015) Activated factor XI increases the procoagulant activity of the extrinsic pathway by inactivating tissue factor pathway inhibitor. *Blood* **125**, 1488-1496
126. Matafonov, A., Cheng, Q., Geng, Y., Verhamme, I. M., Umunakwe, O., Tucker, E. I., Sun, M. F., Serebrov, V., Gruber, A., and Gailani, D. (2013) Evidence for factor IX-independent roles for factor XIa in blood coagulation. *J Thromb Haemost* **11**, 2118-2127
127. Whelihan, M. F., Orfeo, T., Gissel, M. T., and Mann, K. G. (2010) Coagulation procofactor activation by factor XIa. *J Thromb Haemost* **8**, 1532-1539
128. Frantz, C., Stewart, K. M., and Weaver, V. M. (2010) The extracellular matrix at a glance. *J Cell Sci* **123**, 4195-4200
129. Ackley, B. D., Kang, S. H., Crew, J. R., Suh, C., Jin, Y., and Kramer, J. M. (2003) The basement membrane components nidogen and type XVIII collagen regulate organization of neuromuscular junctions in *Caenorhabditis elegans*. *J Neurosci* **23**, 3577-3587
130. Kim, S., and Wadsworth, W. G. (2000) Positioning of longitudinal nerves in *C. elegans* by nidogen. *Science* **288**, 150-154
131. Kuriri, F. A., O'Malley, C. J., and Jackson, D. E. (2019) Molecular mechanisms of immunoreceptors in platelets. *Thromb Res* **176**, 108-114
132. Senis, Y. A., Mazharian, A., and Mori, J. (2014) Src family kinases: at the forefront of platelet activation. *Blood* **124**, 2013-2024
133. Aslan, J. E., Itakura, A., Gertz, J. M., and McCarty, O. J. (2012) Platelet shape change and spreading. *Methods Mol Biol* **788**, 91-100
134. Mangin, P. H., Onselaer, M. B., Receveur, N., Le Lay, N., Hardy, A. T., Wilson, C., Sanchez, X., Loyau, S., Dupuis, A., Babar, A. K., Miller, J. L., Philippou, H., Hughes, C. E., Herr, A. B., Ariens, R. A., Mezzano, D., Jandrot-Perrus, M., Gachet, C., and Watson, S. P. (2018) Immobilized fibrinogen activates human platelets through glycoprotein VI. *Haematologica* **103**, 898-907
135. Mammadova-Bach, E., Ollivier, V., Loyau, S., Schaff, M., Dumont, B., Favier, R., Freyburger, G., Latger-Cannard, V., Nieswandt, B., Gachet, C., Mangin, P. H., and

- Jandrot-Perrus, M. (2015) Platelet glycoprotein VI binds to polymerized fibrin and promotes thrombin generation. *Blood* **126**, 683-691
136. Schonberger, T., Ziegler, M., Borst, O., Konrad, I., Nieswandt, B., Massberg, S., Ochmann, C., Jurgens, T., Seizer, P., Langer, H., Munch, G., Ungerer, M., Preissner, K. T., Elvers, M., and Gawaz, M. (2012) The dimeric platelet collagen receptor GPVI-Fc reduces platelet adhesion to activated endothelium and preserves myocardial function after transient ischemia in mice. *Am J Physiol Cell Physiol* **303**, C757-766
137. Grover, S. P., Bergmeier, W., and Mackman, N. (2018) Platelet Signaling Pathways and New Inhibitors. *Arterioscler Thromb Vasc Biol* **38**, e28-e35
138. Beaulieu, L. M., and Freedman, J. E. (2009) NFkappaB regulation of platelet function: no nucleus, no genes, no problem? *J Thromb Haemost* **7**, 1329-1332
139. Aslan, J. E., Tormoen, G. W., Loren, C. P., Pang, J., and McCarty, O. J. (2011) S6K1 and mTOR regulate Rac1-driven platelet activation and aggregation. *Blood* **118**, 3129-3136
140. Lebozec, K., Jandrot-Perrus, M., Avenard, G., Favre-Bulle, O., and Billiald, P. (2017) Design, development and characterization of ACT017, a humanized Fab that blocks platelet's glycoprotein VI function without causing bleeding risks. *MAbs* **9**, 945-958
141. Voors-Pette, C., Lebozec, K., Dogterom, P., Jullien, L., Billiald, P., Ferlan, P., Renaud, L., Favre-Bulle, O., Avenard, G., Machacek, M., Pletan, Y., and Jandrot-Perrus, M. (2019) Safety and Tolerability, Pharmacokinetics, and Pharmacodynamics of ACT017, an Antiplatelet GPVI (Glycoprotein VI) Fab. *Arterioscler Thromb Vasc Biol* **39**, 956-964
142. Reinhardt, D., Mann, K., Nischt, R., Fox, J. W., Chu, M. L., Krieg, T., and Timpl, R. (1993) Mapping of nidogen binding sites for collagen type IV, heparan sulfate proteoglycan, and zinc. *J Biol Chem* **268**, 10881-10887
143. Jung, S. M., Moroi, M., Soejima, K., Nakagaki, T., Miura, Y., Berndt, M. C., Gardiner, E. E., Howes, J. M., Pugh, N., Bihan, D., Watson, S. P., and Farndale, R. W. (2012) Constitutive dimerization of glycoprotein VI (GPVI) in resting platelets is essential for binding to collagen and activation in flowing blood. *J Biol Chem* **287**, 30000-30013
144. Induruwa, I., Moroi, M., Bonna, A., Malcor, J. D., Howes, J. M., Warburton, E. A., Farndale, R. W., and Jung, S. M. (2018) Platelet collagen receptor Glycoprotein VI-dimer recognizes fibrinogen and fibrin through their D-domains, contributing to platelet adhesion and activation during thrombus formation. *J Thromb Haemost* **16**, 389-404

145. Connors, J. M., and Levy, J. H. (2020) COVID-19 and its implications for thrombosis and anticoagulation. *Blood*
146. Ye, Q., Wang, B., and Mao, J. (2020) The pathogenesis and treatment of the 'Cytokine Storm' in COVID-19. *J Infect* **80**, 607-613
147. Vickers, E. R., McClure, D. L., Naleway, A. L., Jacobsen, S. J., Klein, N. P., Glanz, J. M., Weintraub, E. S., and Belongia, E. A. (2017) Risk of venous thromboembolism following influenza vaccination in adults aged 50 years and older in the Vaccine Safety Datalink. *Vaccine* **35**, 5872-5877
148. Bikdeli, B., Madhavan, M. V., Jimenez, D., Chuich, T., Dreyfus, I., Driggin, E., Nigoghossian, C., Agha, W., Madjid, M., Guo, Y., Tang, L. V., Hu, Y., Giri, J., Cushman, M., Quere, I., Dimakakos, E. P., Gibson, C. M., Lippi, G., Favaloro, E. J., Fareed, J., Caprini, J. A., Tafur, A. J., Burton, J. R., Francese, D. P., Wang, E. Y., Falanga, A., McLintock, C., Hunt, B. J., Spyropoulos, A. C., Barnes, G. D., Eikelboom, J. W., Weinberg, I., Schulman, S., Carrier, M., Piazza, G., Beckman, J. A., Steg, P. G., Stone, G. W., Rosenkranz, S., Goldhaber, S. Z., Parikh, S. A., Monreal, M., Krumholz, H. M., Konstantinides, S. V., Weitz, J. I., and Lip, G. Y. H. (2020) COVID-19 and Thrombotic or Thromboembolic Disease: Implications for Prevention, Antithrombotic Therapy, and Follow-up. *J Am Coll Cardiol*
149. Bunce, P. E., High, S. M., Nadjafi, M., Stanley, K., Liles, W. C., and Christian, M. D. (2011) Pandemic H1N1 Influenza Infection and Vascular Thrombosis. *Clinical Infectious Diseases* **52**, e14-e17
150. Stark, K., and Massberg, S. (2021) Interplay between inflammation and thrombosis in cardiovascular pathology. *Nat Rev Cardiol* **18**, 666-682
151. Sahu, A., and Pangburn, M. K. (1993) Identification of multiple sites of interaction between heparin and the complement system. *Mol Immunol* **30**, 679-684
152. Hao, C., Xu, H., Yu, L., and Zhang, L. (2019) Heparin: An essential drug for modern medicine. *Prog Mol Biol Transl Sci* **163**, 1-19
153. Matafonov, A., Leung, P. Y., Gailani, A. E., Grach, S. L., Puy, C., Cheng, Q., Sun, M. F., McCarty, O. J., Tucker, E. I., Kataoka, H., Renne, T., Morrissey, J. H., Gruber, A., and Gailani, D. (2014) Factor XII inhibition reduces thrombus formation in a primate thrombosis model. *Blood* **123**, 1739-1746
154. Shatzel, J., DeLoughery, E., Lorentz, C., Tucker, E., Aslan, J., Hinds, M., Gailani, D., Weitz, J., McCarty, O., and Gruber, A. The Contact Activation System as a Potential Therapeutic Target in Patients with COVID-19. *Research and Practice in Thrombosis and Haemostasis* **n/a**

155. Sakurai, Y., Hardy, E. T., Ahn, B., Tran, R., Fay, M. E., Ciciliano, J. C., Mannino, R. G., Myers, D. R., Qiu, Y., Carden, M. A., Baldwin, W. H., Meeks, S. L., Gilbert, G. E., Jobe, S. M., and Lam, W. A. (2018) A microengineered vascularized bleeding model that integrates the principal components of hemostasis. *Nature Communications* **9**, 509
156. Schoeman, R. M., Rana, K., Danes, N., Lehmann, M., Di Paola, J. A., Fogelson, A. L., Leiderman, K., and Neeves, K. B. (2017) A microfluidic model of hemostasis sensitive to platelet function and coagulation. *Cell Mol Bioeng* **10**, 3-15
157. Lakshmanan, H. H. S., Melrose, A. R., Sepp, A. I., Mitrugno, A., Ngo, A. T. P., Khader, A., Thompson, R., Sallee, D., Pang, J., Mangin, P. H., Jandrot-Perrus, M., Aslan, J. E., and McCarty, O. J. T. (2020) The basement membrane protein nidogen-1 supports platelet adhesion and activation. *Platelets*, 1-5
158. Zilberman-Rudenko, J., White, R. M., Zilberman, D. A., Lakshmanan, H. H. S., Rigg, R. A., Shatzel, J. J., Maddala, J., and McCarty, O. J. T. (2018) Design and Utility of a Point-of-Care Microfluidic Platform to Assess Hematocrit and Blood Coagulation. *Cell Mol Bioeng* **11**, 519-529
159. Younan, X., and Whitesides, G. M. (1998) Soft Lithography. *Annual Review of Materials Science* **28**, 153-184
160. Qin, D., Xia, Y., and Whitesides, G. M. (2010) Soft lithography for micro- and nanoscale patterning. *Nat Protoc* **5**, 491-502
161. Zilberman-Rudenko, J., Sylman, J. L., Lakshmanan, H. H. S., McCarty, O. J. T., and Maddala, J. (2017) Dynamics of blood flow and thrombus formation in a multi-bypass microfluidic ladder network. *Cell Mol Bioeng* **10**, 16-29
162. Mahalingam, A., Gawandalkar, U. U., Kini, G., Buradi, A., Araki, T., Ikeda, N., Nicolaides, A., Laird, J. R., Saba, L., and Suri, J. S. (2016) Numerical analysis of the effect of turbulence transition on the hemodynamic parameters in human coronary arteries. *Cardiovasc Diagn Ther* **6**, 208-220
163. Stalker, T. J., Traxler, E. A., Wu, J., Wannemacher, K. M., Cermignano, S. L., Voronov, R., Diamond, S. L., and Brass, L. F. (2013) Hierarchical organization in the hemostatic response and its relationship to the platelet-signaling network. *Blood* **121**, 1875-1885
164. Welsh, J. D., Poventud-Fuentes, I., Sampietro, S., Diamond, S. L., Stalker, T. J., and Brass, L. F. (2017) Hierarchical organization of the hemostatic response to penetrating injuries in the mouse macrovasculature. *J Thromb Haemost* **15**, 526-537

165. Tomaiuolo, M., Matzko, C. N., Poventud-Fuentes, I., Weisel, J. W., Brass, L. F., and Stalker, T. J. (2019) Interrelationships between structure and function during the hemostatic response to injury. *Proc Natl Acad Sci U S A* **116**, 2243-2252
166. Klok, F. A., Kruip, M., van der Meer, N. J. M., Arbous, M. S., Gommers, D., Kant, K. M., Kaptein, F. H. J., van Paassen, J., Stals, M. A. M., Huisman, M. V., and Endeman, H. (2020) Incidence of thrombotic complications in critically ill ICU patients with COVID-19. *Thromb Res*
167. Middeldorp, S., Coppens, M., van Haaps, T. F., Foppen, M., Vlaar, A. P., Muller, M. C. A., Bouman, C. C. S., Beenen, L. F. M., Kootte, R. S., Heijmans, J., Smits, L. P., Bonta, P. I., and van Es, N. (2020) Incidence of venous thromboembolism in hospitalized patients with COVID-19. *J Thromb Haemost*
168. Pesonen, E., and Siitonen, O. (1981) Acute myocardial infarction precipitated by infectious disease. *Am Heart J* **101**, 512-513
169. Kearon, C., Akl, E. A., Comerota, A. J., Prandoni, P., Bounameaux, H., Goldhaber, S. Z., Nelson, M. E., Wells, P. S., Gould, M. K., Dentali, F., Crowther, M., and Kahn, S. R. (2012) Antithrombotic therapy for VTE disease: Antithrombotic Therapy and Prevention of Thrombosis, 9th ed: American College of Chest Physicians Evidence-Based Clinical Practice Guidelines. *Chest* **141**, e419S-e496S
170. Amsterdam, E. A., Wenger, N. K., Brindis, R. G., Casey, D. E., Jr., Ganiats, T. G., Holmes, D. R., Jr., Jaffe, A. S., Jneid, H., Kelly, R. F., Kontos, M. C., Levine, G. N., Liebson, P. R., Mukherjee, D., Peterson, E. D., Sabatine, M. S., Smalling, R. W., and Zieman, S. J. (2014) 2014 AHA/ACC Guideline for the Management of Patients with Non-ST-Elevation Acute Coronary Syndromes: a report of the American College of Cardiology/American Heart Association Task Force on Practice Guidelines. *J Am Coll Cardiol* **64**, e139-e228
171. Leiderman, K., and Fogelson, A. (2014) An overview of mathematical modeling of thrombus formation under flow. *Thromb Res* **133 Suppl 1**, S12-14
172. Otero-Cacho, A., Aymerich, M., Flores-Arias, M. T., Abal, M., Alvarez, E., Perez-Munuzuri, V., and Munuzuri, A. P. (2018) Determination of hemodynamic risk for vascular disease in planar artery bifurcations. *Sci Rep* **8**, 2795
173. Morbiducci, U., Kok, A. M., Kwak, B. R., Stone, P. H., Steinman, D. A., and Wentzel, J. J. (2016) Atherosclerosis at arterial bifurcations: evidence for the role of haemodynamics and geometry. *Thromb Haemost* **115**, 484-492
174. Mirramezani, M., Herbig, B. A., Stalker, T. J., Nettey, L., Cooper, M., Weisel, J. W., Diamond, S. L., Sinno, T., Brass, L. F., Shadden, S. C., and Tomaiuolo, M. (2018) Platelet packing density is an independent regulator of the hemostatic response to injury. *J Thromb Haemost* **16**, 973-983

175. Welsh, J. D., Muthard, R. W., Stalker, T. J., Taliaferro, J. P., Diamond, S. L., and Brass, L. F. (2016) A systems approach to hemostasis: 4. How hemostatic thrombi limit the loss of plasma-borne molecules from the microvasculature. *Blood* **127**, 1598-1605
176. Belyaev, A. V., Panteleev, M. A., and Ataulakhanov, F. I. (2015) Threshold of microvascular occlusion: injury size defines the thrombosis scenario. *Biophys J* **109**, 450-456
177. Richardson, P. D. (1973) Letter: Effect of blood flow velocity on growth rate of platelet thrombi. *Nature* **245**, 103-104
178. Sato, M., and Ohshima, N. (1990) Effect of wall shear rate on thrombogenesis in microvessels of the rat mesentery. *Circ Res* **66**, 941-949
179. Colace, T. V., Muthard, R. W., and Diamond, S. L. (2012) Thrombus growth and embolism on tissue factor-bearing collagen surfaces under flow: role of thrombin with and without fibrin. *Arterioscler Thromb Vasc Biol* **32**, 1466-1476
180. Murray, C. D. (1926) The Physiological Principle of Minimum Work Applied to the Angle of Branching of Arteries. *J Gen Physiol* **9**, 835-841
181. Zamir, M., Wrigley, S. M., and Langille, B. L. (1983) Arterial bifurcations in the cardiovascular system of a rat. *J Gen Physiol* **81**, 325-335
182. Rossitti, S., and Lofgren, J. (1993) Optimality principles and flow orderliness at the branching points of cerebral arteries. *Stroke* **24**, 1029-1032
183. Kassab, G. S., and Fung, Y. C. (1995) The pattern of coronary arteriolar bifurcations and the uniform shear hypothesis. *Ann Biomed Eng* **23**, 13-20
184. Zamir, M. (1976) The role of shear forces in arterial branching. *J Gen Physiol* **67**, 213-222
185. Colace, T. V., Jobson, J., and Diamond, S. L. (2011) Relipidated tissue factor linked to collagen surfaces potentiates platelet adhesion and fibrin formation in a microfluidic model of vessel injury. *Bioconjug Chem* **22**, 2104-2109
186. Kniazeva, T., Epshteyn, A. A., Hsiao, J. C., Kim, E. S., Kolachalama, V. B., Charest, J. L., and Borenstein, J. T. (2012) Performance and scaling effects in a multilayer microfluidic extracorporeal lung oxygenation device. *Lab Chip* **12**, 1686-1695
187. Rochow, N., Manan, A., Wu, W. I., Fusch, G., Monkman, S., Leung, J., Chan, E., Nagpal, D., Predescu, D., Brash, J., Selvaganapathy, P. R., and Fusch, C. (2014) An

- integrated array of microfluidic oxygenators as a neonatal lung assist device: in vitro characterization and in vivo demonstration. *Artif Organs* **38**, 856-866
188. Potkay, J. A. (2014) The promise of microfluidic artificial lungs. *Lab Chip* **14**, 4122-4138
 189. Diamond, S. L. (2017) New microfluidic paths to test for bleeding or clotting. *Cell Mol Bioeng* **10**, 1-2
 190. Branchford, B. R., Ng, C. J., Neeves, K. B., and Di Paola, J. (2015) Microfluidic technology as an emerging clinical tool to evaluate thrombosis and hemostasis. *Thromb Res* **136**, 13-19
 191. Neeves, K. B., and Diamond, S. L. (2008) A membrane-based microfluidic device for controlling the flux of platelet agonists into flowing blood. *Lab Chip* **8**, 701-709
 192. Harris, L. F., Castro-Lopez, V., Jenkins, P. V., O'Donnell, J. S., and Killard, A. J. (2011) Comparison of a fluorogenic anti-FXa assay with a central laboratory chromogenic anti-FXa assay for measuring LMWH activity in patient plasmas. *Thromb Res* **128**, e125-129
 193. Danforth, C. M., Orfeo, T., Mann, K. G., Brummel-Ziedins, K. E., and Everse, S. J. (2009) The impact of uncertainty in a blood coagulation model. *Math Med Biol* **26**, 323-336
 194. Link, K. G., Stobb, M. T., Di Paola, J., Neeves, K. B., Fogelson, A. L., Sindi, S. S., and Leiderman, K. (2018) A local and global sensitivity analysis of a mathematical model of coagulation and platelet deposition under flow. *PLoS One* **13**, e0200917
 195. Saltelli, A., Annoni, P., Azzini, I., Campolongo, F., Ratto, M., and Tarantola, S. (2010) Variance based sensitivity analysis of model output. Design and estimator for the total sensitivity index. *Computer Physics Communications* **181**, 259-270

Biographical Sketch

Hari Hara Sudhan Lakshmanan was born on September 23, 1991 in Madurai, Tamil Nadu, India to Lakshmanan and Deivanai. Hari attended the Anna University in Chennai from 2009-2013 to obtain a B.Tech in Chemical Engineering. After graduating, he worked in the Water treatment Industry as a Process Engineer for 2 years in Delhi, India. Driven by curiosity to explore science and pursue research, Hari moved to the Indian Institute of Technology (IIT)-Madras in Chennai to work under Dr. Niket Kaisare in the department of Chemical Engineering as a Project Associate.

In summer 2016, Hari moved to Morgantown, West Virginia to pursue his PhD in Chemical Engineering under the supervision of Dr. Jeevan Maddala at West Virginia University (WVU). During this time Hari had the opportunity to work with Jevgenia Zilberman-Rudenko from Owen McCarty's lab at Oregon Health & Science University on an exciting project that utilized his Chemical engineering skills to build flow models and simulations. As Dr. Jeevan Maddala had to move out of West Virginia University, Hari graduated from the West Virginia University with a Master's degree in Chemical Engineering and moved to OHSU to pursue a PhD in Biomedical Engineering in the lab of Owen McCarty in January 2018. His work is focused on developing and integrating *in vitro* and *in silico* tools to study hemostasis and thrombosis. Hari has published his research in peer-reviewed journals and presented his work at national and International conferences throughout the U.S and Europe, in person and on line. Hari's current publications and presentations are listed below.

Publications/Creative Work:

Peer-reviewed

1. Jevgenia Zilberman-Rudenko, Joanna L Sylman, **Hari Hara Sudhan Lakshmanan**, Owen JT McCarty and Jeevan Maddala, Dynamics of blood flow and thrombus formation in a multi-bypass microfluidic ladder network. *Cellular and Molecular Bioengineering*. 2017; 10(1):16-29.
2. Jevgenia Zilberman-Rudenko, Rachel M White, Dmitriy A Zilberman, **Hari Hara Sudhan Lakshmanan**, Rachel A Rigg, Joseph J Shatzel, Jeevan Maddala and Owen JT McCarty, Design and utility of a point-of-care microfluidic platform to assess hematocrit and blood coagulation. *Cellular and Molecular Bioengineering*. 2018; 11(6):519-529.
3. **Hari Hara Sudhan Lakshmanan**, Joseph J Shatzel, Sven R Olson, Owen JT McCarty and Jeevan Maddala. Modeling the effect of blood vessel bifurcation ratio on occlusive thrombus formation. *Computer Methods in Biomechanics and Biomedical Engineering*. 2019; 22(11):972-980.
4. Michael Wallisch, Christina U Lorentz, **Hari Hara Sudhan Lakshmanan**, Jennifer Johnson, Marschelle R Carris, Cristina Puy, David Gailani, Monica T Hinds, Owen JT McCarty, András Gruber, Erik I Tucker, Antibody inhibition of contact factor XII reduces platelet deposition in a model of extracorporeal membrane oxygenator perfusion in nonhuman primates. *Research and Practice in Thrombosis and Hemostasis*. 2020; 4(2):205-216.
5. **Hari Hara Sudhan Lakshmanan**, Adity A Pore, Tia CL Kohs, Feyza Yazar, Rachel M Thompson, Patrick L Journey, Jeevan Maddala, Sven R Olson, Joseph J Shatzel, Siva A Vanapalli and Owen JT McCarty, Design of a microfluidic bleeding chip to evaluate antithrombotic agents for use in COVID-19 patients. *Cellular and Molecular Bioengineering*. 2021; 13:331-339.
6. **Hari Hara Sudhan Lakshmanan**, Alexander R Melrose, Anna-Liisa I Sepp, Annachiara Mitrugno, Anh TP Ngo, Ayesha Khader, Rachel Thompson, Daniel Sallee, Jiaqing Pang, Pierre H Mangin, Martine Jandrot-Perrus, Joseph E Aslan and Owen JT McCarty, The basement membrane protein nidogen-1 supports platelet adhesion and activation. *Platelets*. 2021; 32(3):424-428.
7. Iván Parra-Izquierdo, **Hari Hara Sudhan Lakshmanan**, Alexander R Melrose, Jiaqing Pang, Tony J Zheng, Kelley R Jordan, Stéphanie E Reitsma, Owen JT McCarty and Joseph E Aslan, The toll-like receptor 2 ligand Pam2CSK4 activates platelet nuclear factor- κ B and Bruton's tyrosine kinase signaling to promote platelet-endothelial cell interactions. *Frontiers in Immunology*. 2021; 12:3492.
8. Tony J Zheng, Elizabeth R Lofurno, Alexander R Melrose, **Hari Hara Sudhan Lakshmanan**, Jiaqing Pang, Kevin G Phillips, Meghan E Fallon, Tia CL Kohs, Anh TP Ngo, Joseph J Shatzel, Monica T Hinds, Owen JT McCarty and Joseph E Aslan, Assessment of the effects of Syk and BTK inhibitors on GPVI-

mediated platelet signaling and function. *American Journal of Physiology: Cell Physiology*. 320(5):C902-C915.

9. Iván Parra-Izquierdo, Alexander R Melrose, Jiaqing Pang, **Hari Hara Sudhan Lakshmanan**, Stéphanie E Reitsma, Sai Hitesh Vavilapalli, Mark K Larson, Joseph J Shatzel, Owen JT McCarty and Joseph E Aslan, Janus kinase inhibitors ruxolitinib and baricitinib impair glycoprotein-VI mediated platelet function. *Platelets*. 2021; 1-12.

Book Chapters

1. Aditya Kasukurti, **Hari Hara Sudhan Lakshmanan**, Sarojini Tiwari and Jeevan Maddala (2019). Integrated multilayer microfluidic platforms with silicon architectures for next generation health diagnostic systems. In Challa SSSR Kumar (Ed.) *Nanotechnology Characterization Tools for Tissue Engineering and Medical Therapy* (1st Edition, 361-396). Springer, Berlin, Heidelberg.

Posters and Presentations at Conferences

1. **Hari Hara Sudhan Lakshmanan**, Jevgenia Zilberman-Rudenko, Owen McCarty, and Jeevan Maddala, “Spatial dependence of thrombolysis”, American Physical Society Division of Fluid Dynamics Meeting, Portland, Oregon, USA (Nov 2016).
2. **Hari Hara Sudhan Lakshmanan** and Jeevan Maddala “Role of bifurcation geometry on stability of thrombus”, 2017 American Institute of Chemical Engineers (AIChE) Annual Meeting, Minneapolis, Minnesota, USA (October 2017).
3. **Hari Hara Sudhan Lakshmanan**, Adity Pore, Rachel Thompson, Jeevan Maddala, Patrick Jurney, Joseph Shatzel, Siva Vanapalli and Owen McCarty, “Design and validation of microfluidic pillar device to study hemostasis under flow”, American Physical Society Division of Fluid Dynamics Meeting, Seattle, Washington, USA (Nov 2019).
4. **Hari Hara Sudhan Lakshmanan**, Owen McCarty and Kristina Haley, “Development of a microfluidic bleeding chip – a tool to assess hemostasis”, Biomedical Engineering Society 2018 Annual Meeting, Atlanta, Georgia, USA (October 2018).
5. **Hari Hara Sudhan Lakshmanan**, Joseph Shatzel, Owen McCarty and Jeevan Maddala, “Microvascular bifurcation ratios and thrombosis,” Biomedical Engineering Society 2018 Annual Meeting, Atlanta, Georgia, USA (October 2018).
6. **Hari Hara Sudhan Lakshmanan**, Adity Pore, Jevgenia Zilberman-Rudenko, Jeevan Maddala, Siva Vanapalli and Owen McCarty, “A microfluidic pillar device to study hemostasis,” Biomedical Engineering Society 2019 Annual Meeting, Atlanta, Philadelphia, USA (October 2019).

7. **Hari Hara Sudhan Lakshmanan**, Daniel Sallee, Stephanie Reitsma, Andras Gruber, Michael Wallisch, Christina Lorentz, Cristina Puy Garcia and Owen McCarty, “Evaluating the safety of targeting coagulation factor XII to prevent vascular device associated thrombus formation under shear”, Biomedical Engineering Society 2019 Annual Meeting, Atlanta, Philadelphia, USA (October 2019).
8. Alexis Flaherty, **Hari Hara Sudhan Lakshmanan**, Toshiaki Shirai and Owen McCarty “Microfluidic device for culturing cells under multiple shear rates,” Biomedical Engineering Society 2019 Annual Meeting, Atlanta, Philadelphia, USA (October 2019).
9. Rachel Thompson, **Hari Hara Sudhan Lakshmanan**, Alexis Flaherty, Joseph Aslan, and Owen McCarty, “Characterization of platelet interactions with the basement membrane protein nidogen-1 under shear flow,” Biomedical Engineering Society 2019 Annual Meeting, Atlanta, Philadelphia, USA (October 2019).
10. Tony Zheng, Elizabeth Lofurno, Alexander Melrose, **Hari hara sudhan Lakshmanan**, Jiaqing Pang, Kevin Phillips, Meghan Fallon, Tia Kohs, Anh Ngo, Joseph Shatzel, Monica Hinds, Owen McCarty and Joseph Aslan. “Assessment of the effects of Syk and BTK inhibitors on GPVI-mediated platelet signaling and function” International Society on Thrombosis and Hemostasis, Philadelphia, USA (Jul 2021).
11. Stephanie Reitsma, Jennifer Johnson, Jiaqing Pang, Iván Parra-Izquierdo, **Hari Hara Sudhan Lakshmanan**, Alexander Melrose, Monica Hinds, Joseph Aslan, Owen McCarty and Jamie Lo “Chronic Edible Dosing of Δ^9 -tetrahydrocannabinol (THC) in Non-human Primates Reduces Systemic Platelet Activity and Function,” International Society on Thrombosis and Hemostasis, Philadelphia, USA (Jul 2021).
12. Benjamin Elstrott, **Hari Hara Sudhan Lakshmanan**, Joseph Aslan and Joseph Shatzel “Iron Repletion Decreases Platelet Count in Iron Deficient Premenopausal Women,” International Society on Thrombosis and Hemostasis, Philadelphia, USA (Jul 2021).
13. **Hari Hara Sudhan Lakshmanan**, Aldrich Estonilo, Cristina Puy, Tony Zheng, Jeevan Maddala, David Gailani, Joseph Shatzel, Andras Gruber, Patrick Journey and Owen McCarty “Refining and validating a model of FXI activation and activity in thrombin generation and blood coagulation,” International Society on Thrombosis and Hemostasis, Philadelphia, USA (Jul 2021).

Appendix A

Modeling the shear rate on the surface of a thrombus in a daughter vessel of a microvascular bifurcation

The following is the mathematical derivation of the analytical model to estimate shear rates on a thrombus of any given length inside a daughter vessel of the bifurcation as described in Chapter 6. The meanings of the notations used below can be found in **Figure 6.1** Modeling a microvasculature bifurcation with a thrombus as a series of resistances.

Equation for shear rate on the thrombus surface for a fully developed steady Newtonian flow reads as

$$\dot{\gamma}_{th} = \frac{8v_{th}}{D_{12}} \quad (A1)$$

$\dot{\gamma}_{th}$ = Shear rate on thrombus surface; v_{th} = velocity near thrombus

D_{12} = Open diameter of the thrombotic region; $D_{12} = (1 - x) * D_1$;

x – occlusion ratio, D_1 – Diameter of vessel before occlusion

$D_1 = r_1 * D$; r_1 – Bifurcation ratio

Substituting for D_{12} in terms of occlusion ratio ‘ x ’ and bifurcation ratio ‘ r_1 ’ in (A1) and simplifying to get (A2)

$$\dot{\gamma}_{th} = \frac{8 v_{th}}{(1 - x)r_1 D} \quad (A2)$$

where $v_{th} = \frac{Q_1}{A_{th}}$

$Q_1 = \text{Blood flow rate through thrombotic vessel}$

$A_{th} = \text{Open area for flow in occluded vessel}$

$$Q_1 = Q \cdot \frac{R_2}{R_2 + R_1}; \text{ where } Q = \frac{\Delta P}{R_t}$$

$$A_{th} = \frac{\pi D_{12}^4}{4} = \frac{\pi(1-x)^2 D_1^2}{4} = \frac{\pi(1-x)^2 r_1^2 D^2}{4}$$

$$\therefore v_{th} = \frac{\Delta P}{R_t} * \frac{R_2}{R_2 + R_1} * \frac{4}{\pi(1-x)^2 r_1^2 D^2}$$

Substituting these in (A2), we get

$$\dot{\gamma}_{th} = \frac{8}{(1-x)r_1 D} \frac{\Delta P}{R_t} \frac{R_2}{R_2 + R_1} \frac{4}{\pi(1-x)^2 r_1^2 D^2}$$

$$\dot{\gamma}_{th} = \frac{32 \Delta P}{\pi D^3} \frac{R_2}{R_t (R_2 + R_1) * (1-x)^3 r_1^3} \quad (A3)$$

This could be further simplified as the first few terms in (A3) could be grouped as the inlet shear rate in the parent vessel.

$$\text{Inlet shear rate, } \dot{\gamma} = \frac{8 * v}{D} = \frac{8 * \Delta P}{R_t * D * \frac{\pi D^2}{4}} = \frac{32 \Delta P}{\pi D^3 R_t}$$

So, equation (A3) is simplified to,

$$\gamma_{th} = \dot{\gamma} \frac{R_2}{(R_2 + R_1) * (1 - x)^3 r_1^3} \quad (A4)$$

$R_1 =$ resistance of the daughter vessel 1 with the thrombus, and is made of three resistances in series, resistance due to the region upstream of the thrombus (R_{11}), resistance due to the thrombus (R_{12}) and resistance due to the region downstream of the thrombus (R_{13}) and can be equated using Hagen-Poiseuille relation for each resistance as follows,

$$R_1 = R_{11} + R_{12} + R_{13} = \frac{128 \mu L_{11}}{\pi D_1^4} + \frac{128 \mu L_{12}}{\pi D_{12}^4} + \frac{128 \mu L_{13}}{\pi D_1^4}; \quad (A5)$$

L_{11}, L_{13} – Lengths of non thrombotic regions of vessel;

L_{12} – Length of thrombus

μ – Blood viscosity;

D_1 – Diameter of daughter vessel 1,

The variables used for resistances, diameters and lengths in these equations are depicted in **Figure 6.1B** and **C**.

Simplifying (A5) we obtain R_1 as

$$R_1 = \frac{128 \mu}{\pi} \lambda_1; \text{ where } \lambda_1 = \frac{L_{11}}{D_1^4} + \frac{L_{12}}{D \cdot r_1 \cdot (1-x)^4} + \frac{L_{13}}{D_1^4} \quad (A6)$$

Similar to R_1 , R_2 can be written as

$$R_2 = \frac{128 \mu}{\pi} \lambda_2; \text{ where } \lambda_2 = \frac{L_2}{D_2^4};$$

To obtain $\frac{R_2}{R_2+R_1}$,

$$\frac{R_2}{R_2 + R_1} = \frac{\lambda_1}{\lambda_1 + \lambda_2} \quad (A7)$$

Substituting (A7) in (A4), we get equation (9) (in Chapter 6) to describe the shear rate on the thrombus surface at different stages of occlusion.

$$\gamma_{th} = \dot{\gamma} \frac{\lambda_1}{(\lambda_1 + \lambda_2) * (1-x)^3 r_1^3} \quad (9)$$

This mathematical relation can be used to estimate the shear rate on thrombus surface growing in one of the vessels in a bifurcation at any stage of occlusion defined by the occlusion ratio 'x'.